2007

High Pressure Testing Of Composite Solid Rocket Propellant Mixtures: Burner Facility Characterization

Rodolphe Valentin Carro
University of Central Florida

HIGH PRESSURE TESTING OF COMPOSITE SOLID ROCKET PROPELLANT MIXTURES: BURNER FACILITY CHARACTERIZATION

by

RODOLPHE VALENTIN CARRO
B.S. Florida Institute of Technology, 2001

A thesis submitted in partial fulfillment of the requirements
for the degree of Master of Science
in the Department of Mechanical Material and Aerospace Engineering
in the College of Engineering and Computer Science
at the University of Central Florida
Orlando, Florida

Fall Term
2007

ABSTRACT

Much Research on composite solid propellants has been performed over the past few decades and much progress has been made, yet many of the fundamental processes are still unknown, and the development of new propellants remains highly empirical. Ways to enhance the performance of solid propellants for rocket and other applications continue to be explored experimentally, including the effects of various additives and the impact of fuel and oxidizer particle sizes on burning behavior. One established method to measure the burning rate of composite propellant mixtures in a controlled laboratory setting is to use a constant-volume pressure vessel, or strand burner. To provide high-pressure burning rate data at pressures up to 360 atm, the authors have installed, characterized and improved a strand burner facility at the University of Central Florida. Details on the facility and its improvements, the measurement procedures, and the data reduction and interpretation are presented. Two common HTPB / ammonium perchlorate (AP) propellant mixtures were tested in the original strand burner. The resulting burning rates were compared to data from the literature with good agreement, thus validating the facility and related test techniques, the data acquisition, data reduction and interpretation.

After more than 380 successful recordings, an upgraded version of the strand burner, SB-II (Strand Burner II) was added to the facility. The details of Strand Burner II, its improvements over Strand Burner I, and its characterization study are presented.

I dedicate my thesis to my grand-parents and my parents

who have always been my source of inspiration,

the foundation of all my achievements,

and a model in my life, each in their own way.

But most of all, I want to dedicate this work to my wife Jaime,

for her unconditional love and support;

and my two boys, Noah and Gabriel, my strength and my purpose in life.

Je dédicace ma thèse à mes grands-parents, et mes parents

qui ont toujours été ma source d'inspiration,

la fondation de tous mes accomplissements,

et un model dans ma vie, chacun a leur propre façon.

Mais avant tout, je veux dédier ce travail à ma femme Jaime,

pour son amour in conditionnel et son support

et à mes deux fils, Noah et Gabriel, ma force et mon dessein.

ACKNOWLEDGMENT

I would like to acknowledge and thanks The Space Launch Corporation and the Missile Defense Agency for partial funding of this research effort.

In addition, this work could not have been complete without the hard work of my coworkers, specifically, Mathew Stephens, Alexander LePage, Jason Arvanetes, David Reid, Thomas Sammet, Steven Wolf, Ollie Rodriguez, Rory Mulcahy, Andrew Lease; and Dr. Eric Petersen who entrusted me with this project.

TABLE OF CONTENTS

LIST OF FIGURES

LIST OF TABLES

LIST OF ACRONYMS AND ABBREVIATIONS

a	temperature coefficient
AIAA	American Institute of Aeronautics and Astronautics
AISI	American Iron and Steel Institute
Al	Aluminum
Amp	Ampere
AP	Ammonium Perchlorate
APS	Air Plasma Spray
Ar	Argon
ASEE	American Society of Engineering Education
ASME	American Society of Mechanical Engineers
atm	Atmosphere
Avg.	Average
CARS	Coherent Anti-Stokes Raman Scattering
CCD	Charge Coupled Device
cm	Centimeter
CSV	Comma-Separated Value
DAS	Data Acquisition System
DC	Direct Current
Dr.	Doctor
et al.	and associates
F	Fahrenheit
FEA	Finite Element Analysis
FEM	Finite Element Model
FOD	Foreign Object Damage
FS	Full Scale
FSS	Focusing Schlieren System
ft	feet
ft^3	feet cube
GUI	Graphical User Interface
HDBK	Handbook
HTPB	Hydroxyl-Terminated-PolyButadiene
IEEE	Institute of Electrical and Electronics Engineers
in	inch

IPDI	IsoPhorone DiIsocynate (curative)
K	Kelvin
kg	kilogram
KVM	Keyboard-Video-Mouse
LASER	Light Amplification by Stimulated Emission Radiation
lb	pound
Log	Logarithmic
m	meter
m^3	meter cube
MIL	Military
mm	millimeter
MS	Margin of Safety
msec	millisecond
n	burning rate exponent
N	Nitrogen
N	Normalized
ND	Neutral Density
Ni	Nickel
nm	nanometer
No.	Number
NPT	National Pipe Thread
P	Pressure (psi)
PCI	Peripheral Component Interconnect
pp.	Page
psi	Pound per Square Inch
Quad	Quadrilaterals
r	burning rate ($in.sec^{-1}$)
R^2	Pearson's linear coefficient of regression (least-squares analysis)
ref	Refer to
REU	Research Experience for Undergraduates
SAE	Society of Automotive Engineers
SB-I	Strand Burner I
SB-II	Strand Burner II
sec	second
SEM	Scanning Electron Microscope
Si	silicon

SLC	Space Launch Corporation
SS	Stainless Steel
Temp.	Temperature (°F)
UCF	University of Central Florida
USB	Universal Serial Bus
UNC	Unified Coarse thread
UNF	Unified Fine thread
V	Volt
VDC	Volt Direct Current
Vol.	Volume (in^2)
vs.	Versus
XPS	X-ray Photoelectron Spectroscope
2D	Bi Dimensional
3D	Tri Dimensional
°	Degree (temperature)
%	Percent
μ	Micro
~	Approximately
σ	Stress (psi)

CHAPTER 1
INTRODUCTION

A solid rocket motor's operation and design depend on the combustion characteristics of the propellant, and the ultimate success of the motor depends significantly on knowledge of its burning rate behavior under all operating and design-limiting conditions (mainly pressure and temperature). However, the fundamental combustion processes within a composite solid rocket motor are very complex and not completely understood.[1, 2] Experimental measurement and validation of a propellant's burning rate are therefore important and involve small-sample testing in laboratory burners, subscale motor firings, and eventually full-scale firings at established test facilities. Composite propellants composed of ammonium perchlorate (AP) oxidizer and hydroxyl-terminated-polybutadiene (HTPB) binder/fuel are commonly found in current production rocket motors. Various additives for influencing an AP / HTPB-based propellant's burning rate, curing characteristics, and structural integrity are routinely added at low weight percent levels. New additives and particle-size permutations are continually being researched in an attempt to increase the performance of a propellant or otherwise modify its physical and chemical characteristics.[3, 4] The initial assessment of new additives is typically conducted by burning small samples of propellant in a high-pressure burner prior to manufacturing a full-scale grain.

In many cases, powdered metals, aluminum in particular, are used in solid propellants because of their promise for high flame temperatures and increased

performance. Nonetheless, problems with melting temperatures, residence times, and oxide coatings often prevent the high potential of metal powders from being fully realized.[5] The physical mechanisms controlling the heating, vaporization, and combustion of aluminized solid propellant ingredients are challenging and continue to be the subject of active research both theoretically and numerically.[6-10]

To further explore alternative composite propellant formulations and their fundamental burning characteristics, the authors established a new, high-pressure strand burner facility at the University of Central Florida (UCF). The strand burner technique is a simple, convenient, and cost effective method for the measurement of the pressure-dependent burning rate of solid propellants.[1, 11, 12] This document describes the self-sufficient solid propellant research laboratory, with an emphasis on the strand burner design details and corresponding burning rate-measurement techniques.

Toward the end of the SLC-sponsored program, and over 400 firings, the original strand burner was showing some signs of wear raising safety concerns. Therefore, based on experience, a new strand burner was designed

- to further extend the pressure range of testing without compromising user safety;
- to increase the internal volume of the pressure vessel, minimizing the effect of the pressure rise over the burning rate;
- to simplify the maintenance of the system, improving turn around time;
- to extend the life time of the overall system;
- to double the number of windows, increasing the number of simultaneous instrumentation ports.

Repeatability in the measurement from two different batches and characterization experiments using two established HTPB / AP formulations are also described. Further examples of the use of the strand burner facility for the assessment of burning rate modifiers are provided in Stephens et al.[13]

CHAPTER 2
LITERATURE REVIEW

During the 1940s, researchers at the Jet Propulsion Laboratory in Pasadena, California, began working on “castable” solid propellants. John Parsons developed asphalt as a fuel and binder (the substance that holds all the chemicals together) together with potassium perchlorate as an oxidizer. By the 1950s, synthetic polymers replaced the asphalt. A major improvement came when the rocket designers and chemists added aluminum powder to the mix, which increased the performance of the propellant substantially. Nowadays, composite solid propellants are commonly utilized in rockets because of their high burning rates and favorable specific impulse (Davenas, 2003).

Development of solid rocket propellants depends on the chemical composition and a variety of parameters; but yet, combustion performance of solid propellant rocket motors can be improved by the following physicochemical parameters:

- Increasing propellant flame temperature without compromising the motor’ structural integrity;
- Reducing the pressure sensitivity of the propellant to promote burn stability and reduce motor damage;
- Quantify the temperature sensitivity of the propellant;
- Measure the casting tensile and compression strength and resistance to erosive burning

- Obtaining a spectrum of propellant burning rate over the operating pressure and temperature range.

All of these items are related to the phenomena of propellant combustion mechanisms.

Extensive substantiation using the principles of chemical kinetics, fluid dynamics and heat transfer must be carried out during the design and conceptual analysis of the rocket propellant to predict some of the complex combustion phenomena occurring during rocket motor operation, such as ignition, erosive burning, oscillatory burning, and combustion termination.

Thanks to the always-increasing availability of computational power, much progress has been made in the modeling of these combustion phenomena. Nonetheless, analysis from theoretical models offers estimation at best of the quantitative properties of the propellant. The determination of the chief propellant combustion characteristic, the *burning rate*, is only accurately determined by experiments.

The motivations for determining this property are different for propellant researchers; design and development, and production engineers:

- Propellant researchers are interested in the influence of new ingredients and new formulations on the burning rate;
- Design, development, and production engineers are interested in the applicability and reproducibility of a propellant with this specific property.

Unlike most liquid propellant rocket engines, a solid propellant rocket motor and its key components cannot be operationally pre-tested. As a result, individual motor reliability must be inferred by substantiating the structural integrity and verifying manufacturing

quality on the entire population of motors. This aspect of solid propellant rocket motors highlights the importance of combustion stability defined by the *combustion index*.

Also, the accuracy of thrust-time prediction has become increasingly more important in the design of solid rockets for multiple boosters in launch vehicles and requires a corresponding improvement of burning rate measurement accuracy. Thus, knowledge of propellant burning rates, whether steady or unsteady, under a variety of operating conditions is of critical importance both for applications (performance, cost, and ageing of motors) and fundamentals (understanding of combustion processes). The desired values are usually measured in a proper experimental setup, also because no theory capable to predict burning rates with accuracies within 1% while including the effects of rate modifiers is yet available. However, while experiments measuring steady burning rates are reasonably feasible, those measuring ignition transient[31, 32, 33] and unsteady values from pressure oscillation are still a matter of research.[34]

2.1 Solid Rocket Propellant Combustion

Whether steady or unsteady, deflagration waves in energetic solid materials in general consist of an initial condensed phase and a final gas phase of reaction products (frequently including particles and/or droplets). The interface between the condensed phase and gas phase is called the burning surface. The propagation rate of this interface is called burning rate; physically, this can be seen as the regression rate of the condensed phase. It is often convenient to define, more precisely, a linear burning (or deflagration) rate as the web thickness burned per unit time in the direction perpendicular to the burning surface. The burning surface regresses in a direction essentially perpendicular to itself.

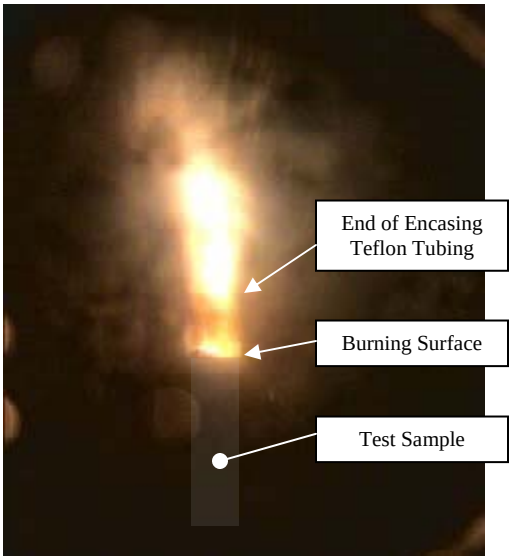

Figure 1: The Typical Linear Regression of the Burning Surface

Solid propellants are considered to burn by parallel layers and the grain "tends to retain its original configuration until the web has burned through" (Robert's law, 1839). This law, originally proposed for homogeneous compositions, can be extended to modern heterogeneous compositions if the propellant heterogeneity is limited to a "sufficiently small scale". The actual burning surface and its time evolution depend on the initial grain geometry (molecules size, distribution, proportion) and overall combustion processes (flame temperature, distance between the flame temperature and burning surface, combustion stability and completeness of the chemical reactions.

Success in rocket motor design and development depends significantly on knowledge of burning rate behavior of the selected propellant under all motor design operating conditions and design limit conditions. Burning rate is a function of the pressure and on the initial propellant grain temperature, cross-flow velocity, propellant type, fuel to oxidizer ratio, and oxidizer particle size in the case of composite propellant. At any instant

the burning rate governs the burning time and the mass flow rate of hot gas generated and flowing from the motor combustion chamber to the nozzle and therefore the thrust, and the specific impulse, of the rocket.

The empirical relation relating the burning rate, r, and the combustion chamber pressure, P, is

$$r = a\,P^{\,n} \tag{1}$$

Where a is a dimensionless empirical constant influenced by ambient grain temperature (the *temperature coefficient*),and n is the *burning rate exponent* also called the *combustion index*. The later is independent of the initial grain temperature and describes the influence of chamber pressure on the burning rate. For stable operation, n has values greater than 0 and less than 1.0. High values of n give a rapid change of burning rate with pressure and can be determined for the motor.

Measuring rocket propellant burning rates covers various phases (research and technology, screening, development, performance verification, and production control) and each requires suitable tools. Correspondingly, a variety of experimental rigs and procedures is in use worldwide, ranging from the simple strand burners to an array of closed or vented vessels, from different small-scale (or subscale) test motors (ballistic evaluation motors) up to full-scale motors tested first on ground and eventually in flight conditions.[1]

2.2 The Strand Burner

For about 60 years, the industry standard apparatus for routine measurements of linear burning rates has been the so-called strand burner or Crawford bomb proposed by

Crawford in 1947.[11] This method, very quick, simple, and economic, is particularly suitable for exploring new propellant compositions, characterizing a propellant's burning rate over a defined pressure and temperature range, or performing quality control of established compositions[37].

The propellant sample being tested, referred to as a *strand*, is burned within the confines of a pressure tank pressurized with an inert gas. The strand is in the form of a pencil-like stick, and is ignited at one end. The time duration for the strand to burn along its length in a cigarette fashion is measured.

The two basic approaches to economical, experimental characterization of a solid propellant's burning rate are closed and isobaric strand burners. The closed burner technique characterizes the isothermal burning rate function in a continuous manner over a small pressure range with a single burn while the isobaric burner method provides a discrete measurement requiring several burns. Over the years, three major advanced techniques to improve the accuracy of the measurement of the regression rate of strands have been implemented and characterized.

- Hermance[17] presented in 1969 a method that consists of using the strand as the dielectric material of a capacitor which forms a part of a resonant inductor-capacitor circuit oscillating at a predetermined center frequency.
- Bozic et al.[18] presented the principle of the measurement and data reduction for their method using microwave reflection interferometry in 1995.
- Lately, high accuracy internal ballistic measurement have been performed using ultrasonic instrumentation.[19, 20]

Refer to Appendix A for the detailed testing procedure used during the experiments. Note that the experiment is designed in a fashion that places efficiency and safety at the highest priority.

Refer to Appendix C and D for detail of the strand burners design.

CHAPTER 3
EXPERIMENTAL DESIGN

The first section of this chapter defines the different components that constitute the solid rocket facility. While most of the major components are unchanged since the original installation started in fall 2003, most of the systems interacting between them and the measurement instrumentation have been upgraded. The motivation for these upgrades was to reach a higher level of safety, accuracy and diversity in our measurements.

3.1 Facility Hardware

At the core of the burner facility are the two high-pressure bombs. The original strand burner, strand burner I or SB-I, was designed and built by Space Launch Corporation (SLC) to handle test pressures in excess of 360 atm (5300 psi). The low-carbon steel alloy body offers one side window along the strand and one end window opposite to the strand. This pressure vessel was described in great detail by the author in an AIAA paper presented during the 41st Joint Propulsion Conference in 2005. [21]

Figure 2 presents the general arrangement of the strand burners. Sitting next to SB-I, at the center of the optical table, is the new and improved strand burner, strand burner II or SB-II. The new pressure vessel is essentially made of the same material and follows the same design outline of SB-I. Table 1 relates the major differences between the two pressure vessels, mainly found in the overall size and quantity of features.

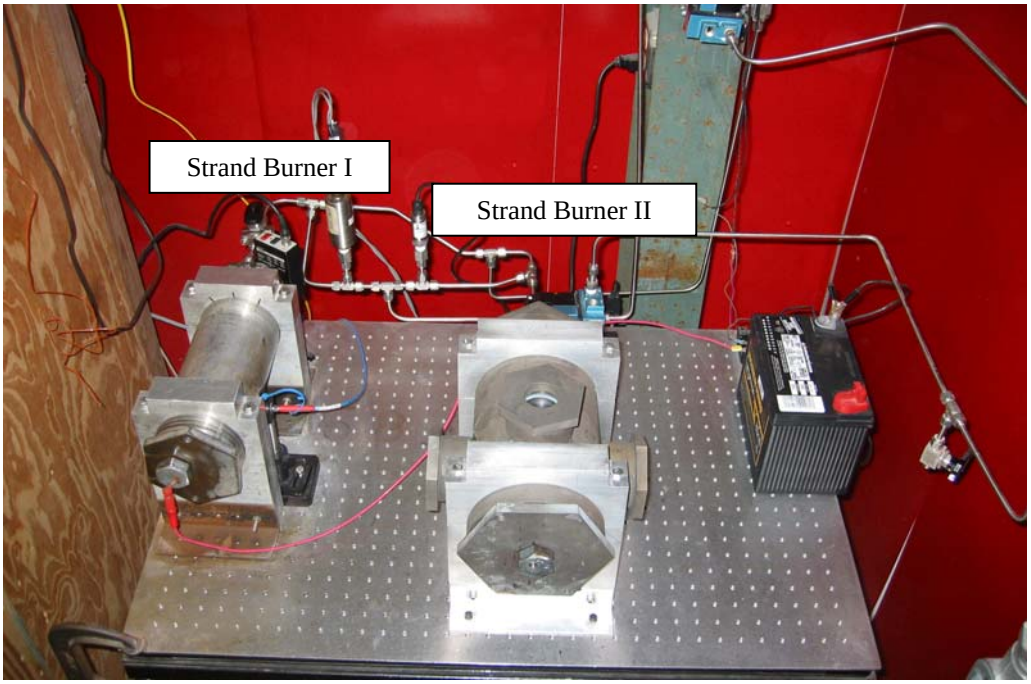

Figure 2: Strand Burner I and Strand Burner II

Table 1: Major SB-I / SB-II Dimensions Comparison

	SB-I	SB-II	% Increase
Inner Diameter (in)	3.13	3.70	18
Outer Diameter (in)	4.25	6.00	41
Wall Thickness (in)	0.56	1.15	104
Outer Length (in)	12.00	12.00	0
Inner Length (in)	8.88	6.50	-27
Maximum Width (in)	5.00	9.80	96
Volume (in^2)	67.76	76.76	13
No. of Windows	2	4	100

The new strand burner was designed following the guidance of the ASME Boiler and Pressure Vessel Code for normal operation up to 340 atm (5000 psi) and positive margin of safety up to 544 atm (8000 psi). A simplified model of the assembly was conceptualized, meshed and subjected to virtual internal pressure loading using a finite element analysis computer software. The pre-processing and definition of the loads,

constraints and assumptions, along with some screenshots of the post-processing visualization are gathered in Appendix H. FEA was used during the design phase to visualize stress concentration areas and validate the stress values found in the hand calculations

The body, the end caps, the window holders and the window end caps were machined out of solid rods of low-carbon steel alloy (SAE 4140). The 30.48 cm (12.0 in) long cylinder has an outer diameter of 15.24 cm (6.00 in) and an inner diameter of 9.398 cm (3.700 in), an 18% increase over SB-I's. Each extremity has a 5.08 cm (2 in) deep 4.0 - 4 UNC internal threads to accept the end-caps. Figure 3 shows the main body and the forward en-cap with an emphasis on the large thread design providing strength, quick assembly / disassembly and prevent galling.

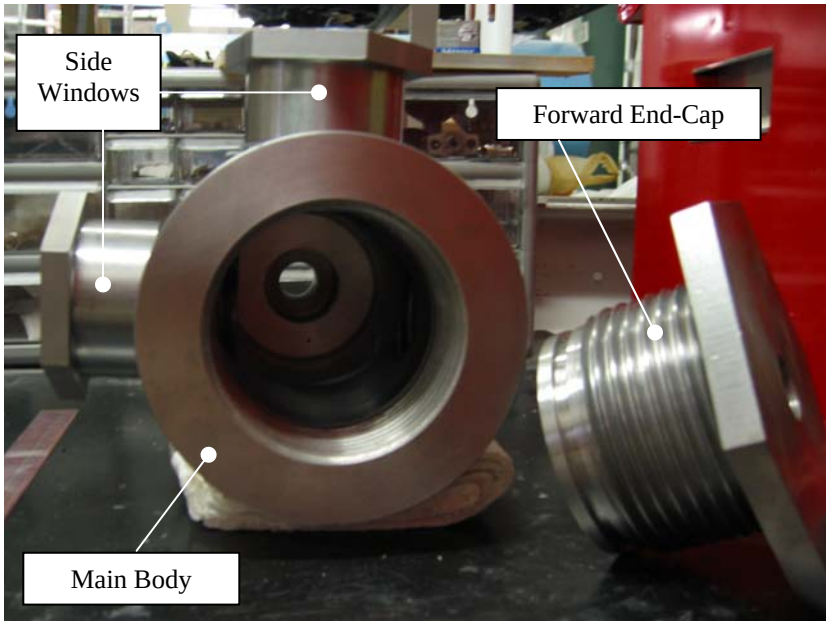

Figure 3: SB-II Main body and the Forward End-Cap

Beyond the threads is a 32 micron finish 2.03 cm (0.80 in) wide. These areas are the seats for the O-rings located on the end-caps sealing the strand burner forward and aft. The hexagonal head of each end-cap is 1.77 cm (0.5 in) thick, making the overall length of the burner 33.02 cm (13 in). Three 5.715 cm (2.25 in) 4 ½ UNC tapped holes were machined through the wall of the cylindrical body in the plan of the strand to accept the window frames. With the window frames and window end-caps installed, the maximum width of the strand burner is 24.89 cm (9.80 in).

Both end-caps have the same overall dimensions and have two diametrically opposed, 0.95 cm (0.375 in) 16 UNC tapped holes through their hexagonal 'heads'. A tool to apply torque to remove the end-caps can be fastened to these holes temporarily. The aft end-cap has a 4.60 cm (1.812 in) hole bored 3.17 cm (1.25 in) deep from the inside to accept the back-end window. This hole then reduces to a 2.54 cm (1.00 in) hole. Next to it is the 0.15 cm (0.06 in) pressure port leading to a ¼ NPT thread. The same port is used to fill and vent the pressure vessel. The forward end-cap has a center 2.54 cm (1.00 in), 14 UNF tapped hole to receive the strand holder. The seal between the strand holder and the end-cap is achieved thanks to the strand holder O-ring seating on the smooth 2.38 cm (0.937 in) hole bored beyond the threads.

The three lateral optical ports are comprised of three removable parts: the window frame, the window and the window end-cap. The window frame is a SAE 4140 steel cylinder threaded on the outside screwed onto the main body and smooth on the inside to accept the window.

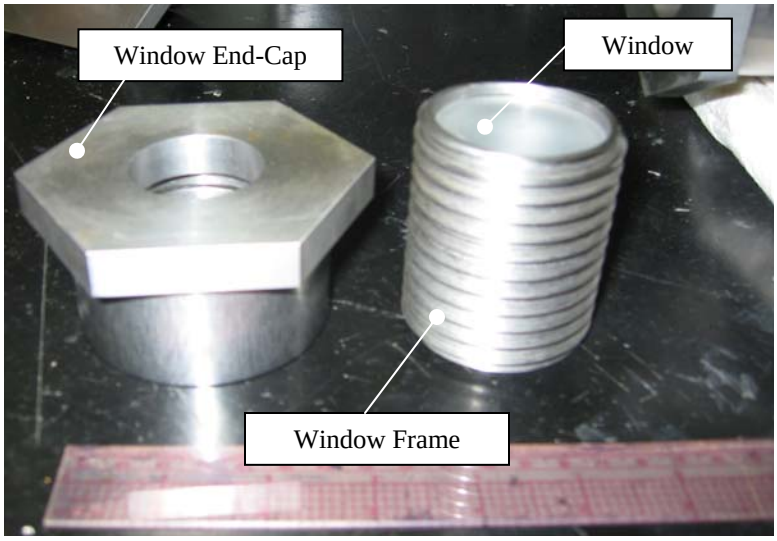

Figure 4: One of the Three Side Window within its Window Frame and a Window End-Cap

After trying several commercial thread sealants, the seal between the window frame and the body was found to be best using ample layers of Teflon tape. Each window (side and back-end) is a 3.175 cm (1.25 in) high, 4.60 cm (1.81 in) diameter polycarbonate (Lexan) cylinder that is press-fitted into the window frame. A greased O-ring and retainer held in a groove machined in the windows provide the seal with the window frame. Optical quality windows for spectroscopic studies can be easily used instead of the Lexan windows. The window end-cap is screwed on the window frame and holds the window within the later.

The strand holder, shown in Figure 5, is a modified McMaster-Carr (92865A524) grade 5, zinc-plated steel hex head, 1 in cap bolt.

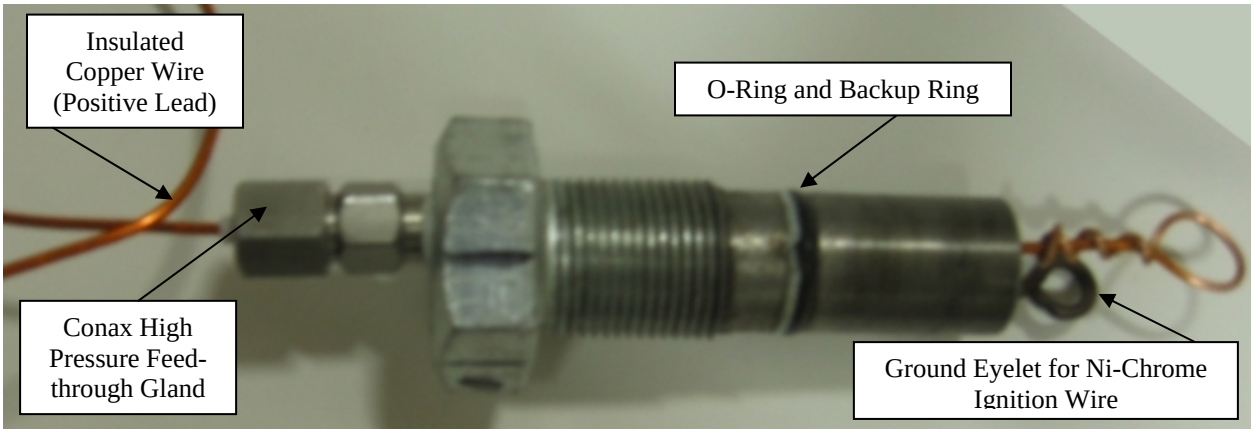

Figure 5: Strand Holder

The modification included machining of part of the thread and the incorporation of a groove to accept a greased O-ring and retainer. The gland for the O-ring was designed following the guidelines presented in the Parker O-ring Handbook. At the tip of the bolt, a 0.635 cm (0.25 in) hole was bored 0.51 cm (0.20 in) deep to hold the strand during tests. On one side of this depression, a hole was tapped to accept a small eyelet (the ground); on the other side, a 0.635 cm (¼-20 UNC) tap and a 0.32 cm (0.125 in) through hole was machined to admit a 14-gage copper wire sealed in a compression seal gland from Conax (PL-14-1) at the other end, which serves as the positive lead. This removable plug design provides easy access for quick turn around between burns. To facilitate the access to the strand holder and because the complete strand burner totals a mass of 41.5 kg (91.5 lb), it is braced horizontally by two, 3.81 cm (1.50 in) thick aluminum stands. When installed on the stands, the top most part of the assembly sits 28.02 cm (11.03 in) above the optical table. Figure 2 presents an overview of the strand burner, as secured within the aluminum strand, centered on the optical table.

The entire surface of the body, from thread to thread, and the inner faces on the end-caps has a 3 mil chrome plating to protect the steel body from chemical attacks from the products of the combustion reaction and from corrosion while the system is not loaded with argon. All the other none-threaded surfaces have been coated with Praxair's FE-101 metal powder (Stainless Steel 316) using a novel technique developed at UCF's Surface Engineering and Nanotech Laboratory: Air Plasma Spray (APS) led by Dr. Sudipta Seal. AISI type 316 stainless steel is an austenitic, low carbon alloy high corrosion resistant steel thanks to its high concentration of chromium and nickel. In addition, the application of this coating by APS created a mostly dense, largely metallic (non-oxidized) coating. The APS thermal spray technique uses large electrical currents to ionize argon and hydrogen gases, to create a 15000 K flame and particle velocities that can reach 300 $m.sec^{-1}$. FE-101 powder is injected directly into the flame, which is melted and blasted towards the substrate fusing with the later. After multiple passes, twenty for this particular application, a suitable thickness is achieved, whereby the coating has no connected porosity between the substrate and the surface. In addition to the protection afforded by a coating, mainly the isolation of the substrate from the corrosive environment, the SS 316 by APS allows a very strong SS 316 due to a fine-grained structure created by APS. This allows it to withstand handling and minor scratches without losing protection. Furthermore, the highly anodic chromium present in the SS 316 neutralizes the galvanic potential of the underlying steel, meaning that a small scratch through the plasma coating will not corrode.

To run the facility, two independent compressed-gas systems are needed: a high-pressure usable gas and a low-pressure working gas (Ref. Figure 6).

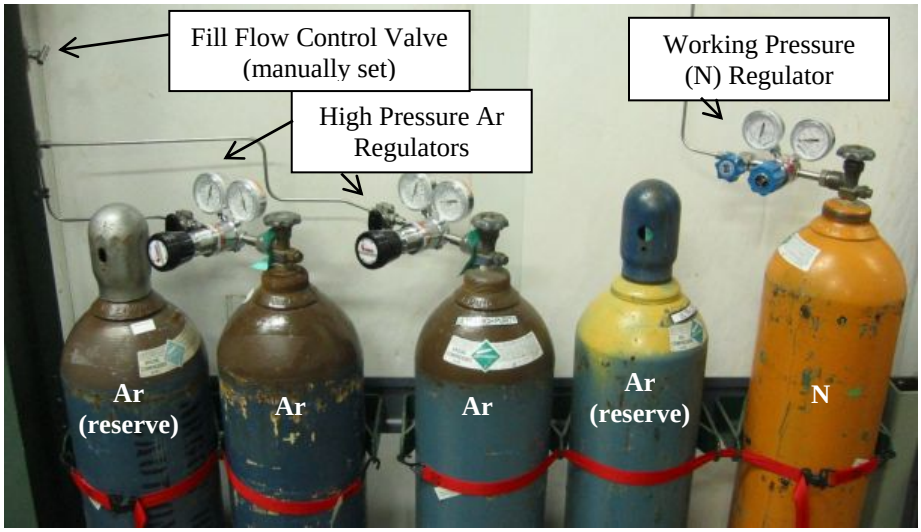

Figure 6: High Pressure Gas Supply

A low-pressure nitrogen circuit is regulated from a single 170 atm (2500 psi) bottle to 5.4 atm (80 psi) to actuate the pneumatic mechanisms of the remotely controlled on/off ball valves.

To duplicate the pressure of the combustion chamber of the rocket motor within which the solid propellant may be burned, the bomb is pressurized with a chemically inert gas. For this purpose, high-pressure argon is supplied by two regulated, 408 atm (6000 psi), 16.14 m^3 (570 ft^3) bottles via 510 atm (7500 psi) rated 0.635 cm (0.25 in) stainless steel tubing (Swagelok SS-T4-S-049). Crawford et al.[11] in their earlier experiments found no significant difference in the burning rate while burning strands in helium, carbon dioxide, nitrogen or argon. Argon was chosen for its price, higher density, and availability. Filling of the strand burner is done remotely by actuating a solenoid-operated, normally closed pneumatic valve; note that two manual quarter turn ON/OFF ball valves are located after each 408 atm (6000 psi) Matheson regulator (3066-1/4) to provide manual override. The filling rate is manually preset with a needle valve. Venting of the

high-pressure inert gas and the products of the combustion outside the laboratory is also operated remotely by actuating another solenoid-operated, normally closed pneumatic valve. For security, venting of the system may be done manually by opening another quarter turn ON / OFF ball valve on the exhaust override line (Ref.

Figure 7). Another needle valve controls the exhaust flow rate to prevent icing of the plumbing or even shock formation during venting.

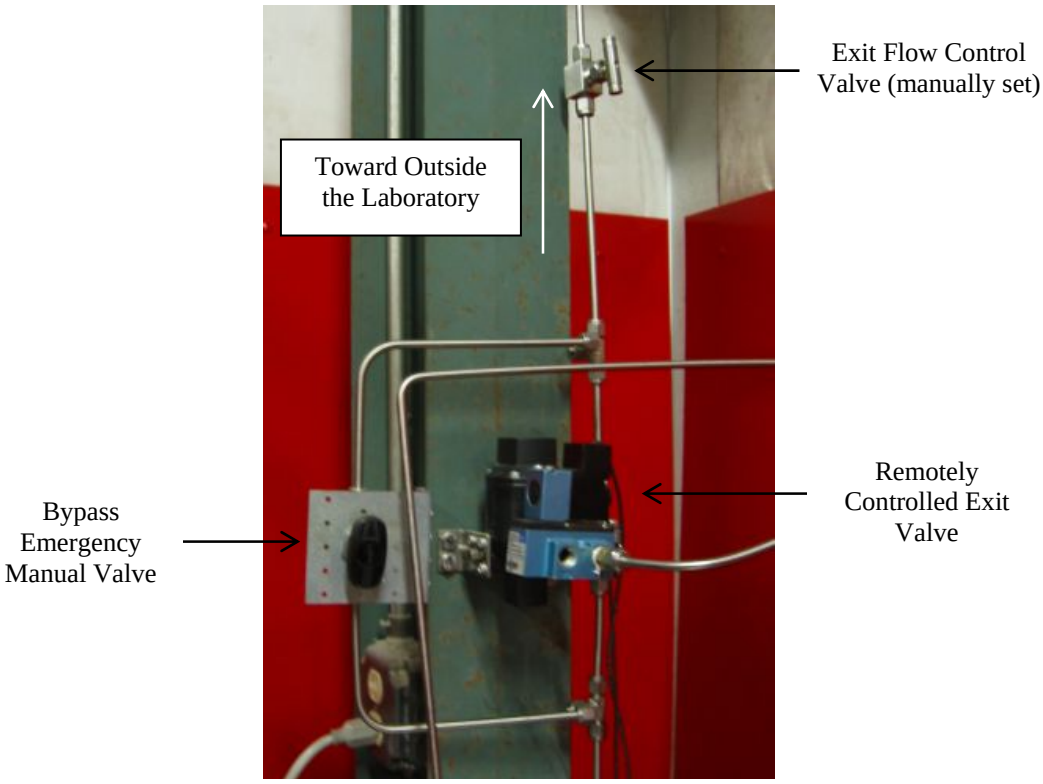

Figure 7: Venting Line Valves

The two pressure transducers are located between the two manual ball valves that isolate either strand burner from the high pressure network. Before burning a batch of propellant, one of the two strand burner is selected by opening one of the two ball valves.

Figure 8 shows the location of the strand burner selector valves, right behind each bomb pressure ports.

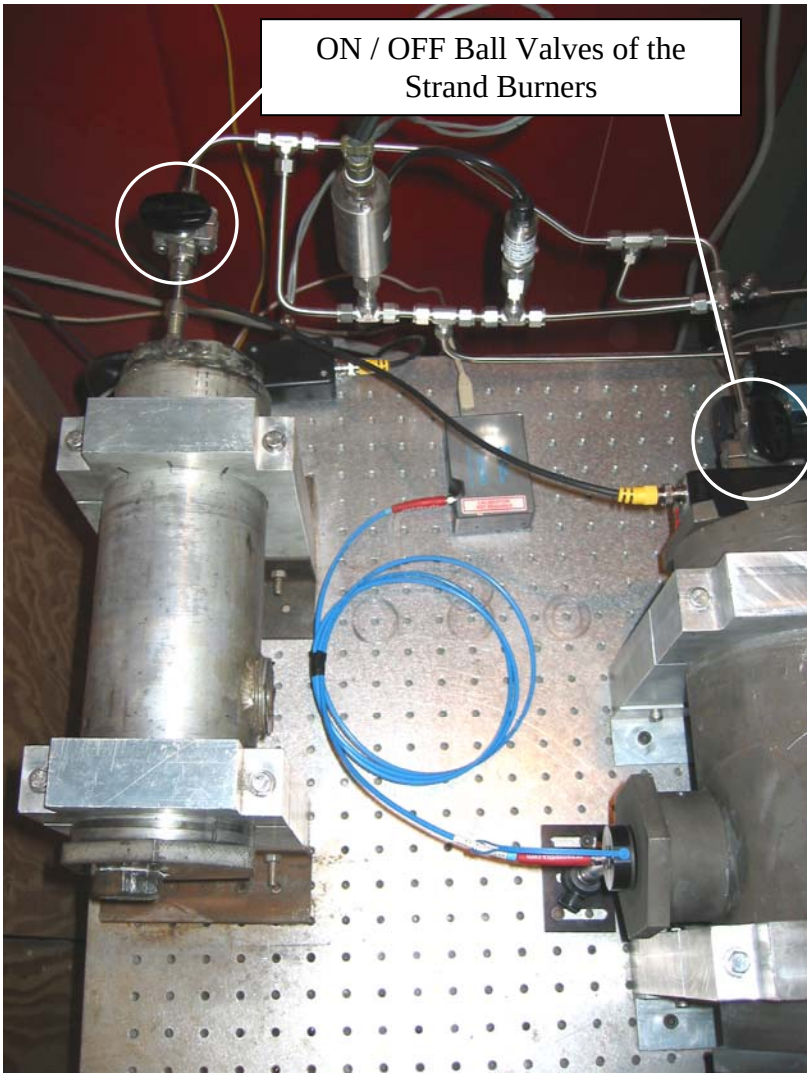

Figure 8: Manual Selection of the Strand Burner

3.2 Procedure

A detailed procedure was established for preparing and burning the propellant samples. This procedure was refined during the course of the setup and early investigations to improve the quality of the data collection and to establish a quicker turn around between samples while increasing the safety of the operations. The length of the strand was chosen to be around 2.54 cm (1 in) for several reasons.

- The first reason was to keep the pressure and temperature increase to a minimum since the vessel pressure and grain temperature directly affect the burning rate. Depending on the mixture, the combustion of a 1-in strand increases the pressure inside the bomb from 5 to 20%. This pressure variation was demonstrated in subsequent experiments to have a minor influence on the burning rate of the tested sample. Howbeit the internal volume of the new strand burner was increased by 13% to further reduce the pressure variation during combustion without altering its distinct onsets and ends. Moreover, each burning time is related to the pressure average between the ignition pressure and the pressure at extinction.

- Secondly, the 1-in strand minimizes the re-circulating flow field generated by the inhibited, end-burning strand in a closed vessel as described and modeled by Glick and Haun.[12]

- Depending on the composition of the strand, burning a longer strand may generate enough smoke to hinder the proper acquisition of the light emitted by the burning surfaces.

- Finally, the strand size selected reduces the material cost, handling and storage of hazardous material, and data storage of each experiment while maintaining adequate resolution and signal-to-noise ratio of the data acquisition.

The following picture (Figure 9) illustrate Al / AP / HTPB strands as extruded in Teflon tubing (bottom right) and once the tubing removed (top left). Each strand is weighed and measured prior to burning. Because the strand burns in a cigarette fashion –thanks to the liquid HTPB coating on the sides for inhibiting the burning at these surfaces– the length of the strand is of prime importance to determine the burning rate of the specimen, while its shape is insignificant. In the present facility, the casting method, which consists of punching out the mixed batch with a ¼ in outer diameter clear Teflon tubing, dictates the strand's cylindrical shape.

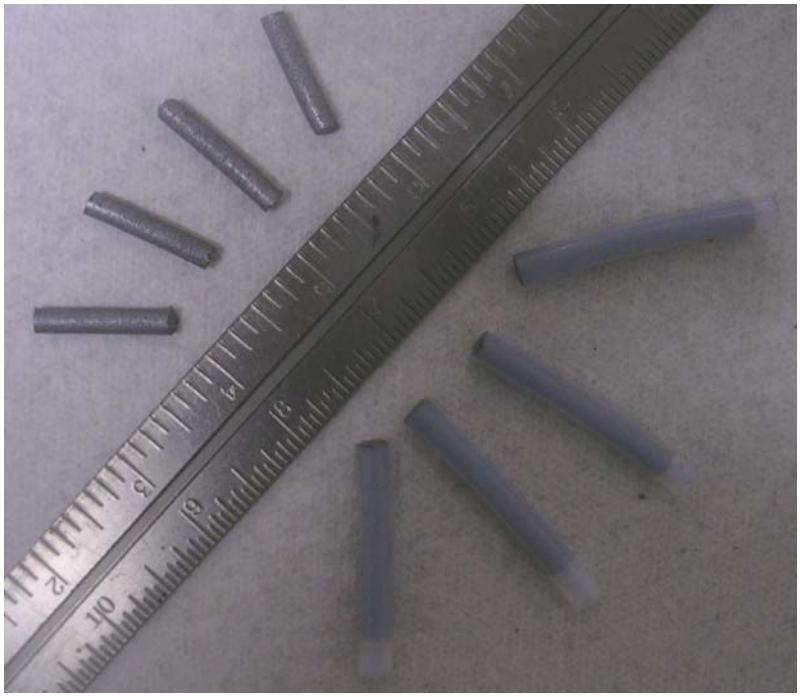

Figure 9: Al / AP / HTPB Strands In and Out of the Teflon Tubing

Each strand is weighed and measured prior to burning. Because the strand burns in a cigarette fashion –thanks to the liquid HTPB coating on the sides for inhibiting the burning at these surfaces– the length of the strand is of prime importance to determine the burning

rate of the specimen, while its shape is insignificant. In the present facility, the casting method, which consists of punching out the mixed batch with a ¼ in outer diameter clear Teflon tubing, dictates the strand's cylindrical shape.

The coated strand is placed on the strand holder which in turn is screwed onto the strand burner. The operator then clears the burning area confined within blasting walls and the rest of the operations, including pressurizing the vessel to the desired pressure, ignition, data acquisition and venting of the tank is conducted remotely on the control board located by the DAS.

The energy necessary to ignite a strand is collected from a spark generated by passing high current in a very high-resistance Ni-chrome wire taut between the two eyelets of the strand holder across the tip of the strand, as shown in Figure 10.

Figure 10: An AP / HTPB Ready to be Loaded Into the Strand Burner

An off-the-shelf 180-amp motorcycle battery provides the high current. The circuit is closed remotely by pushing a button on the command board; this signal triggers a relay installed in series between the battery and the strand holder. Under high pressure, the energy generated by this spark is sufficient to ignite the propellant; the combustion of the strand is then self-sustained. The ignition is normally done without the addition of any explosive that might influence the overall burning rate of the sample under test. The experiment procedure is described in detail in Appendix A.

3.3 Diagnostics

All four available ports of the strain burner have been optimized for monitoring and recording the burning of the strands. Figure 11 provides a layout of the main diagnostics relative to the strand burner.

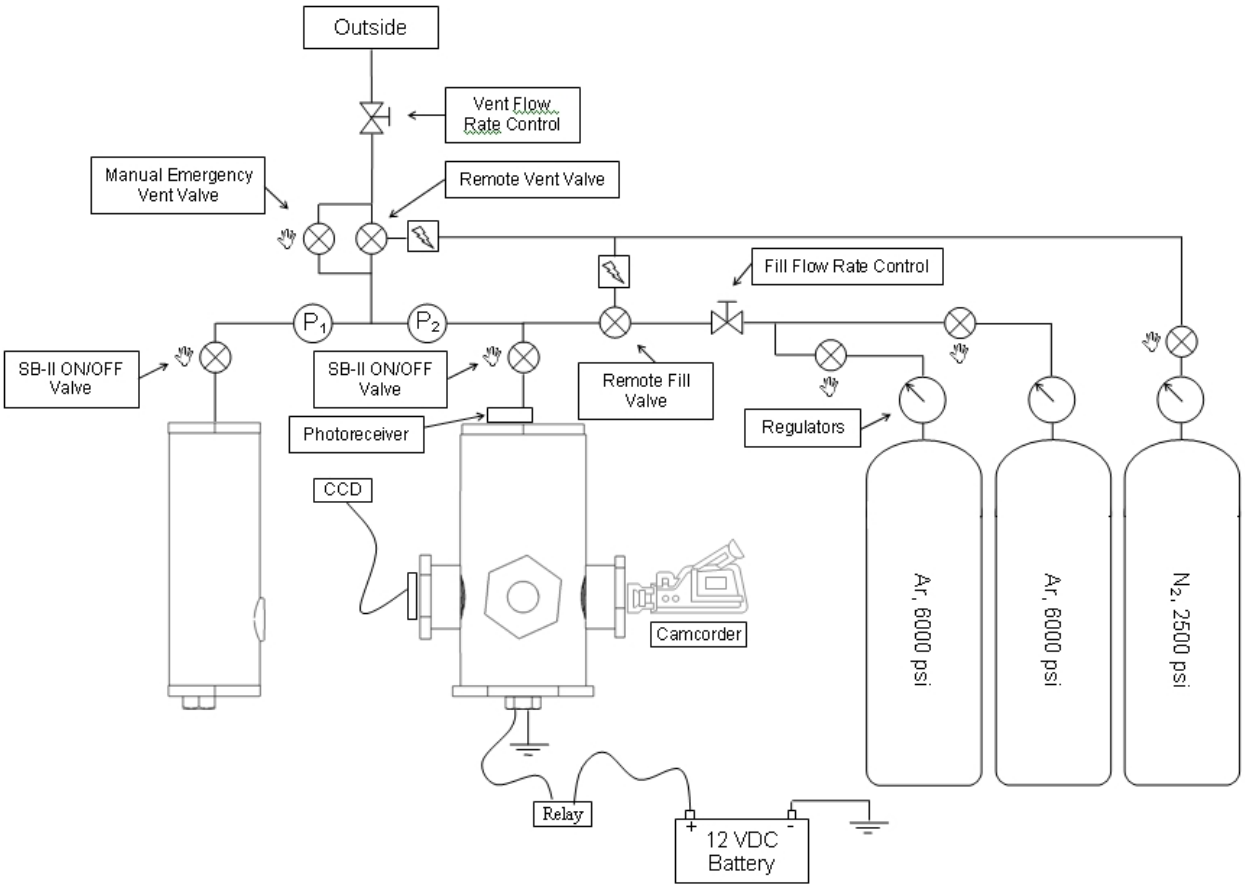

Figure 11: Burner Facility Schematic Illustration

The primary means of measuring and characterizing the burning rate of a selected batch is by measuring the transient pressure increase during the firing. A high accuracy, high response pressure transducer from Omega (PX313-5KG5V) is mounted at the end of the common high-pressure line feeding the strand burners (Figure 12).

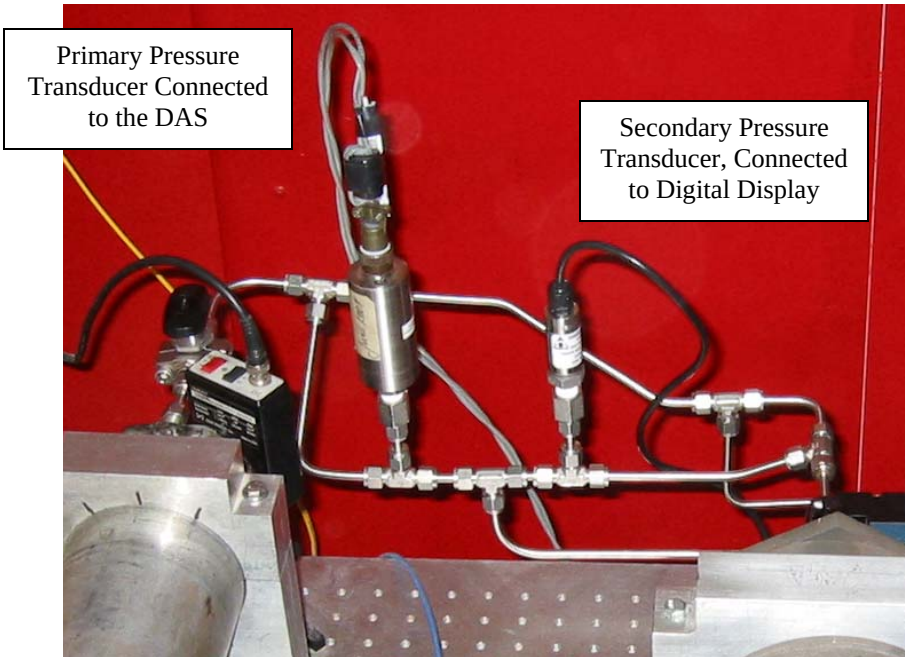

Figure 12: Dual Pressure Transducer Arrangement

The response time of this transducer is approximately 1 msec and offers an accuracy of 0.25% FS (linearity, hysteresis, repeatability) throughout its operating pressure range, 0-345 atm (0-5000 psi). To eliminate ground loops and other disturbances or noise within the output signal, the pressure transducer has a dedicated 12 VDC power supply (Mastech HY3003D). The signal is visualized, acquired, conditioned and logged on a computer-based Data Acquisition System (DAS) via a dual-channel waveform digitizer PCI bus-based card and its corresponding software from Gage Applied Technologies (CompuScope 1540 & GageScope). The oscilloscope board can sample analog signals at speeds up to 50 MS/sec with 14-bit resolution. These performances are possible thanks to the onboard memory. After sampling, logs of data are saved onto the computer for post processing. Another high accuracy Omega pressure transducer (PX02C1-75KG5T), connected to a digital meter from Omega (DP25B-E), displays the pressure inside the vessel in 'real time'

on the command board. This display is used to monitor the pressure inside the vessel during filling and to verify venting is complete after an experiment and prior to removing the strand holder, or any other component of the strand holder or plumbing hardware.

The second channel of the DAS is dedicated to the output signal of the high-speed, 8-mm, Si/PIN large area photoreceiver from New Focus (2031). The back window offers an end view of the strand, ideal for this device, as shown in Figure 13.

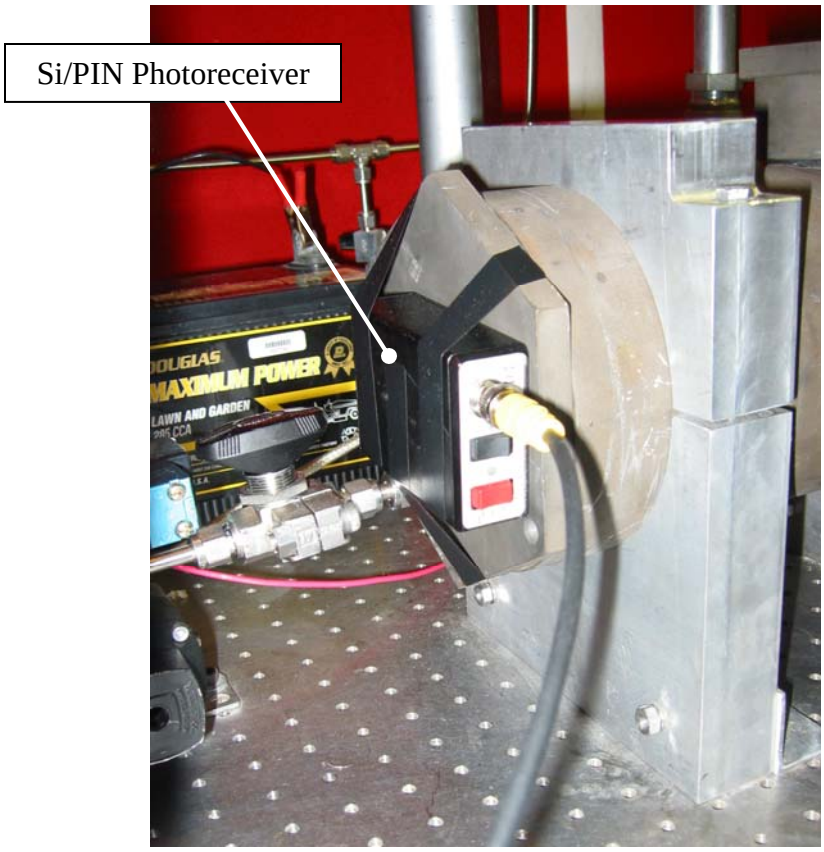

Figure 13: The Photoreceiver as Installed on the Aft End-Cap

Thanks to the large visible wavelength range observed by the silicon-based photoreceiver (400 to 1070 nm), the unfiltered light emitted during a test is fully captured, offering clear beginnings and ends of the burns.

Also available during each test is a 1-Megapixel digital video camera (Sony DCR-TRV38) mounted on an optical pod such that the lens of the camera is in the plan of the side window (Ref. Figure 14).

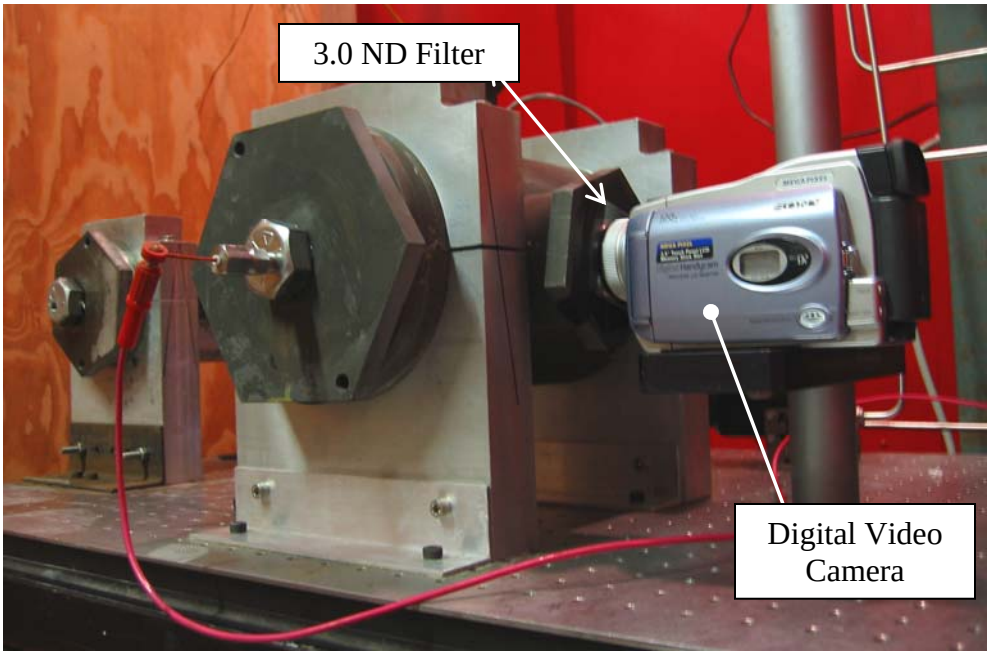

Figure 14: Setup for Digital Video Recording of the Tests

Due to the proximity of the camera lens and the excessive brightness of the flame, the light is dimmed using a 3.0 optical density ND filter. The live experiment is broadcast onto the computer/DAS via a FireWire (IEE 1394), and a qualitative record of each burn is recorded. Note that the footages could also be used to determine the burning rate, but because of the high burning rate of the test samples and the lower accuracy offered by this method when compared to the pressure and emission methods, the videos are only used to verify the quality of the burn. In many cases, the video recordings are used to verify inconsistency in the burns detected by abnormal pressure transients and light traces due to explosions.

Figure 15 illustrates the latest improvement of the diagnostic instrumentation: the design and implementation of an emission spectroscopy diagnostic system from Ocean Optics.[26] The light emitted by the combustion flame is conveyed by a fiber optic held to one of the side window of the strand burner to a Charge Coupled Device (CCD). The CCD diffracts and expands the incoming light to accurately convert it into voltage of different intensity for that specific wavelength.

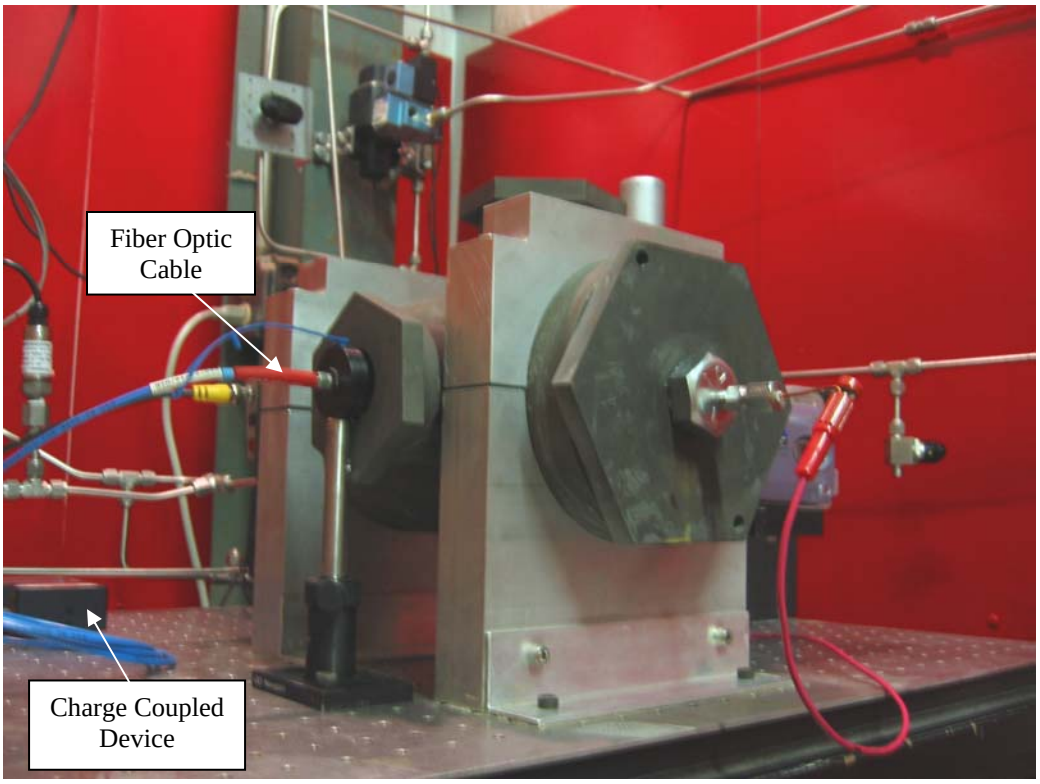

Figure 15: Fiber Optic Installation for Emission Spectroscopy

The output signal is sent to a dedicated DAS via a USB cable; the same cable that powers the spectrometer. The data acquisition is controlled by the SpectraSuite software that offers a graphical user interface to set the spectrometer parameters. Emission spectroscopy is useful to solid propellant research in that the diagnostic can assist in the determination of

the flame temperature and the identification of the species reacting within the combustion zone.

Because A. I. Atwood et al.[32, 33] proved that initial grain temperature significantly influences the propellant burning rate, the room temperature around the strand burner is recorded from a calibrated Omega thermocouple for each burn. This is to attest that each run (approximately ten) of a batch is tested within 5° F of each other, and each batch has been tested within 5° F of each other ruling out the initial grain temperature as a variable influencing the performance of a batch when compared to others.

3.4 Data Analysis and Interpretation

When the propellant sample burns within the pressurized bomb, the phase transition of the solid reactants into liquid at the burning surface then to gas as a result of the combustion create an increase in pressure. This pressure increase varies from batch to batch and lies within 15 to 20 % of the ignition pressure for low pressure testing (~600 psi) and 5 to 8 % for high pressure testing (~2000 psi). Although ideally the samples should be burned in a constant pressure environment, this slight increase in pressure was proven to be of little influence during the characterization testing of SB-I. Also each burning time is related to the pressure average between the ignition pressure and the pressure at extinction. The high response instrumentation in place manages to record this slight increase that spans over time lapses in the order of a second or two –depending on the test pressure and grain potency– with great accuracy. Not only it clearly highlights the beginning and ending of the combustion process, but also records any anomalies or combustion instabilities that

may have occurred during the burn testing offering a quantitative and a qualitative view of the grain combustion.

Once manually triggered, both GageScope and SpectraSuite are set to record 10 sec of data. Experience has shown that 10 sec is plenty for the operator to comfortably trigger SpectraSuite, trigger GageScope, then ignite the propellant. Before saving the data, the researcher must verify the three phases of the burn have been captured (initial pressure, burn, cool off). If not, the test is void and another strand is prepared and burnt at the same pressure. One batch of propellant is usually characterized by 10 discrete burns from 500 to 2000 psi (approximately every 160 psi). During the 10 sec acquisition, GageScope collects 10,000 voltage values between 0 and 5 V from the pressure transducer and 10,000 voltage values between 0 and 5 V from the photoreceiver. These values are logged on two different CSV files where the first column represents the time stamp in second and the second column the voltage output from the transducers. The files are then processed through a Matlab script (ref Appendix G). The code combines the two files into one and converts the voltage output (V) from the pressure transducer into pressure (psi) using a linear law derived from the instrument calibration data (ref Appendix F). The file is then reduced from 10,000 lines to about 5,600 by the SMOOTH.M Matlab function. This function ‘cleans’ the data by deleting outliers and reducing signal noise using a running mean over 2 x N +1 successive points. (N points on each side of the current point, here N = 37). The code then saves the data, ready to be plotted using Microsoft Excel. From Microsoft Excel, the researchers can easily reduce the data file even further to center the plot on the burning phase.

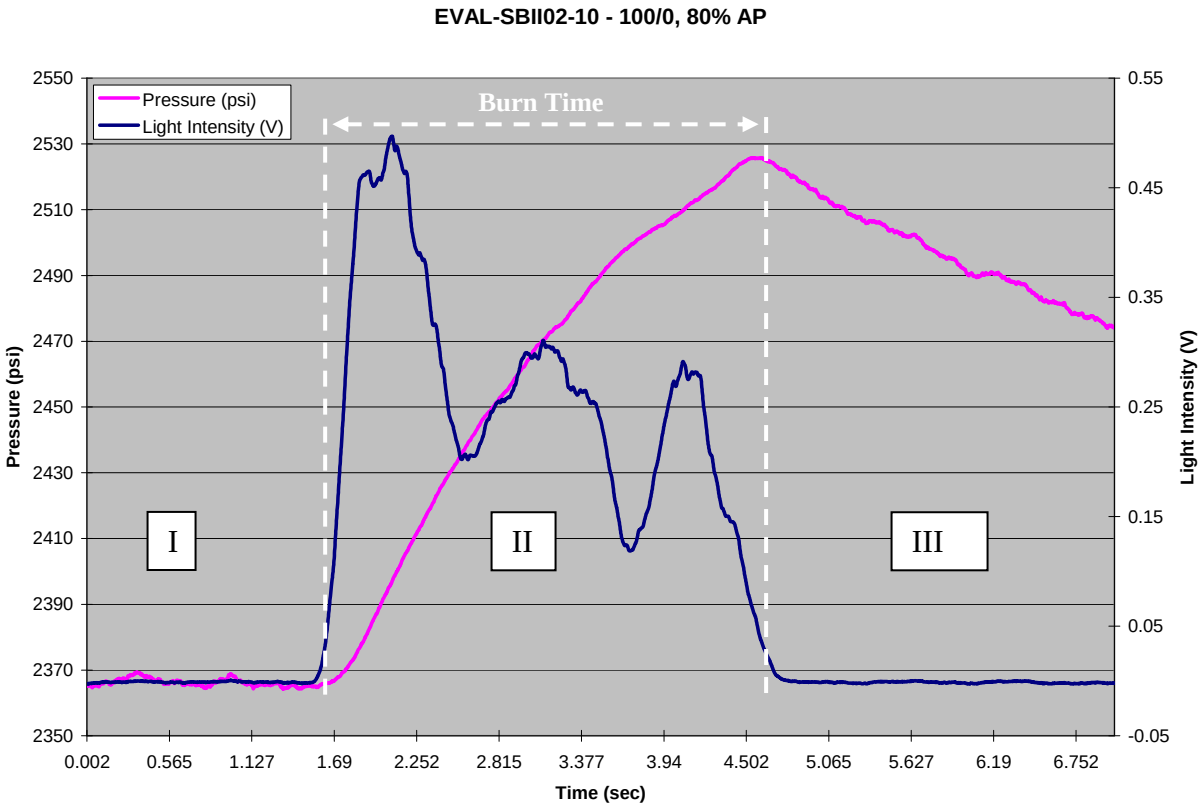

Figure 16: Pressure and Light Intensity Recorded during the SB-II Characterization Exercise

Figure 16 presents a typical pressure signal showing the pressure level before recorded during a burn test from a composite AP / HTPB propellant mixture. The signal can be divided into three distinct phases separated by two pivotal points. The first part of the recording displays the initial pressure within the strand burner. Upon the ignition the pressure starts rising; this is the first inflexion point. This point pressure and time is recorded as 'ignition time' and 'ignition pressure'. As shown, the pressure rises steadily as the flame progresses along the strand and produces gaseous products at a constant rate. When the flame as consumed all of the propellant, the gaseous generation, the gas dynamics and thermodynamic phenomena stop and so does the pressure increase; this is the

second inflexion point. This point pressure and time is recorded as ‘extinction time’ and ‘extinction pressure’. The pressure inside the bomb then decreases slowly until an equilibrium pressure level is attained. The equilibrium pressure level corresponds to the initial pressure of argon gas set by the operator plus the additional gases from the combustion products and a slight increase from the heat generated during the combustion process. It could also be due to condensation of the particulate matter upon cooling. The burn time is clearly illustrated, and the quality of the data seen in Figure 16 is representative of most burns.

The signal recorded from the photoreceiver, the light emission, is recorded by the same software (GageScope) as the pressure signal. The acquisition for both signals falls under the same trigger, this allow the researcher to plot both recordings on the same time axis and use the light emission trace to corroborate the onset and completion of the burning as inferred from the pressure trace. Figure 16 shows that the light increases immediately upon initiation of the burn and ends when the burning has finished. In many cases, the light intensity decreases with time due to the formation of dense and obstructing gases and solid particulates within the tank. The burning rate inferred from the emission signal in most cases is within a 2% of the rate inferred from the pressure signal. In certain cases where there is a problem with the pressure signal transmission, the burning rate can be taken from the light signal with confidence. A closer look at the light and pressure signals recorded during the burn testing for the characterization of SB-II is posted in Section 3.5.

In addition to the quantitative burning rate data, qualitative information can also be obtained from comparing the light and the pressure signals. For some propellant samples,

more so for earlier runs when propellant mixing, casting, curing and burning were still in the development and experimental stages, explosion-like events that violently destroy the sample and invalidate the burning rate measurement were witnessed. When such an explosion event occurs, there is quite often a sharp increase in the pressure rise, but an increase in pressure alone does not conclusively differentiate between a violent explosion of the sample or just an increase in burning rate due to a pressure or an inhomogeneous grain effect. However, the corresponding yet more dramatic increase in the light emission provides a more definitive indication of explosion. A typical case when 'explosion' (excessively high burning rate, or a noticeable burning rate increase) was thought to occur is presented in Figure 17.

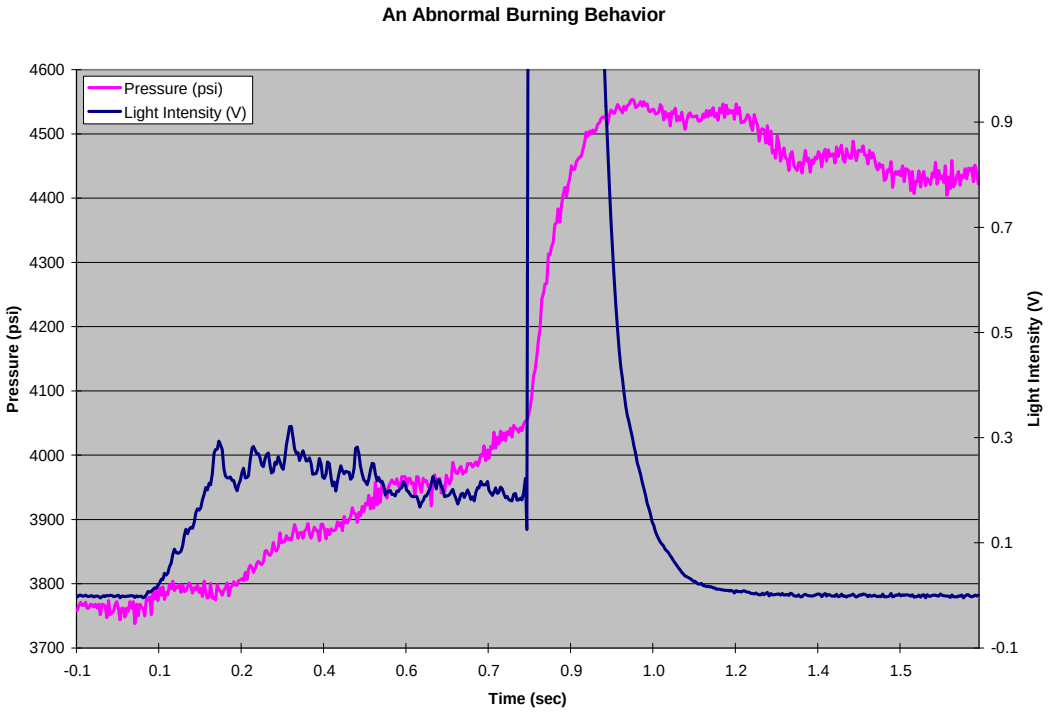

Figure 17: Characteristics of an Abnormal Burning Behaviors

As seen, the light emission very distinctly rises when the explosion event takes place. In many cases, the light emission saturates the detector and/or the data acquisition system by creating an electrical signal greater than 5 V. The digital video data supported these conclusions and aided in diagnosing burning rate problems in earlier measurements such as flame propagation through the strand via voids and cracks, or breaking of the strand during a burn. Videos of the burns were also used to verify the flame surface propagation onto the side of the strand and the effectiveness of the liquid HTPB as inhibitor to restrict the combustion surface to the tip of the strand.

From an array of burning rates measured at different pressures, one can calculate the coefficients a and n of the law of dependence of the burning rate of combustion with pressure established by Vieille at the end of the 19th century:

$$r = a\,P^{\,n} \tag{1}$$

A study on tailoring the behavior of novel rocket propellant is currently underway in the UCF Rocket Propellant Research Facility. The intent of this research is to narrow down the composition of a propellant that becomes impervious to pressure changes (n = 0) at a particular pressure range. Such propellant burning rates are said to “plateau” at that pressure range. High values of the combustion index (n) give rapid changes of burning rate with pressure and are undesirable as they usually lead to structural failure of the rocket motor. Once the coefficients of Vieille’s law are determined, the burning rate of the studied mixture is fully defined. Remember that at any instant the burning rate governs the mass flow rate of hot gas generated and flowing from the motor to the nozzle and therefore the

thrust and the specific impulse of the rocket. Burning rates determined from the strand burner technique provide a means to assess the relative effects that additives, propellant combinations, and manufacturing techniques amongst different propellant mixtures.

3.5 Characterization Tests

To investigate the performance of the new strand burner, a fully characterized propellant was burnt. This propellant was chosen for the simplicity in its formulation, its good handling during the mixing, the extrusion and the curing operations; ruling out any variables from these steps that may influence the outcome of the exercise. The mixture belongs to the smokeless composite category having a monomodal composition of 200 μm particle size ammonium perchlorate at a total weight percentage of 80.0% and HTPB fuel / binder at 18%. The last 2% of the propellant was composed of Tepanol (cross-linking bonding agent) and IPDI (curing agent). Refer to Table 2 for precise batch composition:

Batch	Date of Fab	HTPB %	AP %	IPDI %	Tepanol %	Additive %
EVAL-SBI01	01/26/06	18.001	79.708	2.059	0.232	0.000
EVAL-SBI02	01/27/06	18.067	80.000	1.733	0.200	0.000
EVAL-SBI03	06/23/06	18.075	80.000	1.725	0.200	0.000
EVAL-SBI04	08/17/06	18.050	80.000	1.750	0.200	0.000
EVAL-SBII01	10/09/07	18.050	80.000	1.750	0.200	0.000
EVAL-SBII02	10/11/07	18.041	79.960	1.799	0.200	0.000

Table 2: Mixing Ratios of the Characterization Propellants

All batches were prepared, mixed, extruded and cured at the UCF Rocket Propellant Mixing Facility in accordance with the methodology developed by Matthew Stephens et al.[25]

Reproducibility and repeatability in the measurement of burning rates was verified by burning two different batches mixed with the same ingredients, in the same proportions, EVAL-SBII01 and EVAL-SBII02. A total of 20 samples from these two independent batches were burned in the new strand burner (SB-II), covering a range of average pressures from 658 to 2447 psi. The detail of the information recorded during the EVAL-SBII-01 characterization test runs, pressure rise (psi) and light intensity (V), is as shown in Figure 18:

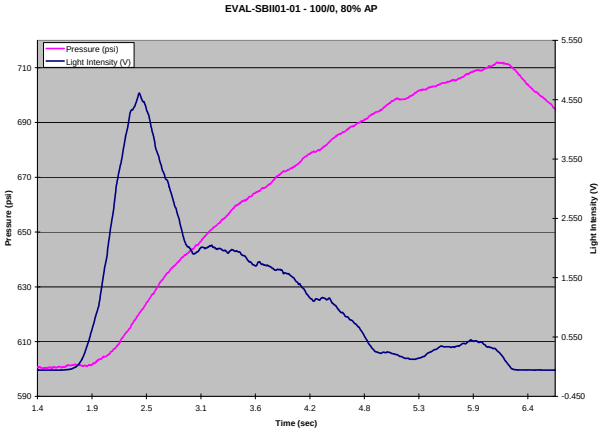

Figure 18.a: EVAL-SBII01-01 Test Runs

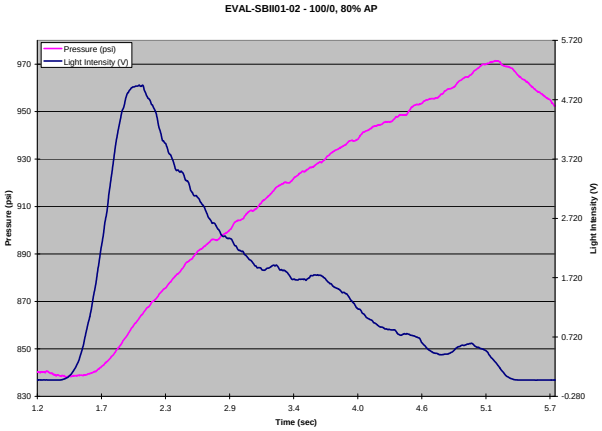

Figure 18.b: EVAL-SBII01-02 Test Runs

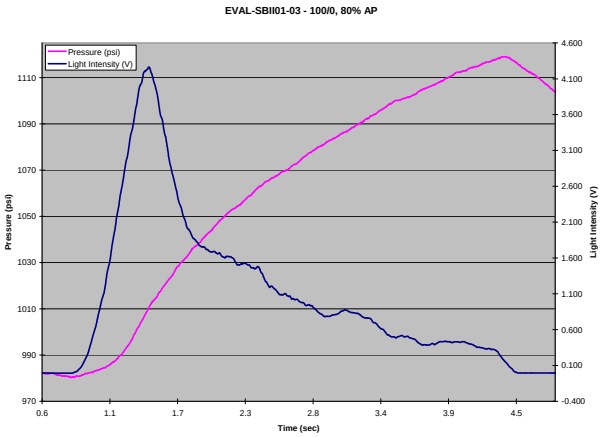

Figure 18.c: EVAL-SBII01-03 Test Runs

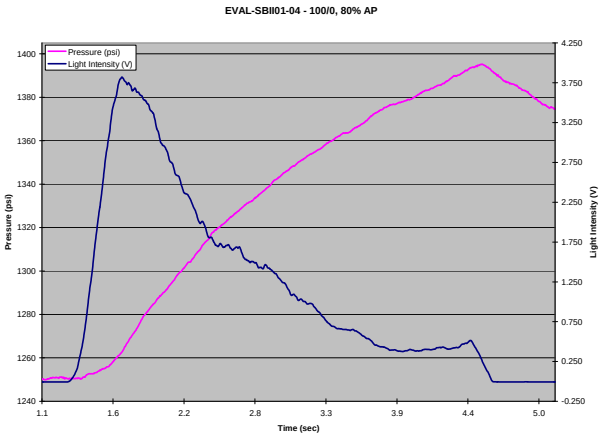

Figure 18.d: EVAL-SBII01-04 Test Runs

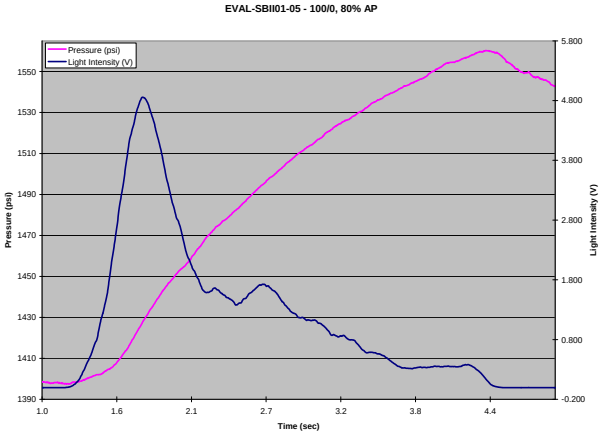

Figure 18.e: EVAL-SBII01-05 Test Runs

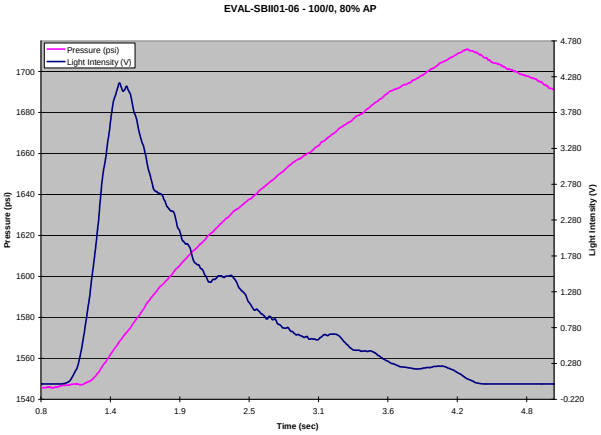

Figure 18.f: EVAL-SBII01-06 Test Runs

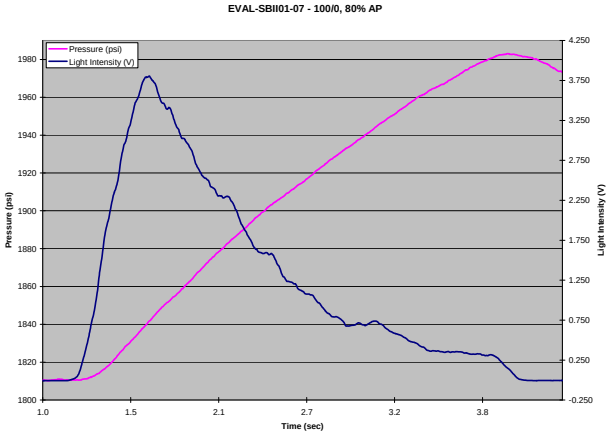

Figure 18.g: EVAL-SBII01-07 Test Runs

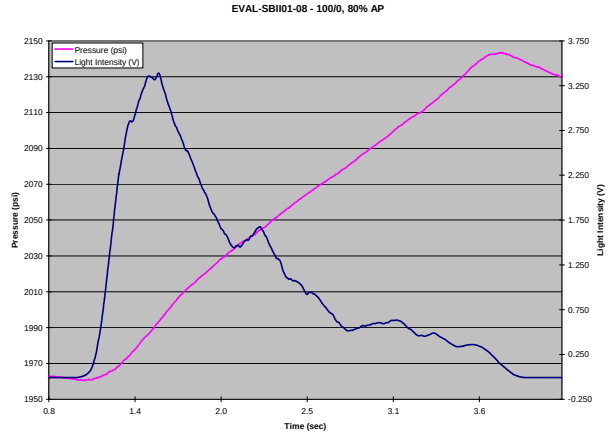

Figure 18.h: EVAL-SBII01-08 Test Runs

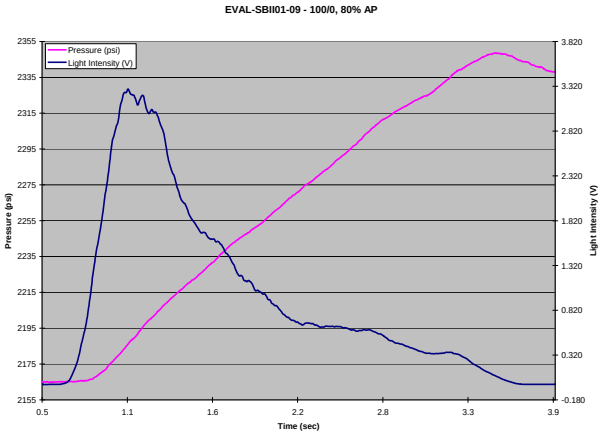

Figure 18.i: EVAL-SBII01-09 Test Runs

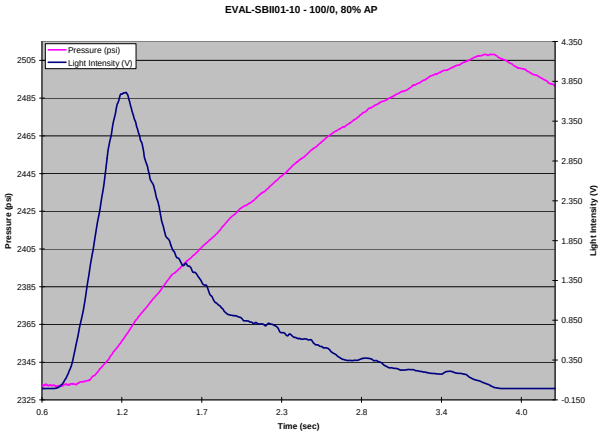

Figure 18.j: EVAL-SBII01-10 Test Runs

Figure 18: EVAL-SBII01 Characterization Test Runs (10)

The ignition and extinction times and corresponding pressure values were recorded as described in Section 3.4. Table 1 summarizes EVAL-SBII01 individual run data.

Table 3: EVAL-SBII01 Ignition and Extinction Time and Pressure Measurements

Batch - Sample	Ignition Pressure	Burn Out Pressure	Avg. Test Pressure	Pressure Increase	Strand Length	Ignition Start	Burnout Time	Burning Rate	Ambient Temp.
	(psi)	(psi)	(psi)	%	(in)	(sec)	(sec)	($in.sec^{-1}$)	(°F)
SBII01-01	605	712	658	18	1.0690	2.070	6.120	0.264	80.2
SBII01-02	840	971	906	16	1.0555	1.681	5.209	0.299	79.7
SBII01-03	985	1119	1052	14	1.0530	1.105	4.418	0.318	80.4
SBII01-04	1254	1395	1324	11	1.0380	1.510	4.571	0.339	80.1
SBII01-05	1402	1560	1481	11	1.0585	1.390	4.360	0.356	80.9
SBII01-06	1549	1711	1630	10	1.0490	1.240	4.270	0.346	80.1
SBII01-07	1812	1983	1897	9	1.0440	1.264	3.989	0.383	80.2
SBII01-08	1961	2143	2052	9	1.0595	1.093	3.788	0.393	80.0
SBII01-09	2167	2349	2258	8	1.0510	0.832	3.505	0.393	80.3
SBII01-10	2337	2508	2422	7	1.0480	0.943	3.710	0.379	80.2

By plotting the burning rate as a function of the average test pressure on a log-log coordinate system, and run a power type curve-fit regression function over the data, one obtain the paramount coefficient A and n of the Vieille's law, and the R^2 parameter to validate the predicting curve. As shown on Figure 19, the burning rate equation for EVAL-SBII01 is $r = 0.039\ P^{0.300}$, and the $R^2 = 0.95$.

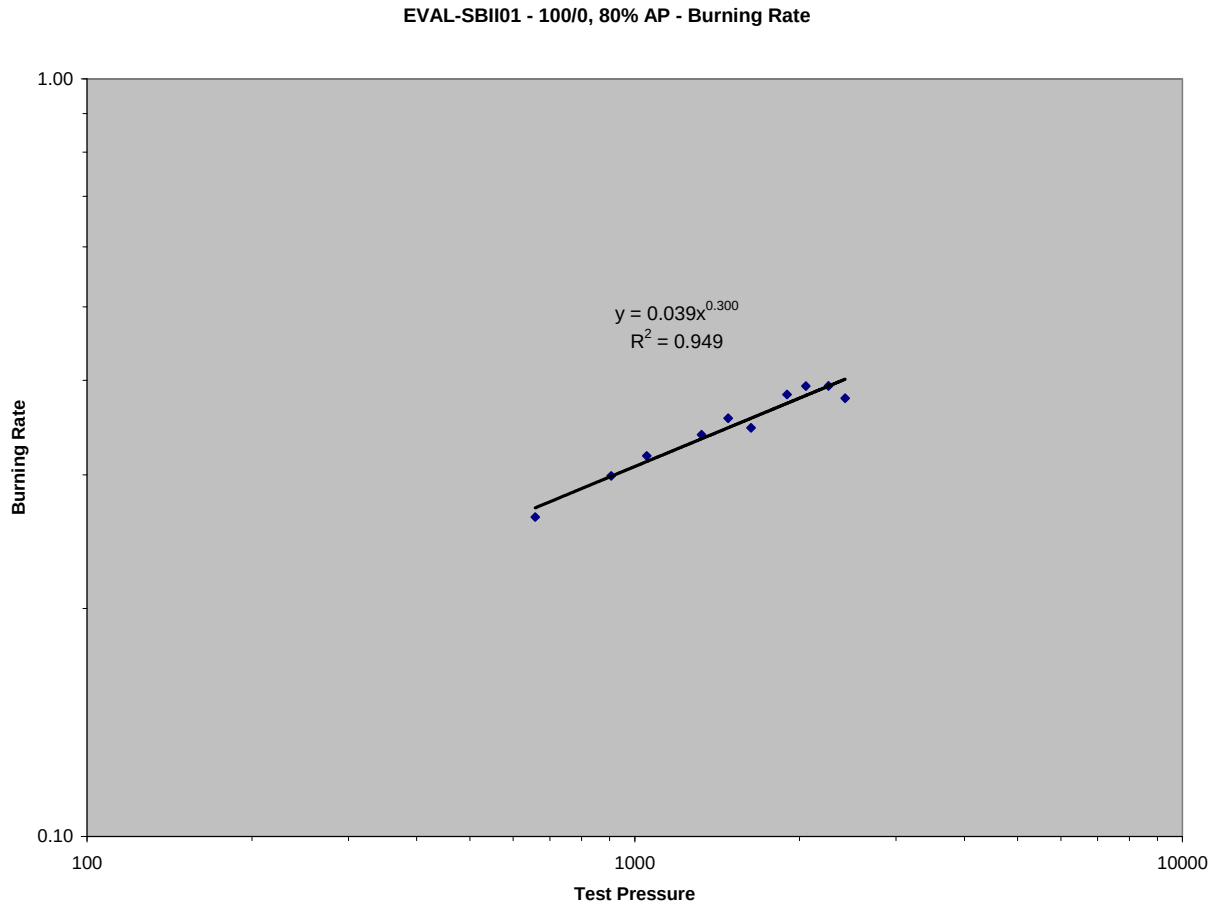

Figure 19: Burning Equation of EVAL-SBII01

Another batch of the same composition was mixed independently then burnt in the new strand burner. Figure 21 shows the recordings of the burn tests of EVAL-SBII02.

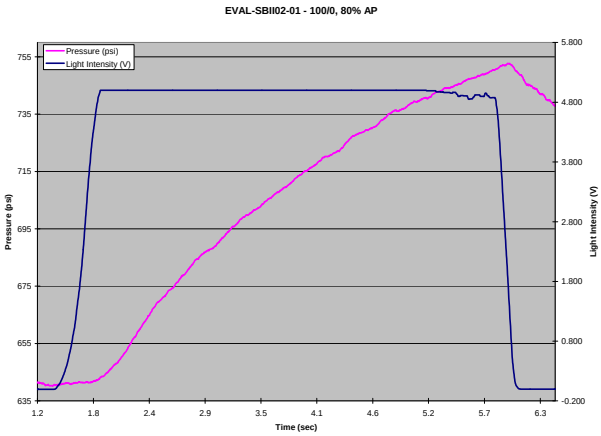

Figure 20.a: EVAL-SBII02-01 Test Runs

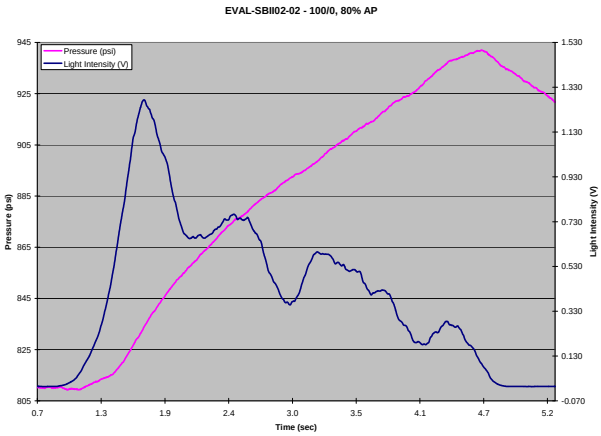

Figure 20.b: EVAL-SBII02-02 Test Runs

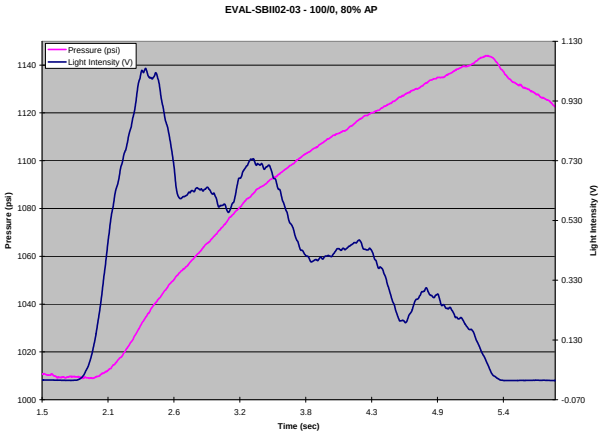

Figure 20.c: EVAL-SBII02-03 Test Runs

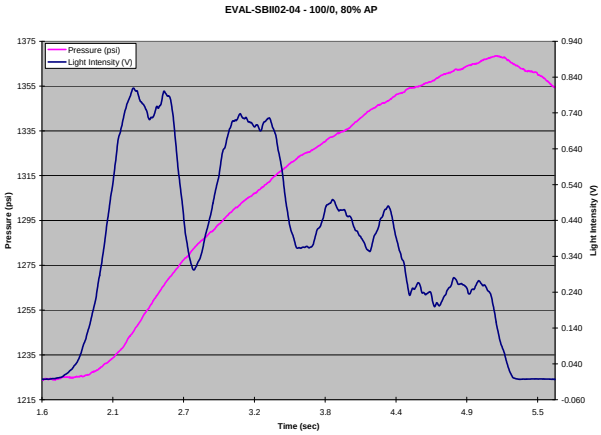

Figure 20.d: EVAL-SBII02-04 Test Runs

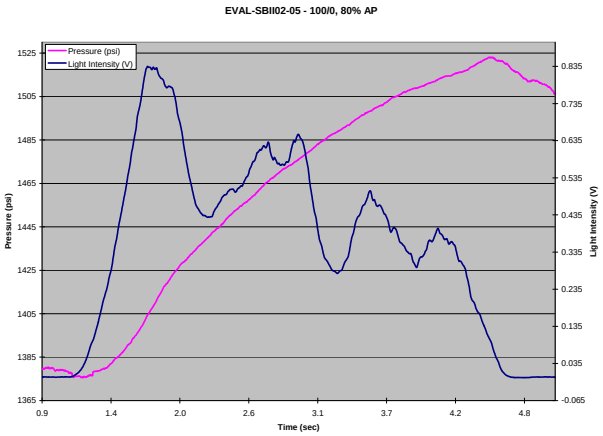

Figure 20.e: EVAL-SBII02-05 Test Runs

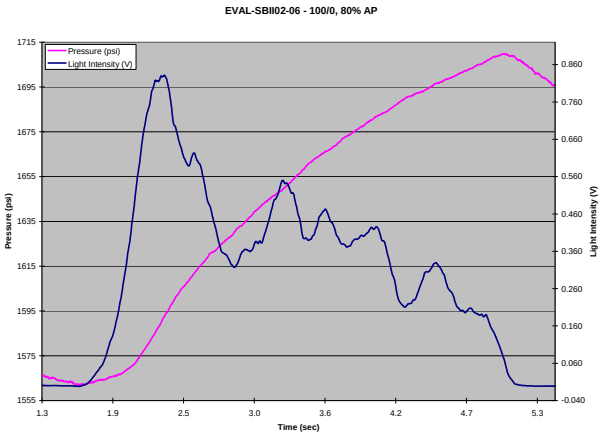

Figure 20.f: EVAL-SBII02-06 Test Runs

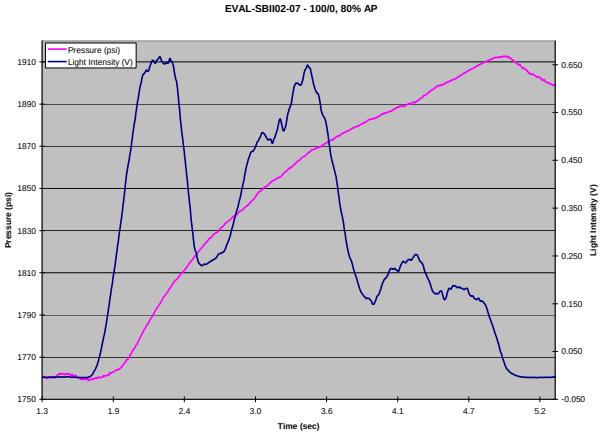

Figure 20.g: EVAL-SBII02-07 Test Runs

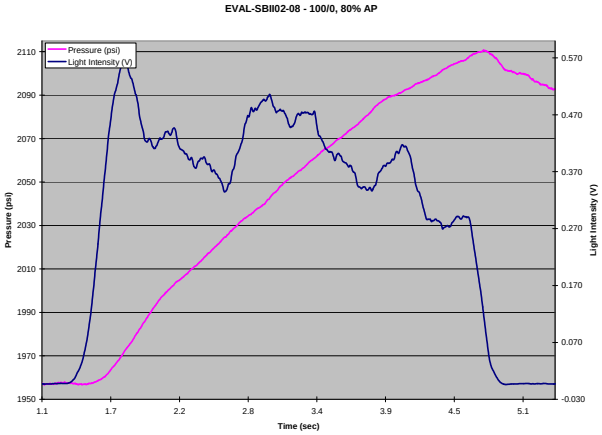

Figure 20.h: EVAL-SBII02-08 Test Runs

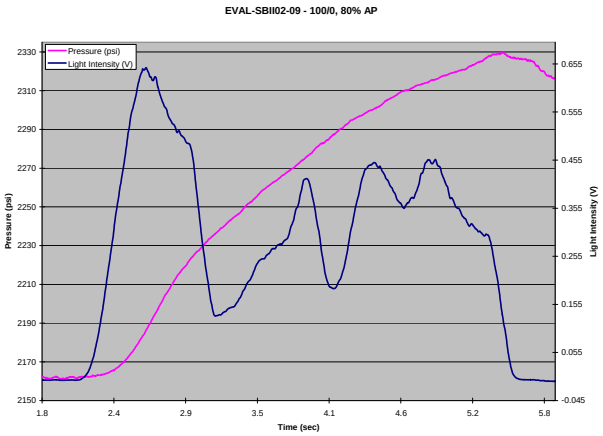

Figure 20.i: EVAL-SBII02-09 Test Runs

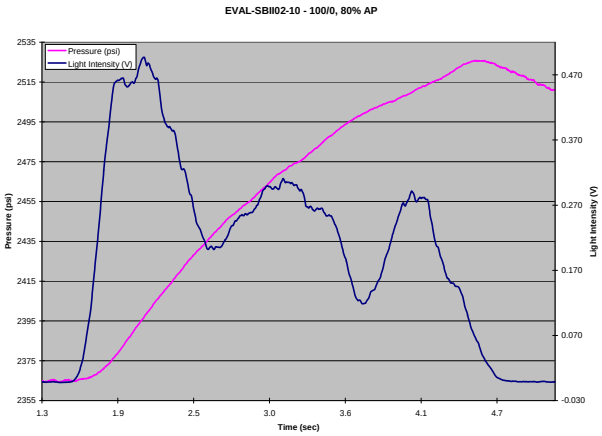

Figure 20.j: EVAL-SBII02-10 Test Runs

Figure 20: EVAL-SBII02 Characterization Test Runs (10)

From these graphs, one can extract the ignition and extinction times and corresponding pressure for EVAL-SBII02 as seen in Table 4.

Table 4: EVAL-SBII02 Ignition and Extinction Time and Pressure Measurements

Batch - Sample	Ignition Pressure	Burn Out Pressure	Avg. Test Pressure	Pressure Increase	Strand Length	Ignition Start	Burnout Time	Burning Rate	Ambient Temp.
	(psi)	(psi)	(psi)	%	(in)	(sec)	(sec)	($in.sec^{-1}$)	(°F)
SBII02-01	643	752	698	17	1.0465	1.780	5.801	0.260	81.0
SBII02-02	810	942	876	16	1.0475	1.090	4.680	0.292	82.7
SBII02-03	1010	1144	1077	13	1.0330	1.950	5.360	0.303	83.1
SBII02-04	1226	1368	1297	12	1.0490	1.862	5.174	0.317	82.1
SBII02-05	1380	1523	1451	10	1.0360	1.385	4.526	0.330	82.0
SBII02-06	1567	1710	1638	9	1.0355	1.982	5.000	0.343	82.1
SBII02-07	1765	1912	1839	8	1.0240	1.930	4.909	0.344	84.3
SBII02-08	1959	2109	2034	8	1.0455	1.580	4.670	0.338	82.6
SBII02-09	2166	2329	2247	8	1.0495	2.390	5.353	0.354	82.3
SBII02-10	2367	2526	2447	7	1.0215	1.740	4.530	0.366	82.0

The burning rate values and test pressures can be plotted one as a function of the other on a log-log coordinate system to obtain the burning rate equation for EVAL-SBII02: $r = 0.055 P^{0.243}$, and the $R^2 = 0.95$ (Ref. Figure 21).

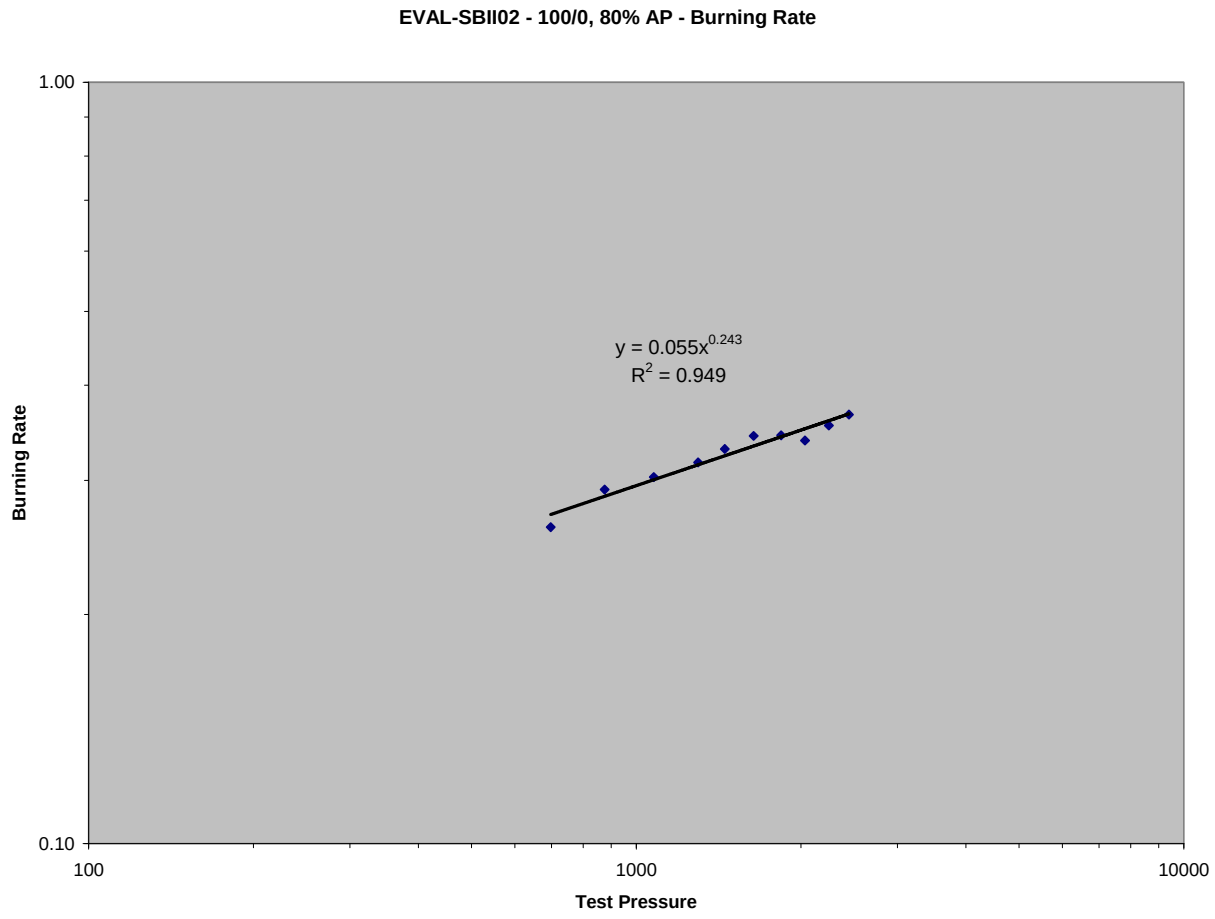

Figure 21: Burning Rate Equation for EVAL-SBII02

The data recorded with the new strand burner and setup arrangement has proven to be very good, and each batch is consistent with its trend (high R^2 values).

Figure 22 show how well each batch agrees with each other by plotting both burning rate equations on the same graph from which one can extract the average burning rate equation for EVAL-SBII01 and EVAL-SBII02.

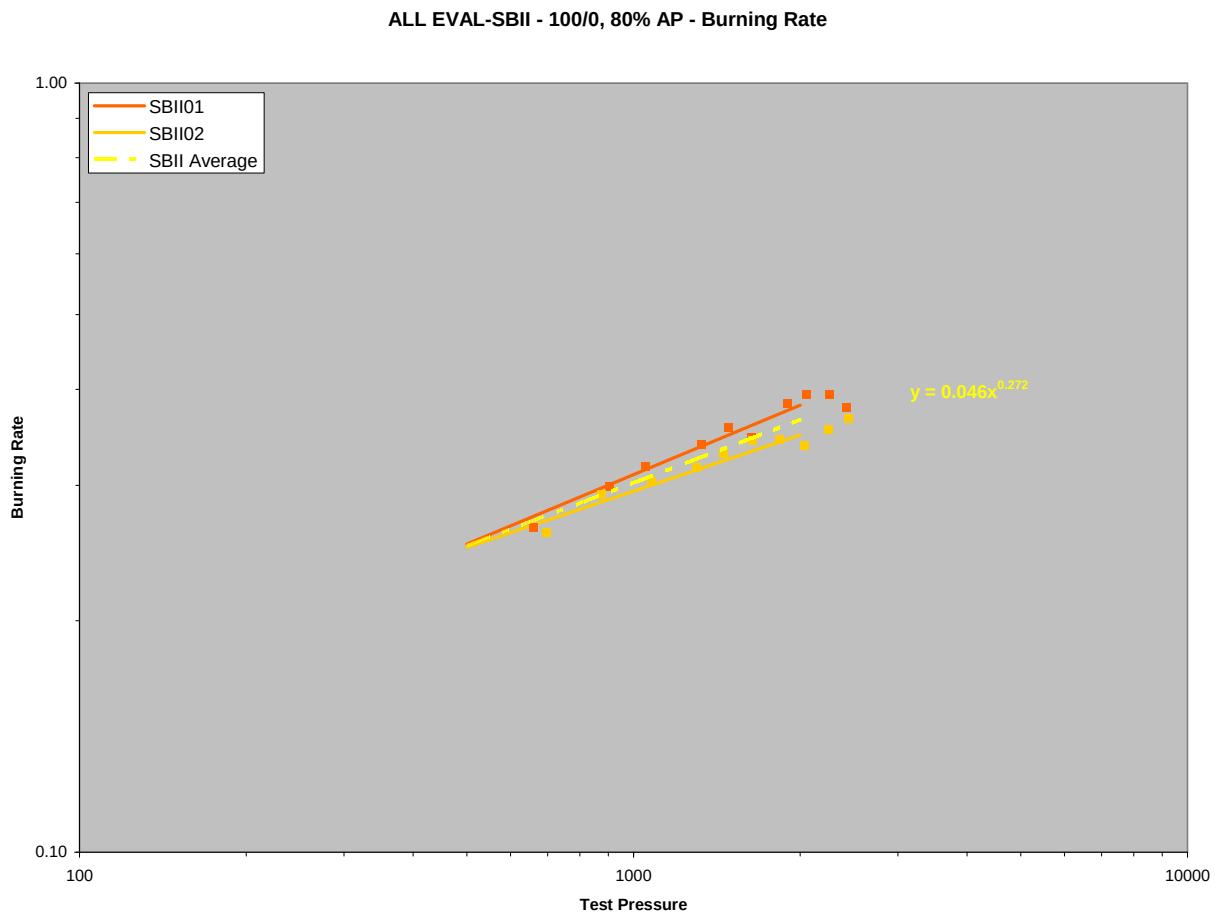

Figure 22: Average Burning Rate Equation for EVAL-SBII01 and EVAL-SBII02

The real narrow band formed by the data is characteristic of small variance from batch to batch, rendering the average data a good approximation of the set. This tight spread demonstrates the high repeatability quality of the new strand burner.

To validate these burning tests, they were compared against 4 other batches of the same propellant burnt using SB-I to support the research on novel burning rate modifiers presented by Matthew Stephens and the author at the 42nd AIAA/ASME/SAE/ASEE Joint Propulsion Conference & Exhibit.[23] Figure 23 reveals the data for EVAL-SBI as a whole (4 batches) and the average burning rate equation.

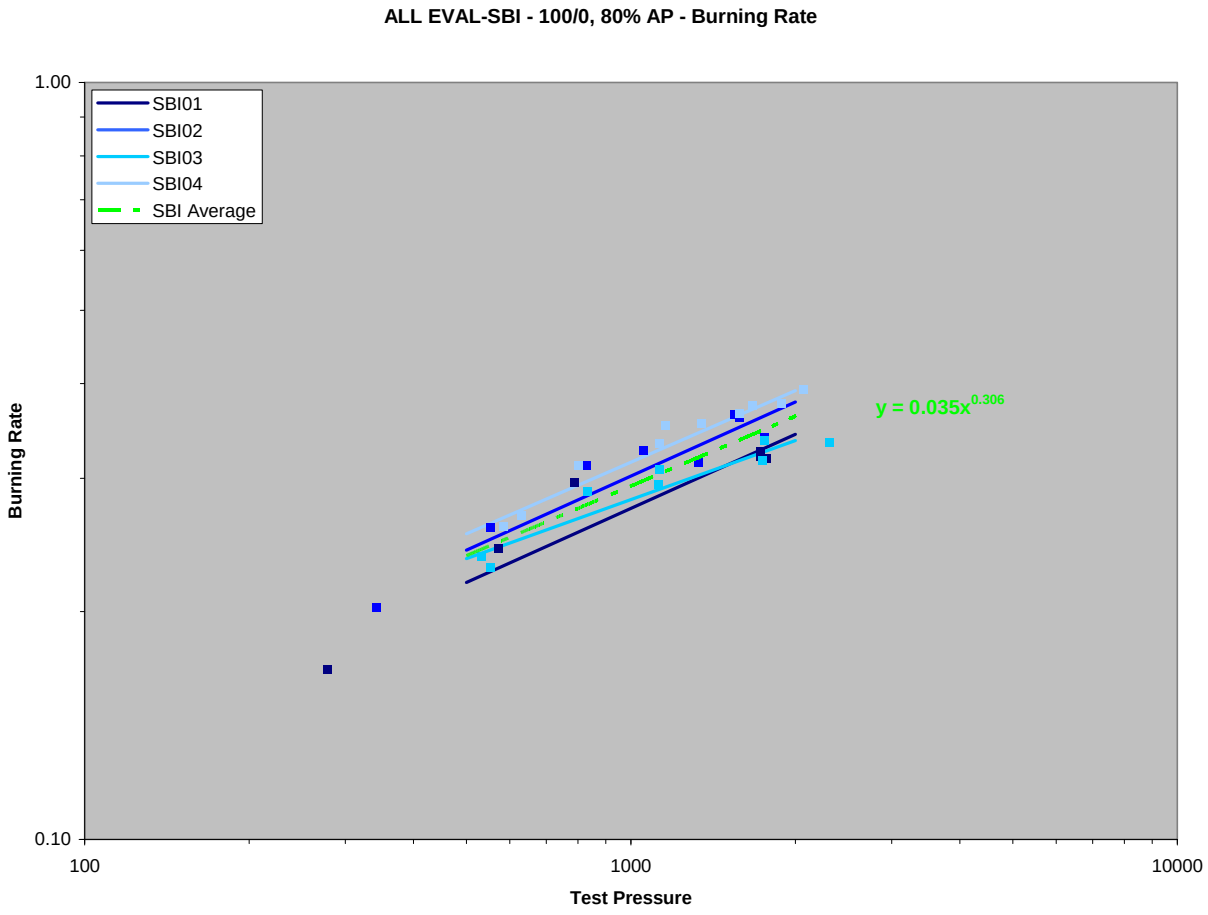

Figure 23: Average Burning Rate Equation for EVAL-SBI01, EVAL-SBI02, EVAL-SBI03 and EVAL-SBI04

The tight band formed by the data is characteristic of small variance from batch to batch, rendering the average data a good approximation for the set which is used next to qualify SB-II.

On the next figure (Figure 24), the 32 samples from the 4 batches making the EVAL-SBI group are plotted together, along with the equation averaging the burning rate over the entire ensemble, this is the reference datum used to benchmark the new setup. The latest 20 samples from the 2 batches making the EVAL-SBII group are also plotted together, along with the equation averaging the burning rate over the entire ensemble.

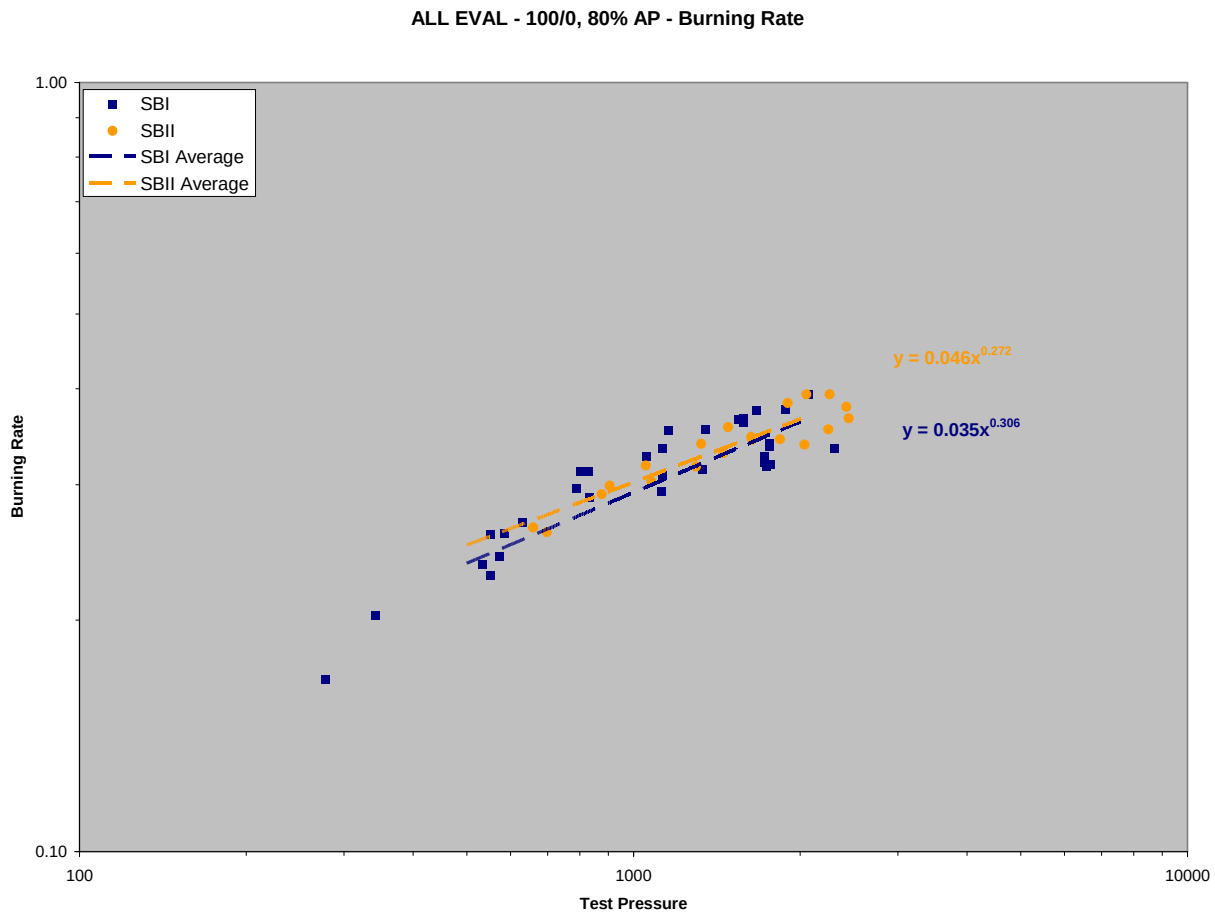

Figure 24: Correlation Between the SBI and SBII Evaluation Test Runs

This graphical representation convey clearly the agreement of the new data collected from the new strand burner with the reference data generated in the original strand burner.

Table 5 shows the average values calculated to represent the 2 groups of batches. The reference group, group EVAL-SBI, comprises batches EVAL-SBI01, SBI02, SBI03 and SBI04. The evaluation group, group EVAL-SBII comprises EVAL-SBII01, SBII02.

Table 5: EVAL-SBI and SBII Burning Rates

			Calcualted Burning Rate ($in.sec^{-1}$)		Average Burning Rate ($in.sec^{-1}$)	
Strand Burner	Batch	Burn Rate Equation	500 (psi)	2000 (psi)	500 (psi)	2000 (psi)
SBI	01	$r = 0.029\ P^{0.325}$	0.219	0.343	0.237	0.362
SBI	02	$r = 0.032\ P^{0.325}$	0.241	0.378		
SBI	03	$r = 0.047\ P^{0.259}$	0.235	0.337		
SBI	04	$r = 0.036\ P^{0.314}$	0.253	0.392		
SBII	01	$r = 0.039\ P^{0.300}$	0.252	0.381	0.250	0.365
SBII	02	$r = 0.055\ P^{0.243}$	0.249	0.349		

These average values are used to quantify the agreement between the groups at 500 psi and 2000 psi as follows

The percentage difference at 500psi (worst case) is calculated as follow:

$$\Delta_{500} = \frac{0.250 - 0.237}{0.237} * 100 = 5.6\%$$

As shown graphically, this small deviation reduces even further at high pressure to

$$\Delta_{2000} = \frac{0.365 - 0.362}{0.362} * 100 = 0.7\%$$

The correlation between SB-I and SB-II is stronger at higher pressures. This finding is in accordance with the fact that the sample burning rate measurement gain in accuracy for

high initial test pressures. This is due to the lower percentage pressure increase at high test pressures, 8 - 9% at 2000 psi compare to 17 - 19% at 600 psi. SB-II internal volume is 13% larger than SB-I's for a better accuracy of the burning rate measurement over the entire operating pressure.

The very good agreement between the averages of the two batch burning rates is consistent with the good concurrence between the data collected with SB-I and SB-II throughout the characterization exercise and reinforce the confidence level in the performance of the new setup.

3.6 Statistical Analysis

To demonstrate the good repeatability in the measurement of the burning rate of a selected propellant mixture, and to quantify our confidence level on the published data, five extra samples of the EVAL-SBII02 batch were burn tested in SB-II at 1000 psi.

These five measurements are collected in Table 6 along with the data collected from sample EVAL-SBII02-03.

Table 6: Collection of Data for Statistical Analysis

Batch - Sample	Ignition Pressure	Burn Out Pressure	Avg. Test Pressure	Pressure Increase	Strand Length	Ignition Start	Burnout Time	Burning Rate
	(psi)	(psi)	(psi)	%	(in)	(sec)	(sec)	($in.sec^{-1}$)
SBII02-03	1010	1144	1077	13	1.0330	1.95	5.36	0.303
SBII02-11	1007	1142	1075	13	1.0550	1.55	5.01	0.305
SBII02-12	1014	1158	1086	14	1.0655	2.55	6.03	0.306
SBII02-13	1010	1144	1077	13	1.0440	2.20	5.64	0.303
SBII02-14	976	1117	1046	14	1.0395	1.76	5.17	0.304
SBII02-15	1010	1150	1080	14	1.0500	3.66	7.04	0.311

Figure 25 displays the very good agreement between all six burning rates sampling carried at an average ignition pressure of 1005 psi

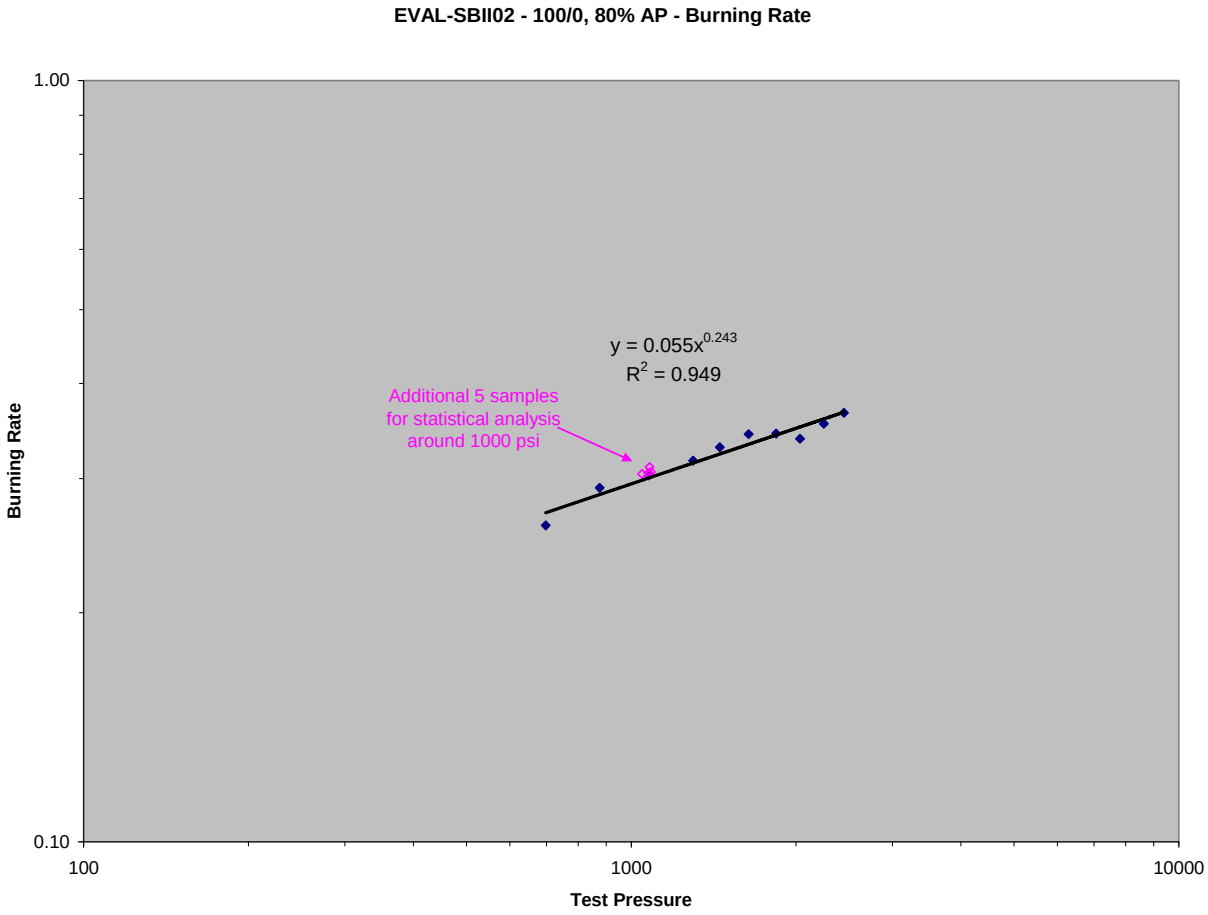

Figure 25: Additional Samples for Statistical Analysis and EVAL-SBII02 Burning Rate

These six samples were tested in an average strand burner pressure ranging from 1046 to 1086 psi, yielding an overall average of 1073.5 psi. The small spread of average test pressures of 40 psi, ensures that all the samples were tested within 3% of the average value. The theoretical burning rate for EVAL-SBII02 at this overall average pressure is

calculated using the burning rate equation determined during the characterization exercise (Ref. Section 3.5) and is used as a reference:

$$r_{1074} = 0.055 \times 1073.5^{\,0.243}$$

$$r_{1074} = 0.300 \text{ in.sec}^{-1}$$

A simple statistical analysis carried on the six burning rates is summarized in Table 7.

Table 7: EVAL-SBI and SBII Burning Rates

Mean	0.30546
Standard Error	0.00114
Median	0.30474
Standard Deviation	0.00280
Sample Variance	0.00001
Kurtosis	2.65448
Skewness	1.56506
Range	0.00772
Minimum	0.30293
Maximum	0.31065
Count	6
Confidence Level (90.0%)	0.00231
Confidence Level (95.0%)	0.00294

Based on this statistical analysis, a 90% confidence interval for the burning rate determination using the new strand burner is $r \pm 0.00231$ in.sec^{-1}, and $r \pm 0.00294$ in.sec^{-1} for a 95% confidence level. Meaning that based on this analysis, the 95% confidence interval for the burning rate of EVAL-SBII02 at 1074 psi has an upper limit of 0.3084 in.sec^{-1} and a lower limit of 0.30252 in.sec^{1}.

Each average burning pressure differs from one to another due to the small differences in the initial strand burner pressure and strand length. The burning rates were

normalized with respect to the overall average pressure using Equation (2) in order to plot each burning rate with respect to a common bomb pressure.

$$r_{normalized} = r_{measured}\left(\frac{P_{av}}{P}\right)^{n} \qquad (2)$$

The results of the normalization are presented in Table 8

Table 8: Measured and Normalized Burning Rates for Statistical Analysis

Batch - Sample	Ignition Pressure (psi)	Burn Out Pressure (psi)	Avg. Test Pressure (psi)	Burning Rate as Measured ($in.sec^{-1}$)	Normalized Burning Rate ($in.sec^{-1}$)
SBII02-03	1010	1144	1077	0.3029	0.3027
SBII02-11	1007	1142	1075	0.3053	0.3052
SBII02-12	1014	1158	1086	0.3062	0.3053
SBII02-13	1010	1144	1077	0.3035	0.3033
SBII02-14	976	1117	1046	0.3042	0.3061
SBII02-15	1010	1150	1080	0.3107	0.3102

The normalized burning rates are plotted with respect to the overall average pressure (1074.5 psi) in Figure 26.

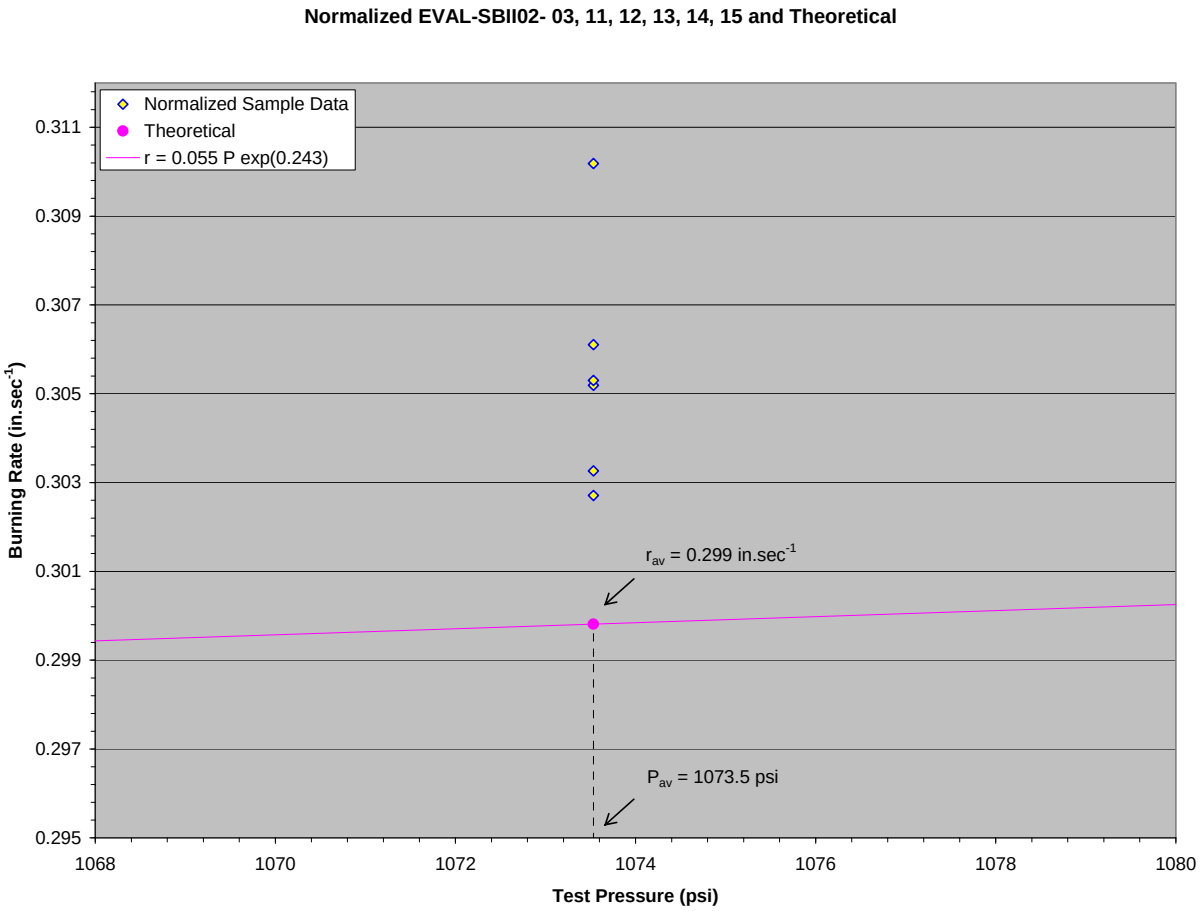

Figure 26: Normalized Burning Rates vs. Overall Average Pressure

Figure 26 allows a visual appreciation of the good correlation between all the repeated tests. The scale of the Burning Rate axis was magnified to provide a better distinction between the points.

Conclusively, the batch to batch comparison and the single pressure comparison furtherance the high level of repeatability achievable with Strand Burner II.

CHAPTER 4
CONCLUSION

4.1 Summary

A new capability exists in the author's laboratory to perform experiments on advanced composite solid propellant formulations. The new strand burner facility is capable of testing 1.8 cm long, 6 mm diameter samples at static pressures as high as 360 atm. Burning rates are obtained from simultaneous pressure and light emission and video acquisition in a safe and low cost environment. The upgrades implemented allow the researchers to conduct emission spectroscopy sampling allowing the researcher to analyze the products reacting within the combustion flame. Outstanding performance of the new strand burner was demonstrated throughout the normal operation range of 500 to 2300 psi. Good correlation was found between the burning rates obtained from the pressure trace and burning rates obtained from the light emission recording providing redundancy. Repeatability in the measurement was verified by burning 20 samples from 2 different batches. The average burning rates equations generated for these batches presented linear regression coefficient in the high 0.9 without suppressing outliers. Because of the very good agreement of the 2 average burning rate equations they were further averaged into 1 equation to represent the propellant mix as a whole and compare with assurance against the data collected in the original setup.

Confidence level in the accuracy was proven by comparing the burning rate of different batches of the same propellant composition in both strand burners. Characterization of the original facility was previously presented for two AP / HTPP-based propellant mixtures;[21] the data compared favorably with existing data from the literature for the same mixture formulas, indicating that the facility produces results consistent with those from established facilities

4.2 Discussion

Theoretical capability to predict the burning rate of real propellants from their ingredients would be an invaluable aid to formulating solid propellants. Unfortunately, no comprehensive means of this sort exist today for solid propellants.[1-3] This short coming is not due to insufficient computational resources, but rather to a lack of fundamental understanding of the combustion mechanisms in the condensed phase, surface interface, and gaseous combustion zones of typical propellant mixtures. Because the setup described herein is best suited for the direct determination of burning rates of solid propellants, it can be used to validate theoretical studies or benchmark statistical computer models of the burning process and behavior of solid rockets or non-propulsion applications of solid propellants (automotive airbags, shut-off vanes, etc.).

A trial-and-error approach has always played a central role in the development of new energetic materials for use as explosives and propellants. It is an approach dictated by necessity, not by choice. Since its creation in the late 1940's,[11] the strand burner has historically been the inevitable first step in the design optimization and final service acceptance of a propellant. The setup described in this thesis was proven to be very

proficient in these tasks. Work conducted to date in this facility includes a comprehensive study on the performance of both non-metallized and metallized composite propellants wherein a fraction of the conventional aluminum content in Al / AP / HTPB mixtures was replaced by nano-sized aluminum.[13] Current activities also include the exploration of additives that increase or otherwise modify the burning rate of composite propellants.[16]

Several improvements to the methodology and diagnostic techniques have been implemented. For example, the light emission intensity that was measured as a whole is now measured for specific wavelengths (200 - 800 nm) by passing the collected light through a spectrometer to monitor. This valuable data allow the researcher to detect the presence of key gas-phase species within the combustion zone by matching the dominant wavelengths to known data. These species could be the result of primary-fuel oxidation or by-products directly related to the presence of various additives of interest. Additional resources also include advanced materials characterization capabilities available through collaboration with materials science personnel at UCF, as in Small et al.[16] Materials characterization such as transmission electron microscopy and x-ray photoelectron spectroscopy of reactant particles and combustion products are possible.

4.3 Recommendations

The characterization tests presented herein demonstrate the validity and the quality of the data collected with the current equipment; nonetheless in the intent of increasing the accuracy and the detail of the experiments without compromising safety the following improvement are recommended.

During the characterization exercise, the Strand Burner II was subjected to pressures as high as 2526 psi without noticeable structural affect and even if the assembly was designed to contain internal pressures as high as 8000 psi it is recommended to secure a third set of braces (SB-02-513 and SB-02-515) at the area of high stress concentration. The finite element analysis conducted on a conservative model of the SB-II assembly pressurized at 5000 psi (Ref Appendix H for a summary of the analysis) highlight a 1 in weak 'ring' on the MAIN BODY (SB-02-503) locate right after the three windows (Ref. Figure 45 and Figure 46). At the worst node, a maximum hoop stress of 53553 psi is predicted. Based on the tensile strength for SAE 4140 N steel, the system still holds a margin of safety of 4 at 5000 psi.

$$MS = \frac{\sigma_{allowable}}{\sigma_{applied}} \tag{2}$$

$$MS = \frac{53553}{215000} = 4$$

During the FEA, a maximum deflection of 0.0257 in was recorded on the AFT END-CAP (SB-02-505) WINDOW (SB-02-301). This is a conservative estimate considering that the 'shoulder' restraining the windows – and lowering the windows surface subjected to the internal pressure – were not modeled. Still, the strength of the windows could be increase by ~ 68% by replacing the polycarbonate windows with 20% glass-filled polycarbonate.

With the addition of the new strand burner, it would now be fairly simple to convert the original strand burner into a ‘dump tank’ and convert the entire setup from isochoric to isobaric burning testing. The experiment is currently performed under constant volume, and the burn time is measured by monitoring the pressure gradient. The resulting burning rate is then associated with the average pressure of the run. A check valve placed between SB-I and SB-II would allow gases to transfer from one tank to another during the burn keeping SB-II at a preset constant pressure. The resulting burning rate / testing pressure relation would be more accurate than the current design. Because a high pressure dump tank is already available, this modification has been qualified as low cost.

Another recommendation is to replace the optical polycarbonate windows with sapphire windows (fused silica). This change would facilitate the cleaning, reduce the damages that occur during the removal, cleaning and even from the hot solid particulates blasted from the combustion surface onto the low melting temperature Lexan, but most of all, sapphire windows manufactured by specialized companies come with a wide transmission range and would not act as a passive filters. To minimize the cost, only the optical ports used for high accuracy emission recording may be replaced.

Upon the completion of the burn testing of an entire propellant batch (~10 samples) the strand burner is dismantled, cleaned, dried, and assembled back together. Because the new strand burner weights over 90 lb this operation is cumbersome. A non-structural 1/8 in thick cylindrical stainless steel liner - with openings for the optical ports of course - that slides right in the strand burner body, would collect the majority of the grime. At the end of a batch testing, the researcher would remove the Forward End-Cap, remove and clean the

liner before putting it back in place. This extra layer of protection would extent the longevity of the system and lowers the frequency of cleaning, reducing the turn around time between batches.

Burning rate variation due to initial grain temperature difference at the time of testing from sample to sample or even batch to batch could be eliminated by keeping the strands, the argon but most of all the strand burner at constant temperature. Furthermore, setting the strands and the strand burner in a temperature controlled environment would allow the researcher to investigate the temperature influence on the burning rate of the propellant mixture.

The energy conveyed by a LASER tuned adequately could be used as a non-intrusive ignition system.[22]

The most substantial and complex change would be to replace the current burning rate measurement methodology with a more sophisticated non-intrusive methods. Intrusive methods such as imbedded timing wires have proven to be accurate and dependable, but require protracted preparations. The most current method in use in the solid rocket propellant research arena is the ultrasonic pulse echo and the transmission microwave interferometry methods. Such methods would bring a greater accuracy in the determination of the burning rate of the propellants. Dauch et al.[36] published a 3.5% to 5% relative uncertainty when comparing the pulse-echo ultrasonic technique with Direct Monte-Carlo simulations. Nevertheless, it is recommended to conduct a cost analysis before integrating such system noting that a full characterization exercise would be needed along with a new testing, data reduction and interpretation procedure.

And finally, upgrading the emission spectroscopy instrumentation would greatly support the UCF solid rocket propellant research group in the investigation of the effect of novel burn rate modifiers. The current emission spectrometry setup offers a 1 nm resolution. Increasing this resolution along with the integration of optical filters to clean background noise and isolate spectral bands of interest would magnify features that are looked after during the interpretation of the data. To reach a higher level of flame emission expertise and further explore the properties and composition of the combustion region both a Focusing Schlieren System (FSS) and a Coherent Anti-Stokes Raman Scattering (CARS) are recommended. While the CARS would provide accurate temperature profile determination above the burning surface, the FSS is devoted to the flame structure study and would back the finding of the CARS up and provide accurate chemical sampling within the combustion zone.[30] Such study could be carried in parallel with XPS or SEM inspection of the structure of the extinguished burning surface by quenching (rapid depressurization of the strand burner).[35]

APPENDIX A: TESTING PROCEDURE

For the operator safety, a lab coat must be worn during all operations. When highlighted within the following procedure, powder free latex gloves, ear protection and ear muff must also be worn. If skin contact occurs during the strand handling and preparation, wash immediately with soap and water. If eye contact occurs during the handling and preparation, do not rub eye, rinse thoroughly using the eye wash solution located in the green case above the sink. Before testing, the pressure system must be inspected and tested for leak up to few hundred psi (~500psi) using a leak detection solution such as Snoop, retighten loose connection accordingly. In the event of a major leak and/or bursting of the pressure system, turn the illuminated switch on the face of the control panel off and exit the laboratory. If noise level is deemed to high, stay away till the system vents completely.

The system is designed such that the results of the combustion are exhausted outside the laboratory, nevertheless the testing area must be kept ventilated throughout the entire procedure.

1. Wearing powder free latex gloves and eye protection, select a ‘good’ strand from a selected batch. Record batch number. A ‘good’ strand is showing continuity (no cracks or voids) and uniformity or consistency (no change in color or FOD).
2. Peel off the clear tubing using a sharp edge without damaging the strand.
3. Cut both ends of the strand till it measures approximately 1 in.
4. Measure and record the strand length, diameter at three different locations with a digital caliper. Weigh and record the strand on a high precision digital scale.

5. Cut a ¼ in of plastic clear tubing. Coat the inside of the tube with HTPB using a Q-tip.
6. Dip one end of the strand in HTPB and fit it into the tube. Coat the rest of the strand except the tip (burning surface) with HTPB using a Q-tip to prevent side burning.
7. Set the strand straight up within a temporary holder to let the HTPB in excess run down (1 to 2 minutes).
8. Clean the strand holder connector by running it under water to remove the dust and soot. Dry right away using Kimwipes. To enhance connectivity brush the connectors with a metallic brush, a metallic file or sand paper.
9. Coat the threads of the strand holder with antiseize compound, and lubricate the O-ring with high pressure grease.
10. Install the strand into the strand holder.
11. Warp Ni-chrome ignition wire between the 2 connectors. The wire must be tight and in contact with the burning surface (uncoated tip of the strand).

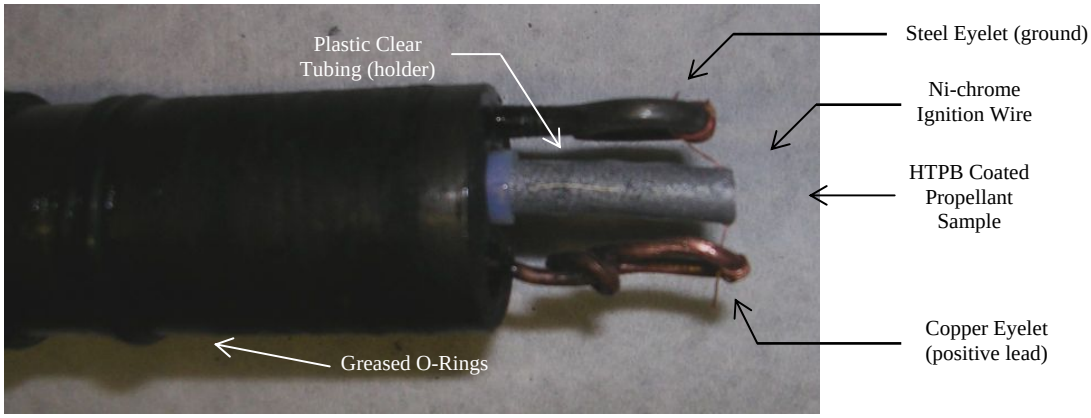

Figure 27: Propellant Sample as Mounted on the Strand Holder

12. Secure the strand holder into the strand burner. From this point forward gloves are not required.
13. Connect the positive lead of the strand holder to the ignition relay, verify connectivity using an Ohmmeter. Connect the ignition relay to the 12 V battery.

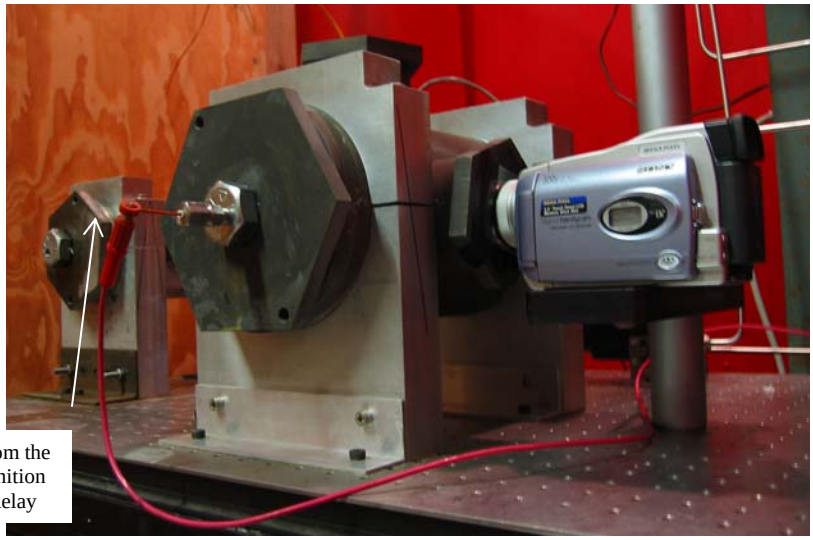

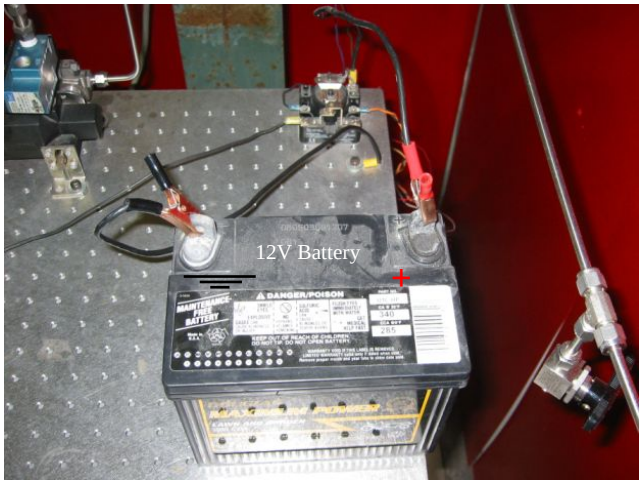

Figure 28: Ignition Circuit

14. Select one strand burner for testing by opening its ball valve and closing the other strand burner's.

15. Close the bypass emergency exit valve.

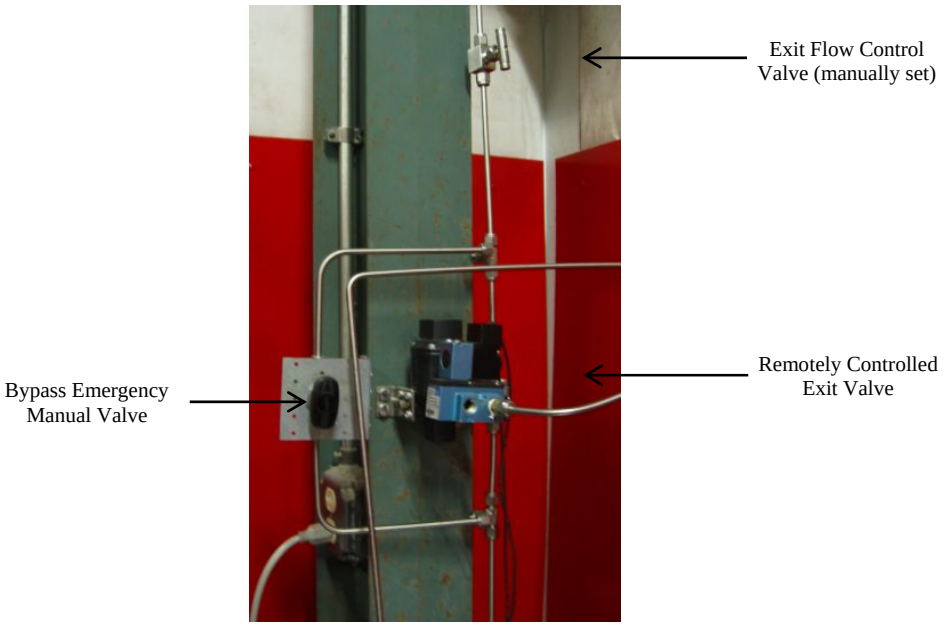

Figure 29: Venting Line Valves

16. Set the working gas (nitrogen) regulator to 60 - 80 psi and turn the ON / OFF regulator valve on. Set the test gas (argon) regulator to a value slightly higher than the test pressure desired.

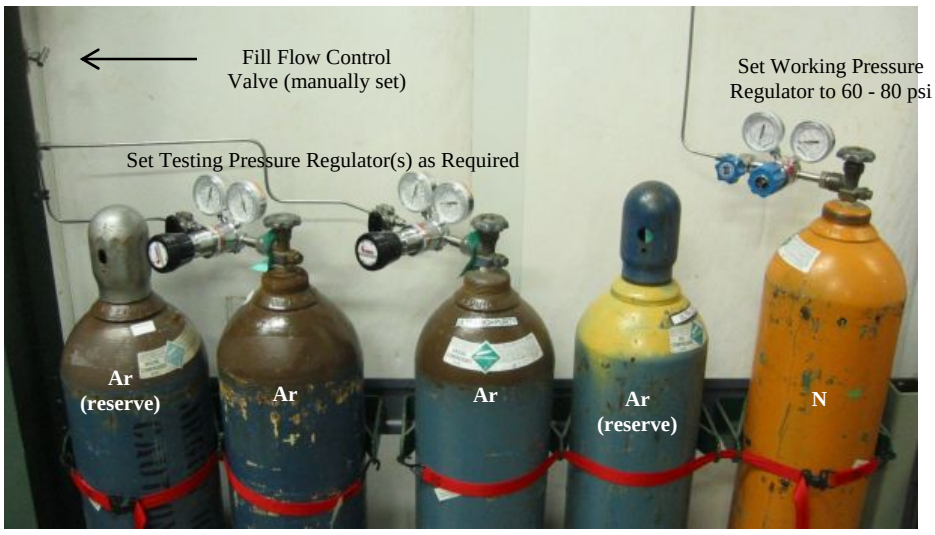

Figure 30: Compress Gas Bottle Arrangement

17. Turn the pressure transducer power supplied ON, verified that it is set to 28.0 V, 0.01 A; and plug the Omega digital display (power supply of the secondary pressure transducer).

Figure 31: Pressure Transducer Power Supply

18. Turn the photoreceiver ON.

Figure 32: Photoreceiver

19. Turn the warning red light and exit the burn testing area (red room) sliding the door shut behind you.

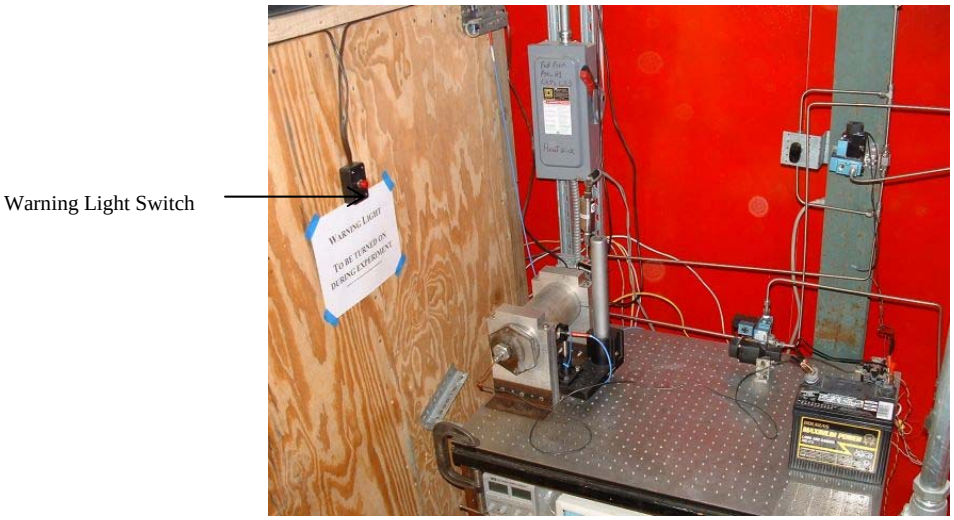

Figure 33: Warning Light Switch

20. The red light is a visual signal to warn all personnel present in the lab that high pressure experiment is in progress meaning that the red room must be evacuated and hearing protection (ear muffs) is required.

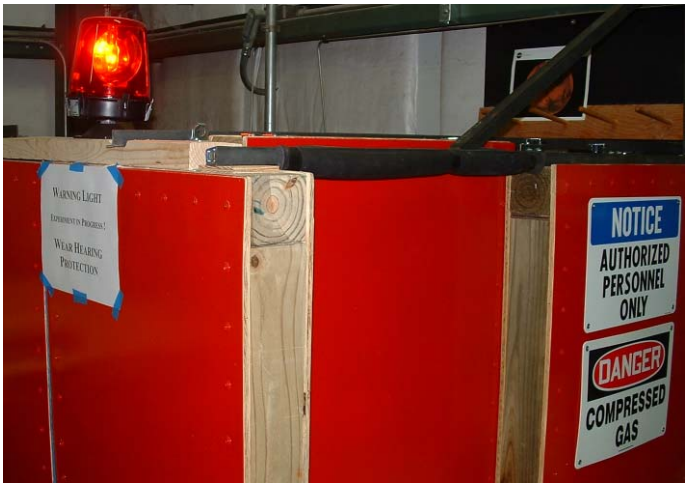

Figure 34: Warning Light

21. At the control panel, power ON the control board. 2 switches: main power, in the back of the panel; and pressure solenoid power, on the face of the panel.

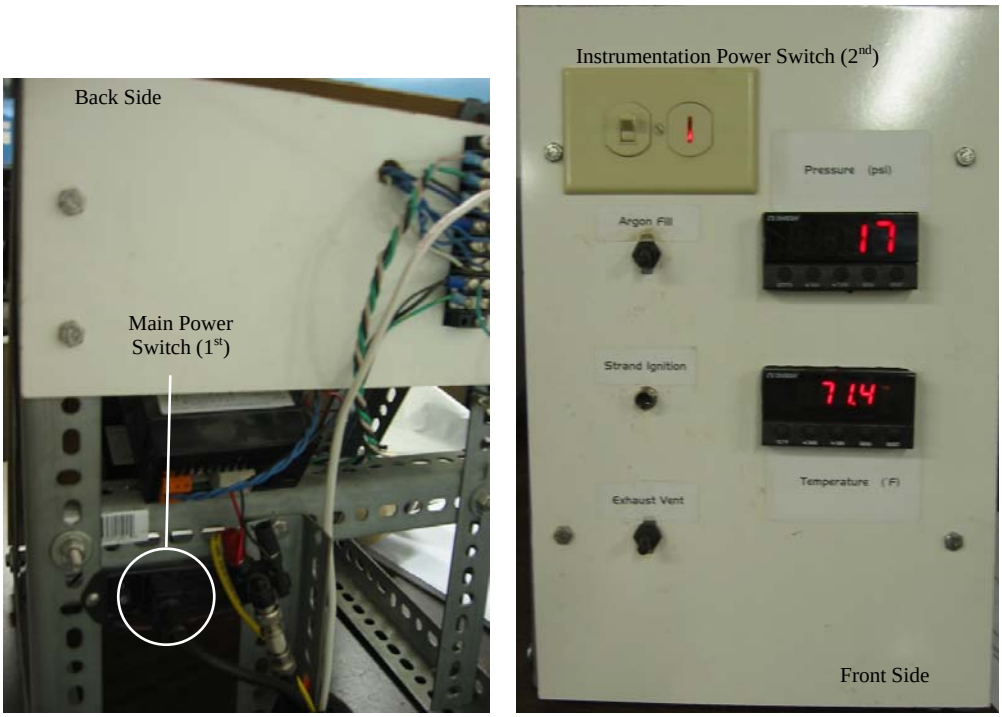

Figure 35: Remote Control Panel

22. Purging: with the exhaust vent closed, open the intake valve momentarily to partially fill the strand burner to 100 to 200 psi then vent it. Repeat once.
23. Open the intake valve to fill the strand burner to the desired test pressure. Record the strand burner pressure and ambient air temperature.
24. Turn the Lab ceiling light off. While this greatly improves the quality of the light emission measurement, it is optional and should not compromise the team safety.
25. Start the emission spectroscopy acquisition from the SpectraSuite GUI.
26. From the GageScope software, trigger the pressure and light emission acquisition. Verify both systems are properly recording.

27. Push the ignition button until ignition (quick raise in pressure on the pressure digital display).
28. Looking at the trace of the pressure transducer output voltage on GageScope, verify that the acquisition recorded the entire burning phase and the ignition and extinction inflection points are apparent.
29. Save the data logs on the computer hard drive.
30. From the control panel open the exhaust valve till the strand pressure reaches 0 psi. Fill up the pressure strand with few hundreds psi of argon; then purge.
31. The red light may be turn off, the red room is now accessible. Open the manual emergency exhaust bypass valve, disconnect the battery from the strand holder. Remove and clean the strand holder. Prepare the next sample for testing. Clean the strand burner every 8 to 10 burns.

APPENDIX B: A TYPICAL LINEAR REGRESSION BURN

The following diaporama presents in a frame by frame sequence, the typical burn test linear regression of the burning surface. These pictures were extracted from a video recording of an early burn for its clarity. The early samples were burnt within their Teflon encasing. This made great video footages as the tubing controlled the flame and the products of the combustion in the plan view, but the confinement of high pressure gases often induced explosion of the sample before the end of the test. This was alleviated by removing the encasing and coating the side of the strand with liquid HTPB.

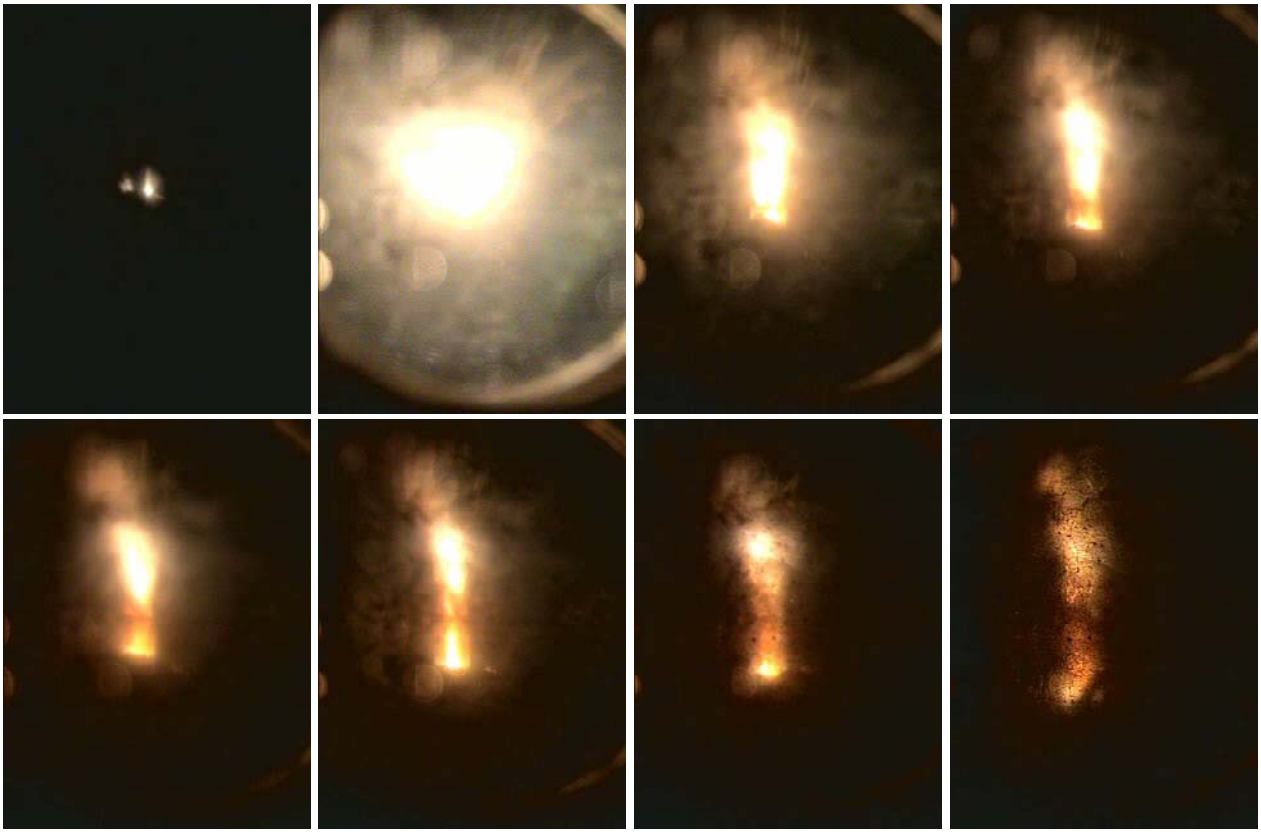

Figure 36: A Typical Burning Sequence

APPENDIX C: STRAND BURNER I OVERVIEW

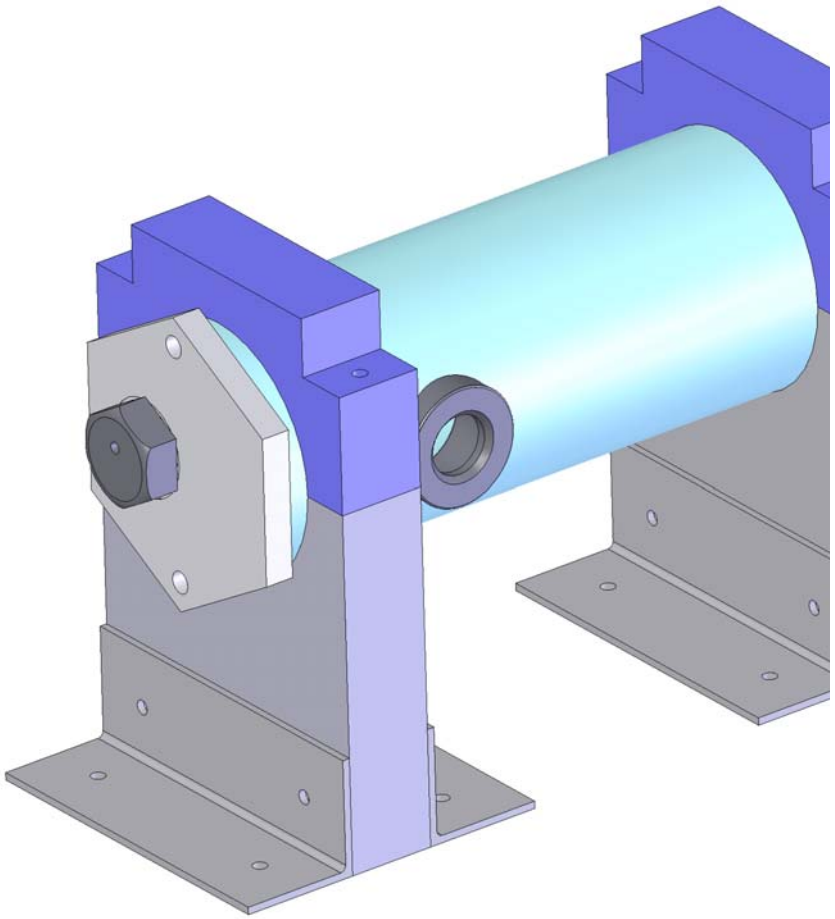

APPENDIX D: STRAND BURNER II DRAWINGS

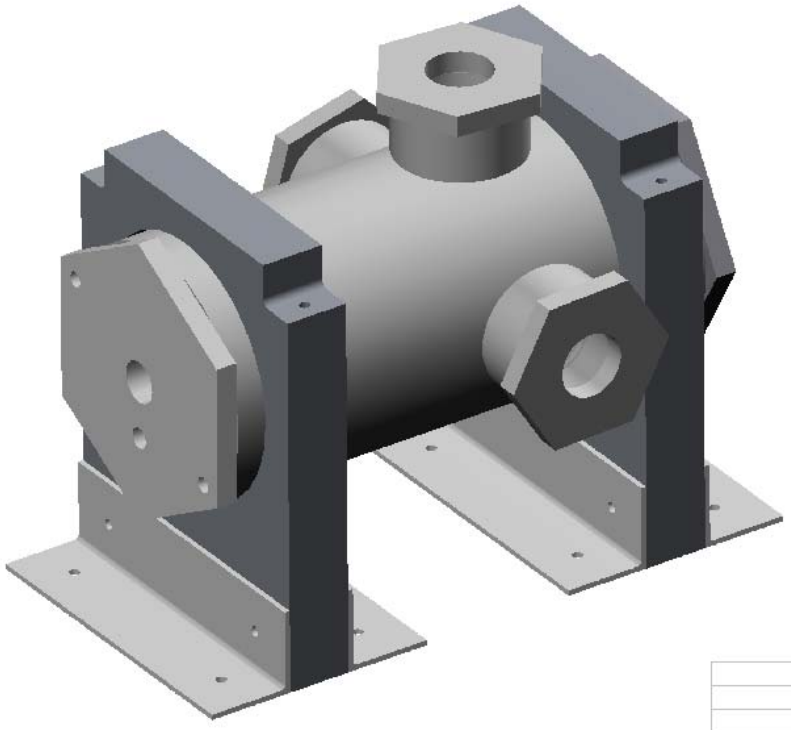

STRAND BURNER ASSEMBLY

		UNLESS OTHERWISE SPECIFIED:		NAME	DATE
		DIMENSIONS ARE IN INCHES TOLERANCES: FRACTIONAL ± 1/16 ANGULAR: MACH ± 2° BEND ± 2° TWO PLACE DECIMAL ± .010 THREE PLACE DECIMAL ± .005	DRAWN	R.J.C.	10/11/07
			CHECKED		
			ENG APPR.		
			MFG APPR.		
		INTERPRET GEOMETRIC TOLERANCING PER: ASME Y14.5M	Q.A.		
		MATERIAL	COMMENTS:		
		FINISH			
NEXT ASSY	USED ON				
APPLICATION		DO NOT SCALE DRAWING			

TITLE: STRAND BURNER TOP ASSY

SIZE	DWG. NO.	REV
B	SB-02-001	A

SCALE: 1:2 WEIGHT: 109.88 lbs. SHEET 1 OF 3

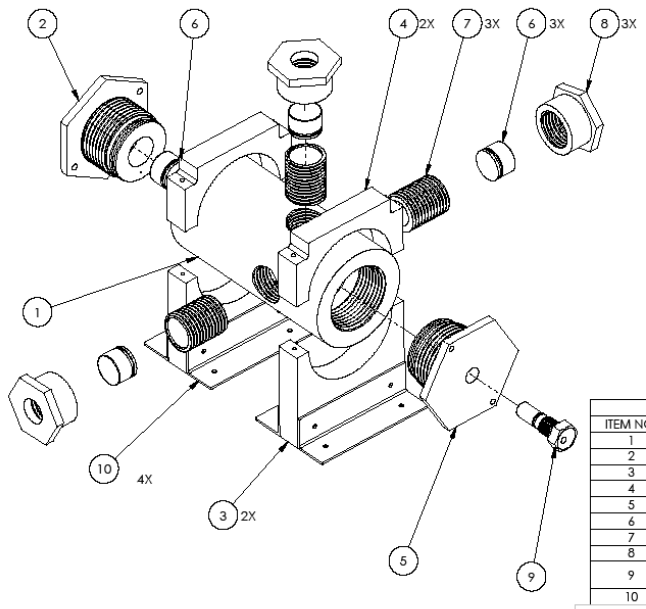

STRAND BURNER ASSEMBLY - EXPLODED VIEW

PARTS LIST				
ITEM NO.	PART NUMBER	DESCRIPTION	QTY.	CALWT
1	SB-02-503	MAIN BODY	1	54.80 lbs.
2	SB-02-505	AFT END-CAP	1	11.57 lbs.
3	SB-02-515	STAND, BOTTOM SUPPORT	2	5.01 lbs.
4	SB-02-513	TOP, STAND	2	2.08 lbs.
5	SB-02-507	FORWARD END-CAP	1	12.19 lbs.
6	SB-02-301	WINDOW	4	0.28 lbs.
7	SB-02-511	WINDOW FRAME	3	1.06 lbs.
8	SB-02-509	WINDOW END-CAP	3	2.60 lbs.
9	SB-02-501	SPECIMEN HOLDER 1 IN, MODIFIED	1	0.82 lbs.
10	SB-02-517	BRACKET, HOLD DOWN	4	1.06 lbs.

UNLESS OTHERWISE SPECIFIED:
DIMENSIONS ARE IN INCHES
TOLERANCES:
FRACTIONAL ± 1/16
ANGULAR: MACH ± 2° BEND ± 2°
TWO PLACE DECIMAL ± .010
THREE PLACE DECIMAL ± .005
INTERPRET GEOMETRIC TOLERANCING PER: ASME Y14.5M
MATERIAL
FINISH
NEXT ASSY | USED ON
APPLICATION | DO NOT SCALE DRAWING

	NAME	DATE
DRAWN	R.J.C.	10/11/07
CHECKED		
ENG APPR.		
MFG APPR.		
Q.A.		
COMMENTS:		

TITLE: STRAND BURNER TOP ASSY

SIZE B | DWG. NO. SB-02-001 | REV A

SCALE: 1:4 | WEIGHT: 109.88 lbs. | SHEET 2 OF 3

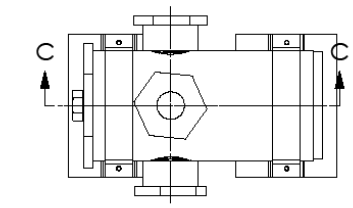

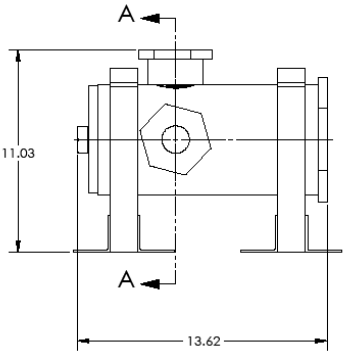

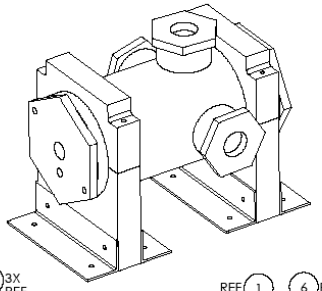

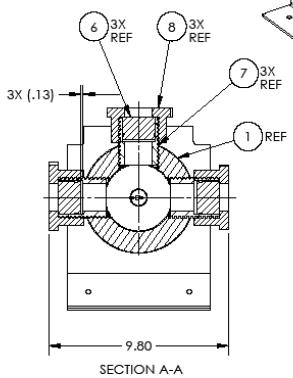

SECTION A-A

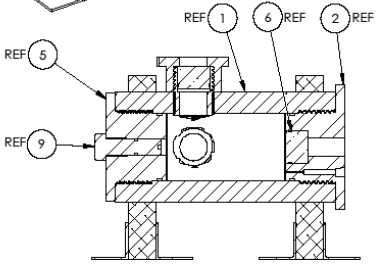

SECTION C-C

UNLESS OTHERWISE SPECIFIED:
DIMENSIONS ARE IN INCHES
TOLERANCES:
FRACTIONAL ± 1/16
ANGULAR: MACH ± 2° BEND ± 2°
TWO PLACE DECIMAL ± .010
THREE PLACE DECIMAL ± .005
INTERPRET GEOMETRIC TOLERANCING PER: ASME Y14.5M
MATERIAL
FINISH
NEXT ASSY | USED ON
APPLICATION | DO NOT SCALE DRAWING

	NAME	DATE
DRAWN	R.J.C.	10/11/07
CHECKED		
ENG APPR.		
MFG APPR.		
Q.A.		
COMMENTS:		

TITLE: STRAND BURNER TOP ASSY

SIZE B | DWG. NO. SB-02-001 | REV A

SCALE: 1:4 | WEIGHT: 109.88 lbs. | SHEET 3 OF 3

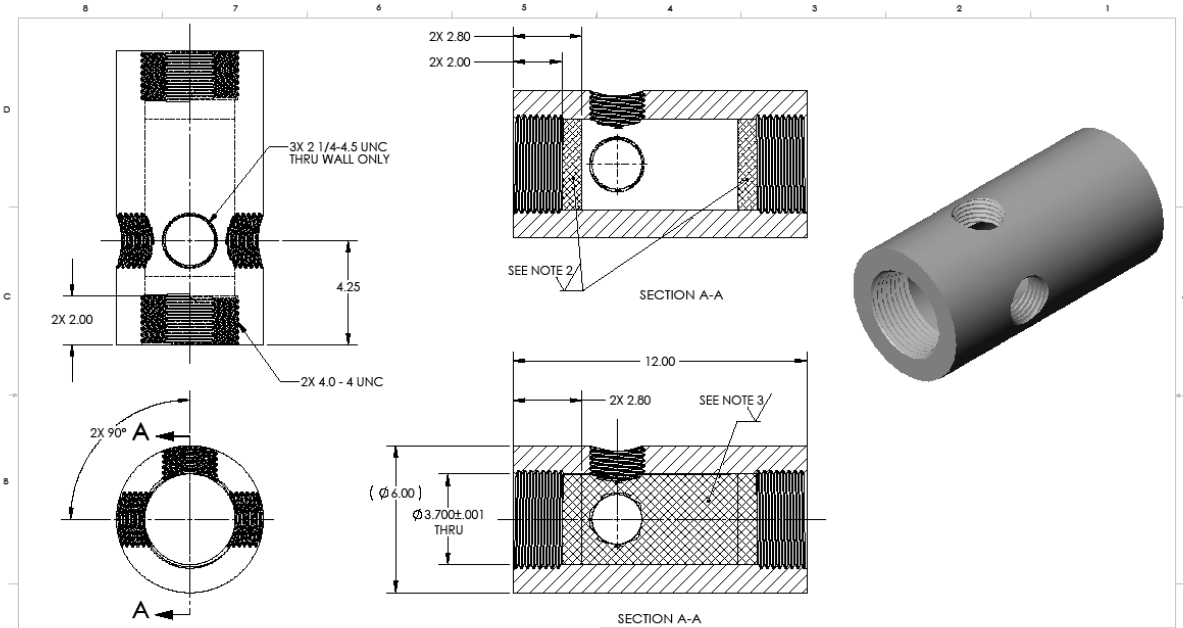

NOTES:
1. BREAK ALL SHARP EDGES.
2. SURFACE FINISH: 32 MICROINCHES (FULL 360° OF ID) PRIOR TO CHROME PLATING (NOTE 3).
3. SURFACE FINISH: 3 MIL CHROME PLATING (FULL 360° OF ID).
4. COAT ALL EXTERNAL SURFACES (NON-CHROMED, NON-THREADED) WITH SS316 USING AIR PLASMA SPRAY.

UNLESS OTHERWISE SPECIFIED:			NAME	DATE	
DIMENSIONS ARE IN INCHES		DRAWN	R.J.C.	10/11/07	TITLE: MAIN BODY
TOLERANCES: FRACTIONAL ± 1/16; ANGULAR: MACH ± 2° BEND ± 2°; TWO PLACE DECIMAL ± .010; THREE PLACE DECIMAL ± .005		CHECKED			
		ENG APPR.			
		MFG APPR.			
INTERPRET GEOMETRIC TOLERANCING PER: ASME Y14.5M		Q.A.			
	SB-02-001	COMMENTS:			SIZE B; DWG. NO. SB-02-503; REV A
MATERIAL: SAE 4140N					
FINISH					
NEXT ASSY / USED ON					SCALE: 1:3; WEIGHT: 54.80 lbs; SHEET 1 OF 1
APPLICATION / DO NOT SCALE DRAWING					

PROPRIETARY AND CONFIDENTIAL
THE INFORMATION CONTAINED IN THIS DRAWING IS THE SOLE PROPERTY OF UNIVERSITY OF CENTRAL FLORIDA. ANY REPRODUCTION IN PART OR AS A WHOLE WITHOUT THE WRITTEN PERMISSION OF UNIVERSITY OF CENTRAL FLORIDA IS PROHIBITED.

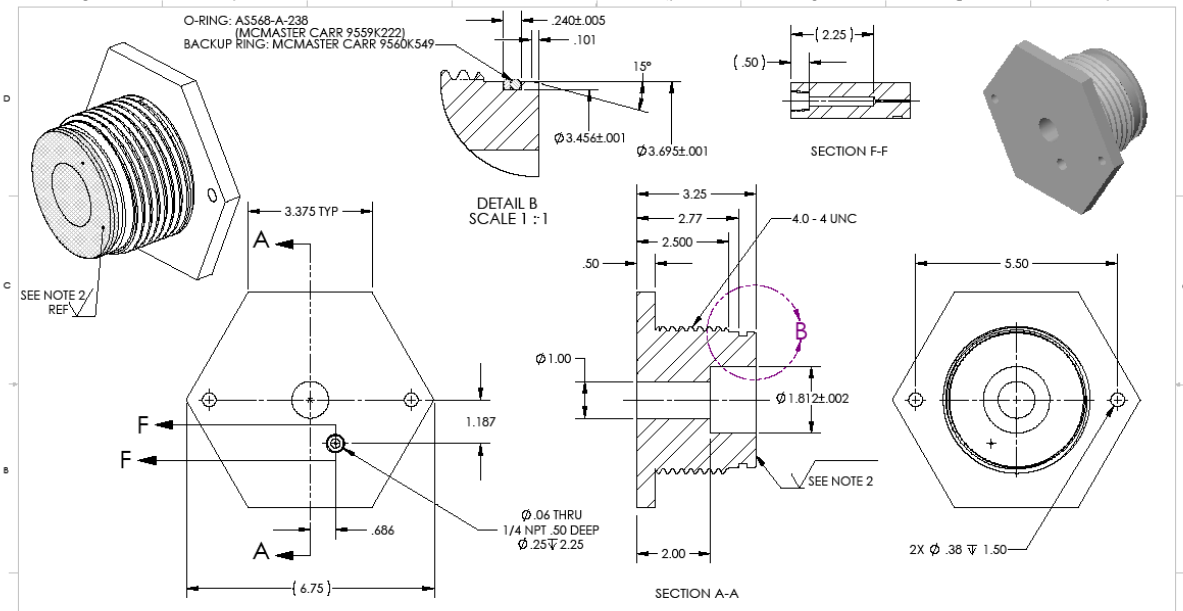

NOTES:
1. BREAK ALL SHARP EDGES.
2. SURFACE FINISH: 3 MIL CHROME PLATING (SURFACE REPRESENTED BY THICK LINES).
3. STANDARD HEX HEAD.
4. COAT ALL EXTERNAL SURFACES (NON-CHROMED, NON-THREADED) WITH SS316 USING AIR PLASMA SPRAY.

UNLESS OTHERWISE SPECIFIED:			NAME	DATE	
DIMENSIONS ARE IN INCHES		DRAWN	R.J.C.	10/11/07	TITLE: AFT END-CAP
TOLERANCES: FRACTIONAL ± 1/16; ANGULAR: MACH ± 2° BEND ± 2°; TWO PLACE DECIMAL ± .010; THREE PLACE DECIMAL ± .005		CHECKED			
		ENG APPR.			
		MFG APPR.			
INTERPRET GEOMETRIC TOLERANCING PER: ASME Y14.5M		Q.A.			
	SB-02-001	COMMENTS:			SIZE B; DWG. NO. SB-02-505; REV
MATERIAL: SAE 4140N					
FINISH					
NEXT ASSY / USED ON					SCALE: 1:2; WEIGHT: 11.57 lbs; SHEET 1 OF 1
APPLICATION / DO NOT SCALE DRAWING					

PROPRIETARY AND CONFIDENTIAL
THE INFORMATION CONTAINED IN THIS DRAWING IS THE SOLE PROPERTY OF UNIVERSITY OF CENTRAL FLORIDA. ANY REPRODUCTION IN PART OR AS A WHOLE WITHOUT THE WRITTEN PERMISSION OF UNIVERSITY OF CENTRAL FLORIDA IS PROHIBITED.

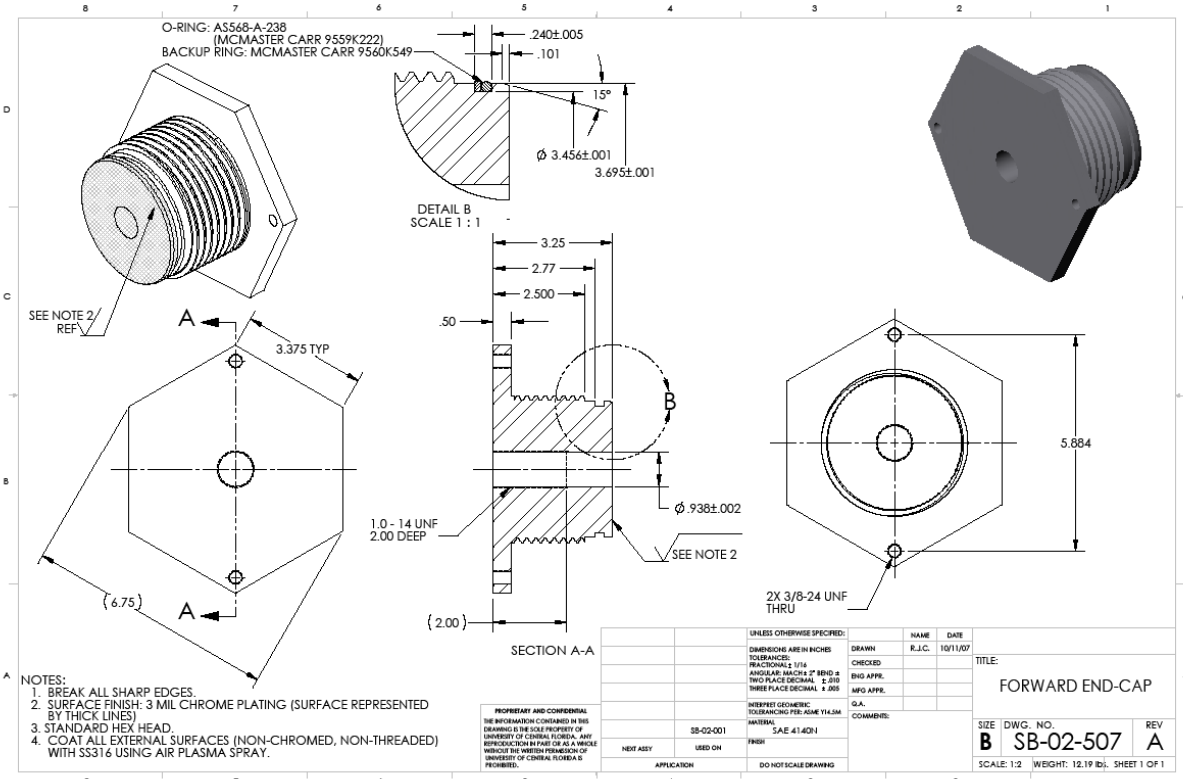

NOTES:
1. BREAK ALL SHARP EDGES.
2. SURFACE FINISH: 3 MIL CHROME PLATING (SURFACE REPRESENTED BY THICK LINES)
3. STANDARD HEX HEAD.
4. COAT ALL EXTERNAL SURFACES (NON-CHROMED, NON-THREADED) WITH SS316 USING AIR PLASMA SPRAY.

PROPRIETARY AND CONFIDENTIAL
THE INFORMATION CONTAINED IN THIS DRAWING IS THE SOLE PROPERTY OF UNIVERSITY OF CENTRAL FLORIDA. ANY REPRODUCTION IN PART OR AS A WHOLE WITHOUT THE WRITTEN PERMISSION OF UNIVERSITY OF CENTRAL FLORIDA IS PROHIBITED.

				NAME	DATE
UNLESS OTHERWISE SPECIFIED:		DRAWN	R.J.C.	10/11/07	
DIMENSIONS ARE IN INCHES TOLERANCES: FRACTIONAL ± 1/16 ANGULAR: MACH ± 2° BEND ± 2° TWO PLACE DECIMAL ± .010 THREE PLACE DECIMAL ± .005		CHECKED			
		ENG APPR.			
		MFG APPR.			
INTERPRET GEOMETRIC TOLERANCING PER: ASME Y14.5M		Q.A.			
MATERIAL	SB-02-001	COMMENTS:			
FINISH	SAE 4140N				
NEXT ASSY	USED ON				
APPLICATION	DO NOT SCALE DRAWING				

TITLE: FORWARD END-CAP

SIZE	DWG. NO.	REV
B	SB-02-507	A

SCALE: 1:2 WEIGHT: 12.19 lbs. SHEET 1 OF 1

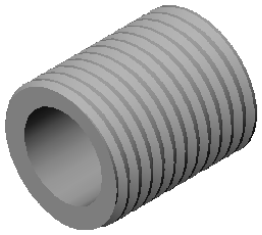

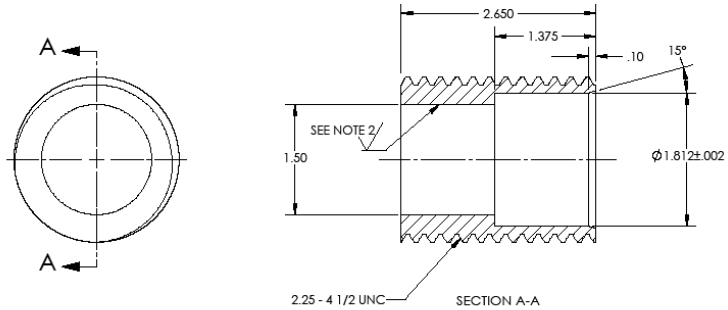

NOTES:
1. BREAK ALL SHARP EDGES.
2. SURFACE FINISH: 3 MIL CHROME PLATING (SURFACE REPRESENTED BY THICK LINES)
3. COAT ALL EXTERNAL SURFACES (NON-CHROMED, NON-THREADED) WITH SS316 USING AIR PLASMA SPRAY.

PROPRIETARY AND CONFIDENTIAL
THE INFORMATION CONTAINED IN THIS DRAWING IS THE SOLE PROPERTY OF UNIVERSITY OF CENTRAL FLORIDA. ANY REPRODUCTION IN PART OR AS A WHOLE WITHOUT THE WRITTEN PERMISSION OF UNIVERSITY OF CENTRAL FLORIDA IS PROHIBITED.

				NAME	DATE
UNLESS OTHERWISE SPECIFIED:		DRAWN	R.J.C.	10/11/07	
DIMENSIONS ARE IN INCHES TOLERANCES: FRACTIONAL ± 1/16 ANGULAR: MACH ± 2° BEND ± 2° TWO PLACE DECIMAL ± .010 THREE PLACE DECIMAL ± .005		CHECKED			
		ENG APPR.			
		MFG APPR.			
INTERPRET GEOMETRIC TOLERANCING PER: ASME Y14.5M		Q.A.			
MATERIAL	SB-02-001	COMMENTS:			
FINISH	SAE 4140N				
NEXT ASSY	USED ON				
APPLICATION	DO NOT SCALE DRAWING				

TITLE: WINDOW FRAME

SIZE	DWG. NO.	REV
B	SB-02-511	A

SCALE: 1:1 WEIGHT: 1.06 lbs. SHEET 1 OF 1

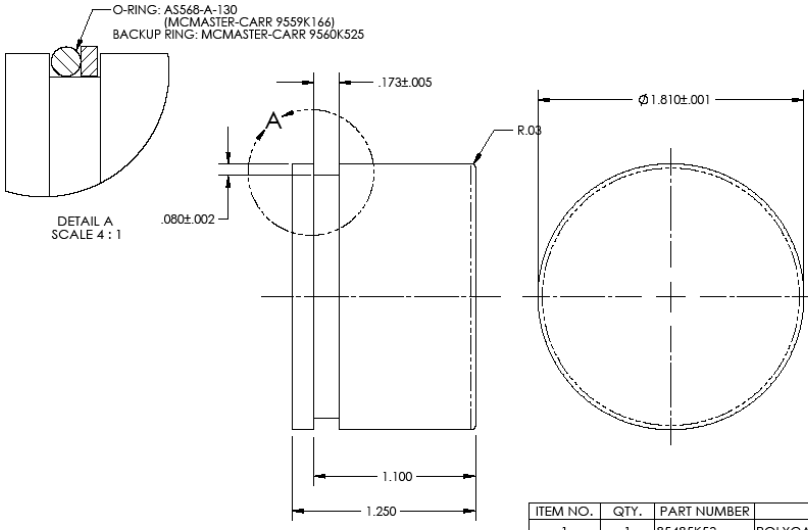

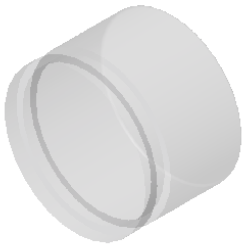

ITEM NO.	QTY.	PART NUMBER	DESCRIPTION	REMARKS
1	1	85485K53	POLYCARBONATE, 2" ROD, CLEAR	McMASTER-CARR
2	1	AS568-A-130	O-RING, PTFE	
3	1	9560K525	BACKUP RING, SPLIT, PTFE	

NOTES:
1. BREAK ALL SHARP EDGES.

UNLESS OTHERWISE SPECIFIED:
DIMENSIONS ARE IN INCHES
TOLERANCES:
FRACTIONAL ± 1/16
ANGULAR: MACH ± 2° BEND ± 2°
TWO PLACE DECIMAL ± .010
THREE PLACE DECIMAL ± .005
INTERPRET GEOMETRIC TOLERANCING PER: ASME Y14.5M
MATERIAL: POLYCARBONATE
FINISH
NEXT ASSY | USED ON
APPLICATION | DO NOT SCALE DRAWING

	NAME	DATE
DRAWN	R.J.C.	10/16/07
CHECKED		
ENG APPR.		
MFG APPR.		
Q.A.		
COMMENTS:		

PROPRIETARY AND CONFIDENTIAL
THE INFORMATION CONTAINED IN THIS DRAWING IS THE SOLE PROPERTY OF UNIVERSITY OF CENTRAL FLORIDA. ANY REPRODUCTION IN PART OR AS A WHOLE WITHOUT THE WRITTEN PERMISSION OF UNIVERSITY OF CENTRAL FLORIDA IS PROHIBITED.

TITLE: WINDOW

SIZE B | DWG. NO. SB-02-301 | REV A
SCALE: 2:1 | WEIGHT: 0.28 lbs. | SHEET 1 OF 1

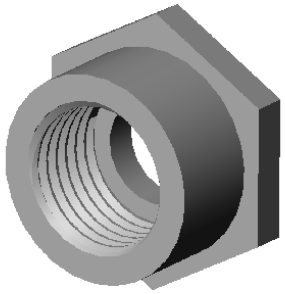

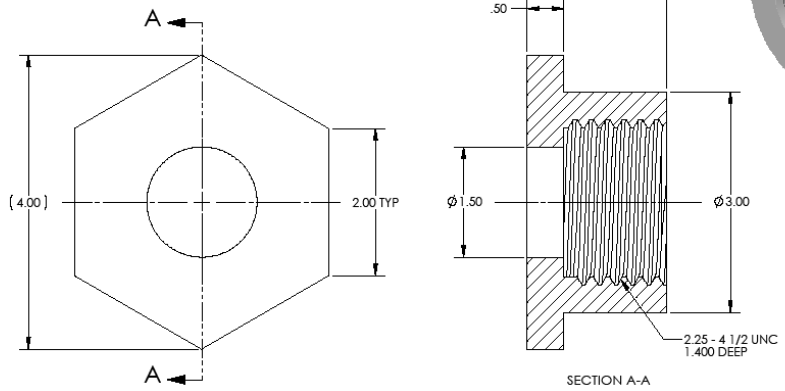

NOTES:
1. BREAK ALL SHARP EDGES.
2. STANDARD HEX HEAD.
3. COAT ALL EXTERNAL SURFACES (NON-CHROMED, NON-THREADED) WITH SS316 USING AIR PLASMA SPRAY.

UNLESS OTHERWISE SPECIFIED:
DIMENSIONS ARE IN INCHES
TOLERANCES:
FRACTIONAL ± 1/16
ANGULAR: MACH ± 2° BEND ± 2°
TWO PLACE DECIMAL ± .010
THREE PLACE DECIMAL ± .005
INTERPRET GEOMETRIC TOLERANCING PER: ASME Y14.5M
MATERIAL: SAE 4140N
FINISH
NEXT ASSY | USED ON
APPLICATION | DO NOT SCALE DRAWING

	NAME	DATE
DRAWN	R.J.C.	10/11/07
CHECKED		
ENG APPR.		
MFG APPR.		
Q.A.		
COMMENTS:		

PROPRIETARY AND CONFIDENTIAL
THE INFORMATION CONTAINED IN THIS DRAWING IS THE SOLE PROPERTY OF UNIVERSITY OF CENTRAL FLORIDA. ANY REPRODUCTION IN PART OR AS A WHOLE WITHOUT THE WRITTEN PERMISSION OF UNIVERSITY OF CENTRAL FLORIDA IS PROHIBITED.

TITLE: WINDOW END-CAP

SIZE B | DWG. NO. SB-02-509 | REV A
SCALE: 1:1 | WEIGHT: 2.60 lbs. | SHEET 1 OF 1

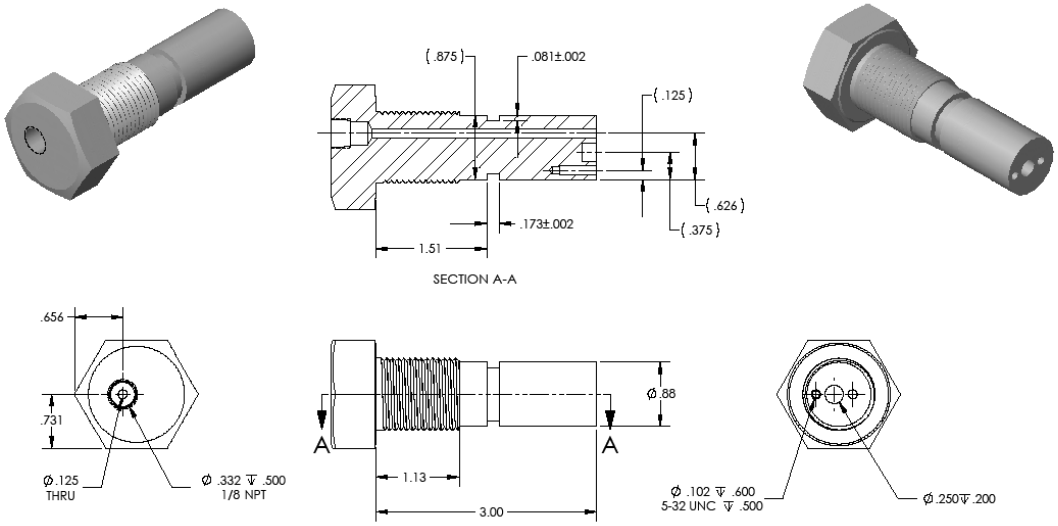

NOTES:
1. CREATE FROM McMASTER-CARR P/N 92865A524
2. COAT ALL EXTERNAL SURFACES (NON-CHROMED, NON-THREADED) WITH SS316 USING AIR PLASMA SPRAY.

PROPRIETARY AND CONFIDENTIAL
THE INFORMATION CONTAINED IN THIS DRAWING IS THE SOLE PROPERTY OF UNIVERSITY OF CENTRAL FLORIDA. ANY REPRODUCTION IN PART OR AS A WHOLE WITHOUT THE WRITTEN PERMISSION OF UNIVERSITY OF CENTRAL FLORIDA IS PROHIBITED.

				NAME	DATE
UNLESS OTHERWISE SPECIFIED:		DRAWN	R.J.C.	9/25/07	
DIMENSIONS ARE IN INCHES TOLERANCES: FRACTIONAL ± 1/16 ANGULAR: MACH ± 2° BEND ± 2° TWO PLACE DECIMAL ± .010 THREE PLACE DECIMAL ± .005		CHECKED			TITLE: SPECIMEN HOLDER 1 IN, MODIFIED
		ENG APPR.			
		MFG APPR.			
INTERPRET GEOMETRIC TOLERANCING PER: ASME Y14.5M		Q.A.			
MATERIAL		COMMENTS:			SIZE B | DWG. NO. SB-02-501 | REV A
FINISH					
NEXT ASSY	USED ON				
APPLICATION	DO NOT SCALE DRAWING				SCALE: 1:1 | WEIGHT: 0.82 lbs. | SHEET 1 OF 1

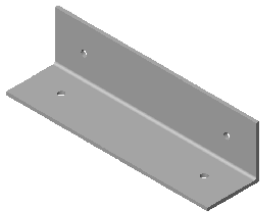

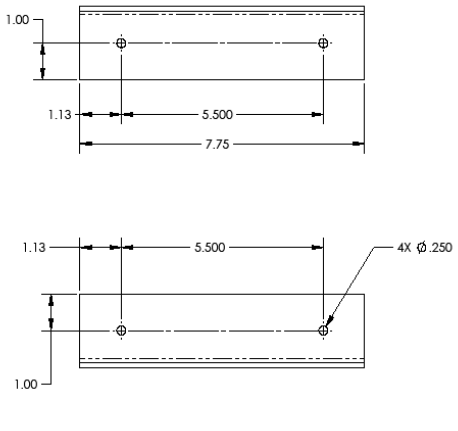

NOTES:
1. BREAK ALL SHARP EDGES.

PROPRIETARY AND CONFIDENTIAL
THE INFORMATION CONTAINED IN THIS DRAWING IS THE SOLE PROPERTY OF UNIVERSITY OF CENTRAL FLORIDA. ANY REPRODUCTION IN PART OR AS A WHOLE WITHOUT THE WRITTEN PERMISSION OF UNIVERSITY OF CENTRAL FLORIDA IS PROHIBITED.

				NAME	DATE
UNLESS OTHERWISE SPECIFIED:		DRAWN	R.J.C.	10/11/07	
DIMENSIONS ARE IN INCHES TOLERANCES: FRACTIONAL ± 1/16 ANGULAR: MACH ± 2° BEND ± 2° TWO PLACE DECIMAL ± .010 THREE PLACE DECIMAL ± .005		CHECKED			TITLE: BRACKET, HOLD DOWN
		ENG APPR.			
		MFG APPR.			
INTERPRET GEOMETRIC TOLERANCING PER: ASME Y14.5M		Q.A.			
MATERIAL	SB-02-001	COMMENTS:			SIZE B | DWG. NO. SB-02-517 | REV A
	Plain Carbon Steel				
FINISH					
NEXT ASSY	USED ON				
APPLICATION	DO NOT SCALE DRAWING				SCALE: 1:2 | WEIGHT: [illegible] | SHEET 1 OF 1

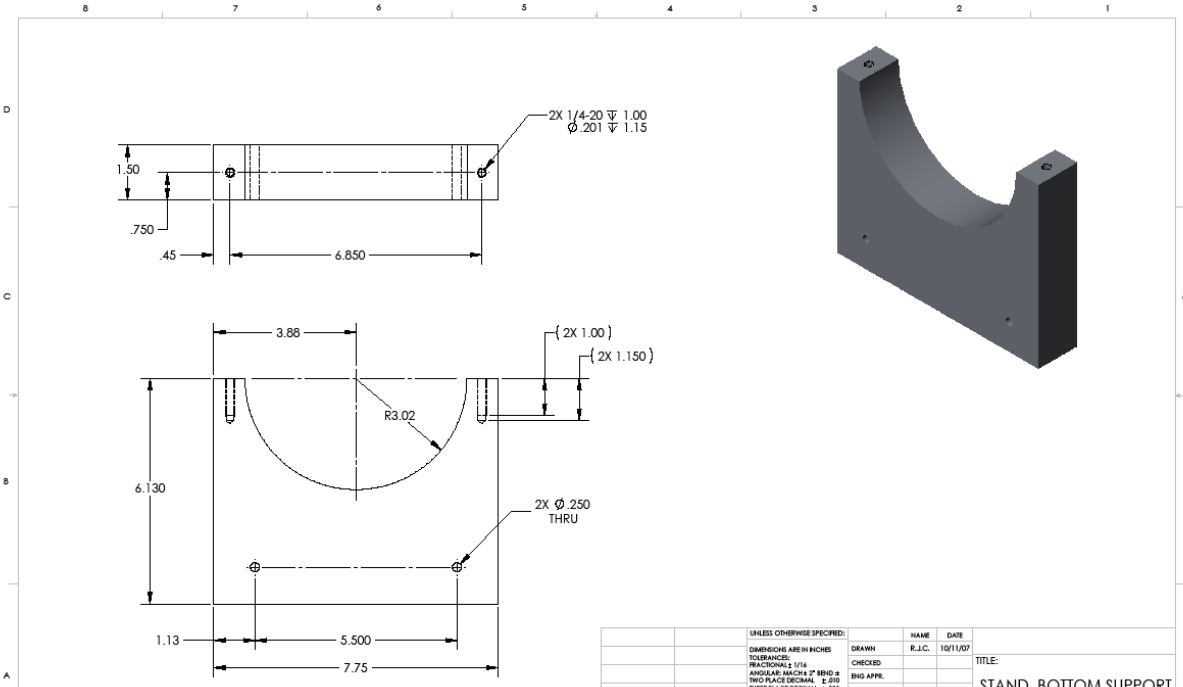
2X 1/4-20 ↧ 1.00
Ø.201 ↧ 1.15
1.50
.750
.45
6.850
3.88
(2X 1.00)
(2X 1.150)
R3.02
6.130
2X Ø.250
THRU
1.13
5.500
7.75
NOTES:
1. BREAK ALL SHARP EDGES.
UNLESS OTHERWISE SPECIFIED:
DIMENSIONS ARE IN INCHES
TOLERANCES:
FRACTIONAL ± 1/16
ANGULAR: MACH ± 2° BEND ± 2°
TWO PLACE DECIMAL ± .010
THREE PLACE DECIMAL ± .005
INTERPRET GEOMETRIC TOLERANCING PER: ASME Y14.5M
MATERIAL
2024 Alloy
FINISH
DO NOT SCALE DRAWING
NAME
DATE
DRAWN
R.J.C.
10/11/07
CHECKED
ENG APPR.
MFG APPR.
Q.A.
COMMENTS:
TITLE:
STAND, BOTTOM SUPPORT
SIZE
B
DWG. NO.
SB-02-515
REV
A
SCALE: 1:2
WEIGHT: 5.01 lbs.
SHEET 1 OF 1
SB-02-001
NEXT ASSY
USED ON
APPLICATION
PROPRIETARY AND CONFIDENTIAL
THE INFORMATION CONTAINED IN THIS DRAWING IS THE SOLE PROPERTY OF UNIVERSITY OF CENTRAL FLORIDA. ANY REPRODUCTION IN PART OR AS A WHOLE WITHOUT THE WRITTEN PERMISSION OF UNIVERSITY OF CENTRAL FLORIDA IS PROHIBITED.

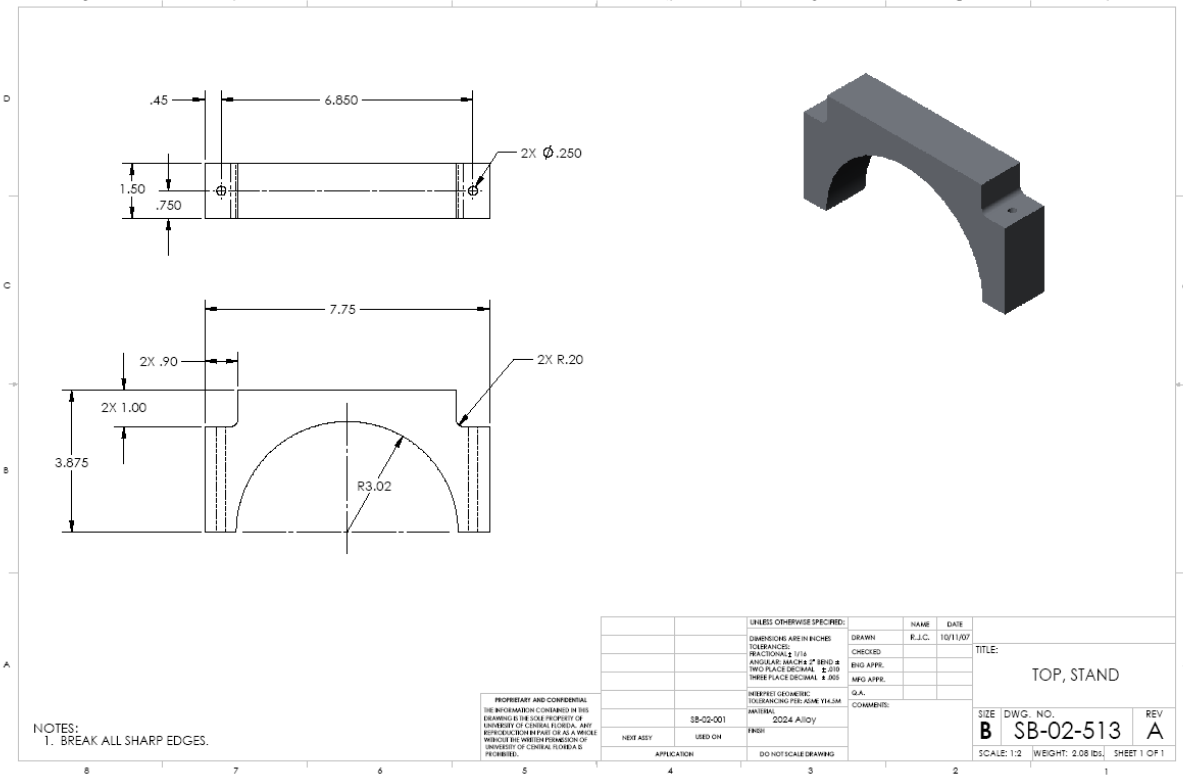
.45
6.850
2X Ø.250
1.50
.750
7.75
2X .90
2X R.20
2X 1.00
3.875
R3.02
NOTES:
1. BREAK ALL SHARP EDGES.
UNLESS OTHERWISE SPECIFIED:
DIMENSIONS ARE IN INCHES
TOLERANCES:
FRACTIONAL ± 1/16
ANGULAR: MACH ± 2° BEND ± 2°
TWO PLACE DECIMAL ± .010
THREE PLACE DECIMAL ± .005
INTERPRET GEOMETRIC TOLERANCING PER: ASME Y14.5M
MATERIAL
2024 Alloy
FINISH
DO NOT SCALE DRAWING
NAME
DATE
DRAWN
R.J.C.
10/11/07
CHECKED
ENG APPR.
MFG APPR.
Q.A.
COMMENTS:
TITLE:
TOP, STAND
SIZE
B
DWG. NO.
SB-02-513
REV
A
SCALE: 1:2
WEIGHT: 2.08 lbs.
SHEET 1 OF 1
SB-02-001
NEXT ASSY
USED ON
APPLICATION
PROPRIETARY AND CONFIDENTIAL
THE INFORMATION CONTAINED IN THIS DRAWING IS THE SOLE PROPERTY OF UNIVERSITY OF CENTRAL FLORIDA. ANY REPRODUCTION IN PART OR AS A WHOLE WITHOUT THE WRITTEN PERMISSION OF UNIVERSITY OF CENTRAL FLORIDA IS PROHIBITED.

APPENDIX E: INSTRUMENTATION CALIBRATION

HIGH ACCURACY AMPLIFIED VOLTAGE OUTPUT PRESSURE TRANSDUCER

7/16-20 OR 1/4 NPT CONNECTIONS

Connector / NPT Model
PX02K1-100G5T
Shown Smaller than Actual Size

PX02
$649
Model Shown

Cable / NPT Model
PX02C0-100G5T
Shown Smaller than Actual Size

PX02 Series

0 to 5 Vdc Output
0-2 to 0-30,000 psi
0-150 mbar to 0-2000 bar

- Internal Shunt Resistor for Easy System Checks
- FM Intrinsically Safe
- All Stainless Steel Construction
- Hermetically Sealed Double Diaphragm Design for Harsh Environments
- Available in Gage, Absolute, Sealed Gage, psi and Metric Ranges
- Cable or Connector Models
- Optional Pressure Ports to Fit Most Industrial Applications

OMEGA's PX02 Series is a high accuracy, amplified voltage output, industrial pressure transducer. All stainless steel construction and a hermetically sealed case makes the PX02 suitable for harsh industrial environments. It is a true high accuracy industrial device with FM Intrinsically Safe rating standard. A broad temperature compensated range of 16 to 71°C (60-160°F) and excellent temperature compensation make this transducer very stable with fluctuating temperatures. The PX02 is available in gage, absolute or sealed models as well as PSI or metric ranges. NPT and 7/16-20 O-ring seal fittings are available for industrial and Hydraulic applications.

To Order *(Specify Model Number)*

RANGE (psi)	7/16-20 MODEL	PRICE	1/4 NPT MODEL	PRICE	COMPAT METERS
Connector Style – Absolute Pressure *(All Ranges Available In Absolute Pressure)*					
0 to 10	PX02K1-010A5T	$745	PX02C1-010A5T	$754	DP41-E, DP25-E
0 to 15	PX02K1-015A5T	745	PX02C1-015A5T	754	DP41-E, DP25-E
0 to 20	PX02K1-020A5T	745	PX02C1-020A5T	754	DP41-E, DP25-E
0 to 25	PX02K1-025A5T	745	PX02C1-025A5T	754	DP41-E, DP25-E
0 to 50	PX02K1-050A5T	685	PX02C1-050A5T	694	DP41-E, DP25-E
Connector Style – Gage Pressure *(All Ranges Also Available In Sealed Gage Pressure)*					
0 to 2	PX02K1-002G5T	$695	PX02C1-002G5T	$714	DP41-E, DP25-E
0 to 5	PX02K1-005G5T	695	PX02C1-005G5T	714	DP41-E, DP25-E
0 to 10	PX02K1-010G5T	695	PX02C1-010G5T	714	DP41-E, DP25-E
0 to 15	PX02K1-015G5T	695	PX02C1-015G5T	714	DP41-E, DP25-E
0 to 50	PX02K1-050G5T	630	PX02C1-050G5T	714	DP41-E, DP25-E
0 to 75	PX02K1-075G5T	630	PX02C1-075G5T	649	DP41-E, DP25-E
0 to 100	PX02K1-100G5T	630	PX02C1-100G5T	649	DP41-E, DP25-E
0 to 200	PX02K1-200G5T	630	PX02C1-200G5T	649	DP41-E, DP25-E
0 to 300	PX02K1-300G5T	630	PX02C1-300G5T	649	DP41-E, DP25-E
0 to 500	PX02K1-500G5T	630	PX02C1-500G5T	649	DP41-E, DP25-E
0 to 1000	PX02K1-1KG5T	630	PX02C1-1KG5T	649	DP41-E, DP25-E
0 to 1500	PX02K1-1.5KG5T	630	PX02C1-1.5KG5T	649	DP41-E, DP25-E
0 to 2000	PX02K1-2KG5T	630	PX02C1-2KG5T	649	DP41-E, DP25-E
0 to 3500	PX02K1-3.5KG5T	630	PX02C1-3.5KG5T	649	DP41-E, DP25-E
0 to 5000	PX02K1-5KG5T	630	PX02C1-5KG5T	649	DP41-E, DP25-E
0 to 7500	PX02K1-7.5KG5T	630	PX02C1-7.5KG5T	649	DP41-E, DP25-E
0 to 10000**	PX02S1-10KG5T	730	not available		DP41-E, DP25-E*
0 to 20000**	PX02S1-20KG5T	730	not available		DP41-E, DP25-E*
0 to 30000**	PX02S1-30KG5T	730	not available		DP41-E, DP25-E*

** 4 digit meter, counts in increments of 10.* *** 1/4HP Tube Fitting*

To order Absolute Pressure replace the "G" in model number with "A" ($50 additional).
To order Sealed Gage units replace "G" in model number with "S" (no charge).
Ordering Examples: 1.) PX02K1-1KG5T is a 1,000 psi gage transducer with 0-5 V output, twist lock connector and 7/16-20 female pressure connection, $630. Mating Connector (not included) PT06F-10-6S, $26.50. 2.) PX02C0-010G5T is a 10 psi gage transducer with 0-5 V output, 10 Ft Cable and 1/4 NPT male pressure connection, $714. Mating Connector (not included) PT06F-10-6S, $26.50.

ALL STAINLESS STEEL TRANSDUCER
MULTIMEDIA COMPATIBILITY
HIGH-PERFORMANCE SILICON TECHNOLOGY

PX309 Series
0 to 5 Vdc Output
0-1 to 0-10,000 psi
0-70 mbar to 0-690 bar

Starts at
$225

- 1, 2, and 5 psi Ranges
- Rugged, Solid State Design
- All Stainless Steel
- High Stability, Low Drift
- 0.25% Accuracy Typical
- RoHS Compliant
- IP65 Protection Class

SPECIFICATIONS

Excitation: 9 to 30 Vdc (<10 mA) (reverse polarity and overvoltage protected)
Output: 0 to 5 Vdc
Accuracy: ±0.25% includes linearity, hysteresis and repeatability
Zero Offset: ±2% FSO; ±4% 1 and 2 psi ranges
Span Setting: ±2% FSO; ±4% 1 and 2 psi ranges
Total Error Band: ±2% FSO, includes linearity, hysteresis, repeatability, thermal hysteresis and thermal errors (except 1 psi = ±4.5% and 2 psi = ±3%)
Long-Term Stability (1 Year): ±0.25% typical
Typical Life: 10 million cycles
Operating Temperature: -40 to 85°C (-40 to 185°F)
Compensated Temperature:
>5 psi Range: -20 to 85°C (-4 to 185°F)
≤5 psi Range: 0 to 50°C (-18 to 122°F)
Proof Pressure:
psia and ≤50 psig: 3x capacity or 20 psi, whichever is greater
≥100 psi: 2x capacity
Burst Pressure: 5x capacity or 25 psi, whichever is greater
Response Time: <1 ms
Shock: 50 g, 11 ms half-sine shock
Vibration: ±20 g
Wetted Parts: 316 SS for all psia ranges and 1 to 50 psig; 17-4 PH SS for ranges 100 to 10,000 psig
Pressure Port: ¼-18 MNPT
Electrical Connections:
PX309: 1.5 m (5') 3-conductor cable
PX319: Mini DIN connector with mating connector included
PX329: Twist-lock connector, mating connector sold separately (PT06V-10-6S)
Weight: 155 g (5.4 oz) max
Note: Units 100 psig and above may be subjected to vacuum on the pressure port without damage
For alternative performance specifications contact Engineering.

Order a snubber to protect your pressure transducer!

PS-4G, $10, shown actual size.
Snubbers protect sensors from fluid hammers/spikes.

Strain, Process & Temperature Meters

with Optional Relays and Analog Output

OMEGA MONOGRAM SERIES

DP25B Series

$245 Basic Unit

U.S. and International Patents.
Used Under License.

Inputs

- Thermocouple
- RTD
- Process (dc Voltage and Current)
- Strain Gage

Options

- Relay Output with Adjustable Deadband
- Isolated or Non-Isolated Analog Output
- Totally Programmable Color Display
- Low Voltage Power Options

Panel Meters/Controllers

The unparalleled accuracy of the OMEGA® DP25B signal conditioner is available in an economical series of panel meters/controllers. The OMEGA® DP25B series of meter/controllers feature a four-digit, 9-segment display plus optional dual 6 amp SPDT relays (Single Pole Double Throw; Form C) and a choice of isolated or non-isolated analog output. The scalable 0-10 Vdc, 0-20 mA, or 4-20 mA analog output can be used for retransmission of the display value or as a proportional control output, as required.
The microprocessor-based DP25B series includes instruments for process (dc voltage and current) strain gage, thermocouple, and RTD.

Common Specifications

Display: 4-digit, 9-segment, 21 mm (0.83") Red, Amber or Green LED (programmable)
Analog-to-Digital Technique: Dual slope
Internal Resolution: 15-bit
Polarity: Automatic
Read Rate: 3/sec
Step Response: 2 seconds
Power: 115 Vac, 230 Vac, 10-32 Vdc, 26-56 Vdc; 6 Watts
Operating Temperature: 0 to 60°C (32 to 140°F)
Storage Temperature: -40 to 85°C (-40 to 185°F)
Relative Humidity: 90% @ 40°C (104°F) (non-condensing)
Dimensions: 48 H x 96 W x 152 mm D (1.89 x 3.78 x 6.0") x 7.0 for DP25
Panel Cutout: 45 x 92 mm (1.772 x 3.622")
Weight: 36 g (1.27 lb)

Thermocouple and RTD Models

The DP25B Series for thermocouple and RTD inputs is a versatile panel meter and limit alarm in one easily programmable instrument. The DP25B-TC is selectable for J, K, T, or J DIN thermocouples. The DP25B-RTD accepts 100 Ω PT (0.00385 curve) RTD's.

DP25B-TC (Thermocouple)

Input Type	Range		Accuracy
J	-210 to 760°C	-346 to 1400°F	0.5°C (0.9°F)
K	-270 to 1372°C	-454 to 2500°F	
T	-210 to 400°C	-346 to 752°F	
J DIN	-200 to 900°C	-328 to 1652°F	

Thermocouple Meter Specifications

Input: Thermocouples types, J, K, T, and J DIN
Outputs: 2 Form C (SPDT) relays, rated 6 Amp 250 Vac; programmable for active high/low alarms with latching/non-latching relays.
Relay Hysteresis: Programmable from 0 to 9999
Accuracy: ±0.50°C (0.9°F) after 30 min. warm-up
Temperature Coefficient: ±50 PPM/°C
Read Rate: 3/sec
Step Response: 2 seconds
Power: 115 Vac, 230 Vac, 10-32 Vdc, 26-56 Vdc; 6 Watts; 240 V RMS overvoltage protection
Isolation: 1500 V peak per Hv test; 354 V peak per IEC spacing
NMR: 60 dB
CMR: 120 dB
Input Resistance: 100 MΩ
Operating Temperature: 0 to 60°C (32 to 140°F)
Storage Temperature: -40 to 85°C (-40 to 185°F)
Analog Output: Scalable

Large-Area Photoreceivers

- *Large photodetector diameter for easy alignment*
- *Adjustable gain settings*
- *Compact housing for tight spaces*

With the extra-large 5- or 8-mm-diameter photodetectors in these photoreceivers, you'll be able to tweak your experiment without worrying about the beam wandering off the photodetector. Just position the photodetector close to where you think the laser beam is and you'll see a signal. No more time-consuming and tedious alignment procedures. To keep your signal from going off scale while you're adjusting your experiment, you can easily switch among the three gain settings of 2×10^3, 10^5, and 2×10^6 V/A.

These photoreceivers are battery powered so you'll need only a single coaxial cable to connect the photodetector to other instruments. This eliminates ground loops, the most common source of noise. (A non-conductive pad electrically isolates the case from the table, further eliminating noise pickup.) To ensure long battery life, we build these photoreceivers using amplifiers with low-current draws. In fact, you can leave these photoreceivers on for three weeks (or 500 hours) before the battery needs to be changed. If you're unsure about the battery status, the built-in battery check can tell you instantly whether or not the battery is good.

The compact housing lets you slide the photoreceiver in wherever you need to quickly check your signal. Since all switches and connectors are located on the top of the housing, you won't have to worry about access or about cables that drag on the table and block your beam. See page 140 for compatible filter holders and FC-fiber adapters.

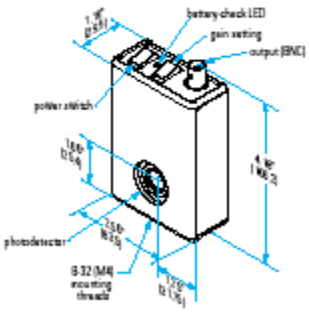

Models 203X

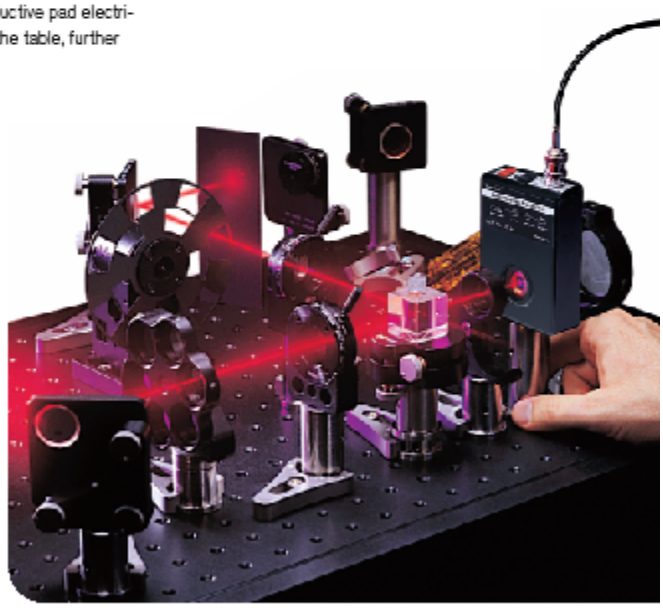

Their slim housing (with the output BNC and switches conveniently located on the top) makes it easy to place these photodetectors right where you want them, even between closely spaced optics.

Model 2031

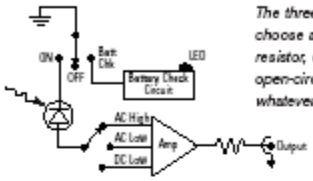

The three-position switch lets you choose a 50-Ω or 10-kΩ load resistor, or you can select the open-circuit setting and provide whatever load resistor you like.

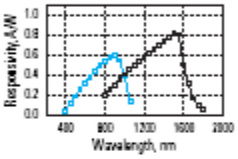

■ *Typical responsivity of the photodetector in the Model 2031.*
■ *Typical responsivity of the photodetector in the Model 2033.*

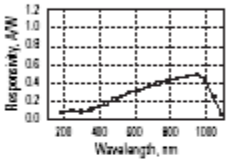

Typical responsivity of the photodetector in the Model 2032.

Wavelength Range	400–1070 nm	190–1100 nm	800–1750 nm
3-dB Bandwidth†	1 MHz, 150 kHz, and 90 kHz	900 kHz, 150 kHz, and 150 kHz	200 kHz, 30 kHz, and 20 kHz
Peak Conversion Gain	1.2×10^6 V/W	1×10^6 V/W	1×10^6 V/W
Typical Maximum Responsivity	0.6 A/W	0.5 A/W	0.8 A/W
Transimpedance Gain†	2×10^3, 10^5, and 2×10^6 V/A	2×10^3, 10^5, and 2×10^6 V/A	2×10^3, 10^5, and 2×10^6 V/A
Output Impedance	100 Ω	100 Ω	100 Ω
Minimum NEP	43 pW/√Hz	58 pW/√Hz	44 pW/√Hz
cw Saturation Power	4 mW	5 mW	3 mW
Maximum Power Density	10 mW/mm²	10 mW/mm²	6 mW/mm²
Photodetector Diameter	8 mm	5.8 mm	5 mm
Power Requirements	Internal 9-V Battery	Internal 9-V Battery	Internal 9-V Battery
Electrical Output	BNC	BNC	BNC
Metric Versions	Add M to Model #	Add M to Model #	Add M to Model #
Model #	**2031**	**2032**	**2033**
Price*	$875	$845	$795
Price, 3-yr Extended Warranty††*	$125	$125	$125

†*As the gain is increased, the bandwidth decreases, as shown in the table above.*
††*See our terms and conditions of sale for more details.*

Related Products: Filter Holders and FC-Fiber Adapters (page 140) • Pedestals and Holding Forks (pages 256, 260) Breakout Cable (page 136)

Definitions of Characteristics (page 142)

For international prices add 10%

CompuScope 1450

Ultra-fast Waveform Digitizer Card for PCI Bus

CompuScope 1450 is a family of 50 MS/s, 14 bit IBM PC based Waveform Digitizer cards for the PCI Bus with very deep, on-board acquisition memory of up to 1 Billion Samples.

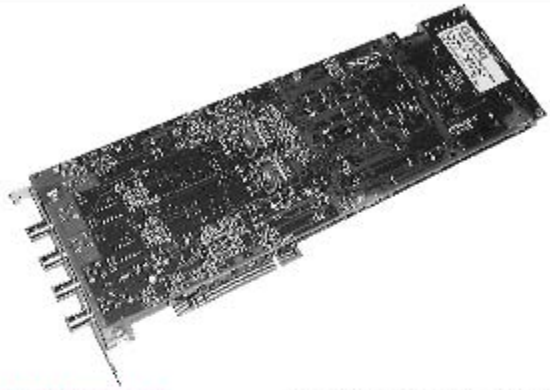

COMPUSCOPE 1450

CompuScope 1450 can sample analog signals at speeds up to 50 MS/s with 14 bit resolution and store the data in the on-board memory.

50 MS/S SAMPLING

CompuScope 1450 uses two monolithic sub-ranging A/D converters, each running at 25 MS/s, to provide a dual-channel simultaneous real-time sampling rate of 50 MS/s.

In the single-channel mode the two ADCs are clocked in a "ping-pong" mode to achieve up to 50 MS/s sampling. An on-board crystal-controlled timing circuit ensures timebase accuracy and long-term thermal stability.

The on-board auto-calibration circuitry allows the two channels to be matched in order to reduce the image signal.

HIGH IMMUNITY TO DIGITAL NOISE

In order to isolate the high-frequency analog circuitry from PCI bus–related digital electronics, a two-board piggy-back configuration is used. This scheme allows maximum separation of analog and digital grounds, thereby providing high immunity to digital noise.

MEMORY DEPTH

CompuScope 1450 is available with memory depths of 1M, 8M, 128M, 512M and 1G (14-bit samples). This memory can be used as a circular buffer for storage of pre- and post-trigger data.

In the single-channel mode, the maximum number of sample points is equal to the memory depth of the CompuScope 1450 model being used, whereas in the dual-channel mode the maximum number of sample points is half the memory depth.

The data stored in the CompuScope 1450 memory can be transferred to the system RAM for post-processing, display or storage to hard disk without any interface bus (no GPIB bus required).

FAST BUS THROUGHPUT

The high-speed, 32 bit, bus-mastering interface to the PCI bus allows the data from the on-board memory of the CompuScope 1450 to be transferred to the system RAM, or any other PCI destination, at sustained rates of up to 80 MB/s under single-tasking operating systems. Under Windows, this rate depends on the architecture of the user application. Under controlled conditions, it is still possible to achieve 80 MB/s recording speed to the system RAM.

BUS MASTERING

CompuScope 1450 is fully capable of becoming a PCI bus master in order to transfer data at the maximum rate of 80 MB/s.

A PCI bus Master is a card which can take control of the bus and transfer data to any PCI target device such as system RAM without any involvement from the CPU.

FLEXIBLE TRIGGERING

CompuScope 1450 features state-of-the-art analog triggering.

An analog comparator provides triggering from either one of the input channels, or from an external signal or from software.

In addition to the trigger source, trigger level and slope are also selectable by software, making the trigger system similar to traditional oscilloscopes.

GAGESCOPE SOFTWARE

CompuScope 1450 is compatible with the powerful and easy-to-use GageScope Software which has become an industry standard for high speed data capture from A/D cards.

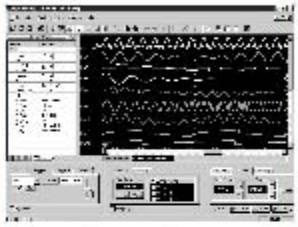

GageScope Software, which sells separately, allows the user to capture data in a Windows environment without having to write a single line of programming code.

Not only can data be captured, manipulated and shared, GageScope allows easy storage of signal files which you can e-mail to your colleagues and share the data.

Some of the powerful features of GageScope include FFT, Averaging, Waveform Parameters, unattended transient capture, remote operation etc.

COMPUSCOPE 1450 FEATURES

- 14 Bit, 50 MS/s A/D
- Up to 1 Gigasample of On-board Acquisition Memory
- 63 dB Signal to Noise Ratio
- Multi-Card Systems of up to 8 channels at 50 MS/s (16 channels at 25 MS/s)
- Fast Data Transfer Rate to System RAM
- Compatible with GageScope Software
- SDKs for C/C++, MATLAB, LabVIEW under Win 95/98/ME and Win NT/2000/XP

GaGe
A Tektronix Technology Company

USB2000+ Miniature Fiber Optic Spectrometer

The USB2000+ Miniature Fiber Optic Spectrometer is a unique combination of technologies a powerful 2-MHz analog-to-digital (A/D) converter, programmable electronics, a 2048-element CCD-array detector, and a high-speed USB 2.0 port. This innovative combination produces our fastest spectrometer yet and provides resolution to 0.35 nm (FWHM). The USB2000+ allows users to capture and store a full spectrum into memory every millisecond (that's 1,000 full spectra every second) when the spectrometer is interfaced to a computer via a USB 2.0 port. The USB2000+ is perfect for chemical, biochemical and other applications where fast reactions need to be monitored.
The USB2000+ offers the following features:

- 1,000 Full Spectra/Second
- Programmable Microcontroller
- Modular design
- User-configured wavelength range and resolution
- Automatically reads the wavelength calibration coefficients of the spectrometer and configures operating software
- USB-to-PC interface; no external power requirements
- RoHS and CE compliance

1,000 Full Spectra/Second

The USB2000+ utilizes an onboard, 2-MHz A/D converter, which allows you to capture and transfer one full spectrum into memory every millisecond when the spectrometer is interfaced to a PC via the USB port.

Programmable Microcontroller

The USB2000+ has an onboard programmable microcontroller that provides flexibility in controlling the spectrometer and accessories. Through a 20-pin connector, you can implement all operating parameters in the software, such as controlling external light sources, creating processes and routines and retrieving data from external devices. The USB2000+ gives you access to 10 user-programmable digital I/Os for interfacing to other equipment; one analog input and one analog output; and a pulse generator for triggering other devices. (Programming the I/Os requires SpectraSuite Spectroscopy Operating Software.)

Facilitated Operation

Setting up the USB2000+ Spectrometer is easy. The user simply installs our Spectrometer Operating Software and then connects the USB cable from the spectrometer to the computer. Wavelength calibration coefficients unique to each spectrometer are programmed into a memory chip right on the USB2000+; the software simply reads these values from the spectrometer. What's more, the USB2000+ requires no external power supply; it draws its power from the computer. In fact, the USB port can be used to power light sources that connect to the spectrometer.

Optimal Performance

The USB2000+ couples a low-cost, high-performance 2048-element linear CCD-array detector with an optical bench that's small enough to fit into the palm of your hand -- the same detector and optical bench that have provided superior performance to the users of our 90,000+ systems out in the field. The USB2000+ also works the same way as other Ocean Optics spectrometers in that it accepts light energy transmitted through single-strand optical fiber and disperses it via a fixed grating across the linear CCD array detector, which is responsive from 200-1100 nm.

Modular Design

Just as with all other Ocean Optics user-configured spectrometers, users work with our applications scientists when selecting the USB2000+ -- choosing from 14 gratings, 6 slits and hundreds of fiber optic accessories such as light sources, probes and optical fibers to create the optimal system for their application.
Users can also choose from Ocean Optics' complete line of spectroscopic accessories to use with the USB2000+. Most accessories have SMA connectors for application flexibility. Changing the sampling system is as easy as unscrewing a connector and adding new components or accessories, such as light sources, sampling holders, filter holders, flow cells, fiber optic probes and sensors, collimating lenses, attenuators, diffuse reflectance standards, integrating spheres and an extensive line of optical fibers.

USB Optical Bench Options

What makes the USB spectrometers (USB2000+ and USB4000) so special are the options that allow you to configure the bench for your application. Our Applications Scientists can help you choose the optimum components, or you can follow this guide to choose an entrance aperture size, detector accessories, filters, a grating and more. The diagram below shows how light moves through the asymmetrical crossed Czerny-Turner optical bench, which has no moving parts that can wear or break; all components specified are fixed in place at the time of manufacture.

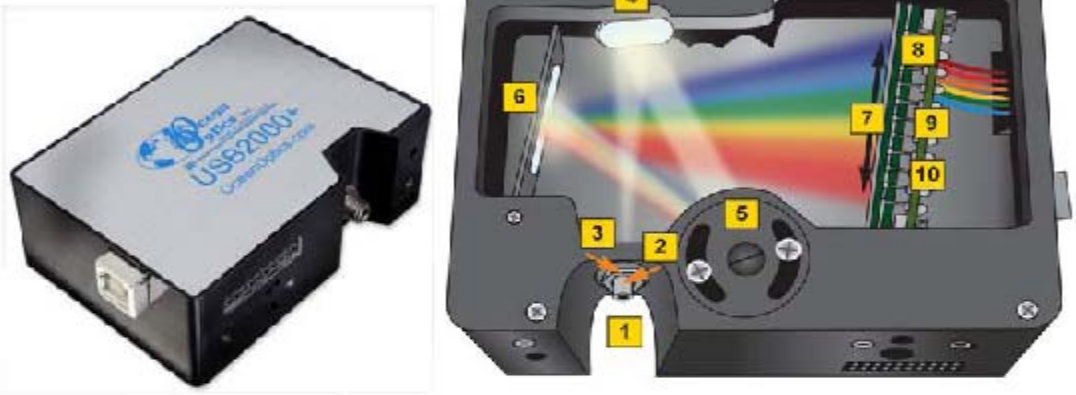

1	SMA 905 Connector	Light from a fiber enters the optical bench through the SMA 905 Connector. The SMA 905 bulkhead provides a precise locus for the end of the optical fiber, fixed slit, absorbance filter and fiber clad mode aperture.
2	Fixed Entrance Slit (specify slit size)	Light passes through the installed slit, which acts as the entrance aperture. Slits come in various widths from 5 µm to 200 µm. The slit is fixed in the SMA 905 bulkhead to sit against the end of a fiber.
3	Longpass Absorbing Filter (optional)	If selected, an absorbance filter is installed between the slit and the clad mode aperture in the SMA 905 bulkhead. The filter is used to block second- and third-order effects or to balance color.
4	Collimating Mirror (specify standard or SAG+)	The collimating mirror is matched to the 0.22 numerical aperture of our optical fiber. Light reflects from this mirror, as a collimated beam, toward the grating. You can opt to install a standard mirror or a UV absorbing SAG+ mirror.
5	Grating & Wavelength Range (specify grating & starting wavelength)	We install the grating on a platform that we then rotate to select the starting wavelength you've specified. Then we permanently fix the grating in place to eliminate mechanical shifts or drift.
6	Focusing Mirror (specify standard or SAG+)	This mirror focuses first-order spectra on the detector plane. Both the collimating and focusing mirrors are made in-house to guarantee the highest reflectance and the lowest stray light possible. You can opt to install a standard or SAG+ mirror.
7	L2 & L4 Detector Collection Lenses (optional)	One of these cylindrical lenses, made in-house to ensure aberration-free performance, is fixed to the detector to focus the light from the tall slit onto the shorter detector elements. It increases light-collection efficiency. The L2 is for the USB2000+; the L4 is for the USB4000.
8	Detector	For the USB2000+ we offer the 2048-element Sony ILX511 linear CCD array detector. For the USB4000, we offer the 3648-element Toshiba TCD1304AP linear CCD array detector. Each pixel responds to the wavelength of light that strikes it. Electronics bring the complete spectrum to the software.
9	OFLV Variable Longpass Order-sorting Filter (optional)	Our proprietary filters precisely block second- and third-order light from reaching specific detector elements.
10	UV2 & UV4 Detector Upgrades (optional)	When selected, the detector's standard BK7 window is replaced with a quartz window to enhance the performance of the spectrometer for applications <340 nm. The UV2 is for the USB2000+; the UV4 is for the USB4000.

Specifications

Physical	
Dimensions:	89.1 mm x 63.3 mm x 34.4 mm
Weight:	190 grams
Detector	
Detector:	Sony ILX511 linear silicon CCD array
Detector range:	200-1100 nm
Pixels:	2048 pixels
Pixel size:	14 µm x 200 µm
Pixel well depth:	~62,500 electrons
Sensitivity:	75 photons/count at 400 nm; 41 photons/count at 600 nm
Optical Bench	
Design:	f/4, Symmetrical crossed Czerny-Turner
Focal length:	42 mm input; 68 mm output
Entrance aperture:	5, 10, 25, 50, 100 or 200 µm wide slits or fiber (no slit)
Grating options:	14 different gratings, UV through Shortwave NIR
HC-1 grating option:	No
Detector collection lens option:	Yes, L2
OFLV filter options:	OFLV-200-850; OFLV-350-1000
Other bench filter options:	Longpass OF-1 filters
Collimating and focusing mirrors:	Standard or SAG+
UV enhanced window:	Yes, UV2
Fiber optic connector:	SMA 905 to 0.22 numerical aperture single-strand optical fiber
Spectroscopic	
Wavelength range:	Grating dependent
Optical resolution:	~0.3-10.0 nm FWHM
Signal-to-noise ratio:	250:1 (at full signal)
A/D resolution:	16 bit
Dark noise:	50 RMS counts
Dynamic range:	2 x 10^8 (system); 1300:1 for a single acquisition
Integration time:	1 ms to 65 seconds
Stray light:	<0.05% at 600 nm; <0.10% at 435 nm
Corrected linearity:	>99.8%
Electronics	
Power consumption:	90 mA @ 5 VDC
Data transfer speed:	Full scans to memory every 1 ms with USB 2.0 or 1.1 port, 300 ms with serial port
Inputs/Outputs:	No
Analog channels:	No
Auto nulling:	No
Breakout box compatibility:	No
Trigger modes:	3 modes

Strobe functions:	Yes
Gated delay feature:	Yes
Connector:	10-pin connector
Computer	
Operating systems:	Windows 98/Me/2000/XP, Mac OS X and Linux with USB port; Any 32-bit Windows OS with serial port
Computer interfaces:	USB 2.0 @ 480 Mbps; RS-232 (2-wire) @ 57.6 K baud
Peripheral interfaces:	I2C inter-integrated circuit

Insulated Leadwire

Conax Buffalo Model PL (Power Lead) Glands seal on insulated leadwire for use in transformers, motors, conduit boxes and pressure/vacuum chambers and as power or instrument feedthroughs. The soft sealant technology seals against gases or liquids and resists element movement under pressure. Immersion length adjustments and easy replacement of elements can be accomplished in the field.

PL glands may be purchased with or without wire. If supplied with wire, solid copper wire with Kapton® insulation is standard. This is provided as 24" total with the gland centered at mid-point. Standard sealants are Grafoil or Teflon. Other materials for wire and sealants can be provided for special applications. Consult your Conax Buffalo sales engineer for more information on available options.

Terminals can be furnished on all wire ends if specified, at additional cost. Bulk wire is available from Conax Buffalo for field assembly of PL glands. (See the Accessories Section, page 152.)

PL gland bodies with NPT threads and SAE threads are constructed from 303SST standard. Weld-neck style gland bodies are constructed from 316LSST standard. Caps and followers for all styles are constructed from 303SST standard. Many optional materials are also available, including 316LSST, Monel 405, Hastelloy C276, Inconel and more. For information on alternative materials, see page 7. Cap Style A offers a mounting thread only. Cap Style B provides threading on both ends for attachment to conduit or terminal heads. Alternative sealant materials are available. Please consult a Conax Buffalo sales engineer for custom needs.

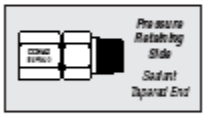

Type A has mounting thread only.

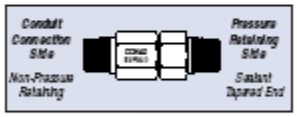

Type B has cap end threaded. B Cap NPT matches the standard mounting NPT.

- Temperature Range: -300° F to +450° F (-185° C to +232° C)
- Pressure Range: Vacuum to 10,000 PSIG (690 bar) – see Pressure Ratings in Specifications Chart.
- 600 Volts to 55 amps
- Seals 1-18 Wires
- Easy installation – no "potting"
- Wire Identification Markers applied
- Thermocouple Material conductors available, 18 gauge standard, other wire gauges optional

Accessories

The replaceable sealant permits repeated use of the same fitting. Assembly is simple and may be done in the field. Simply insert the elements and torque the cap. To replace the sealant or elements, simply loosen the cap, replace the necessary items, relubricate and retorque the cap.

Glands are supplied factory lubricated. When reused, the glands should be relubricated to maintain the published torque and pressure ratings. If glands are cleaned prior to assembly, they should be relubricated. On weld mount models, the heat from the welding process will destroy the lubricant. These models must be relubricated prior to use. See page 153 for information on our lubrication kit.

Replacement Packing Sets are available. These consist of a sealant and two insulators. Replacement sealants may also be ordered separately.

To order a Replacement Packing Set, order
RPS – (Gland) – (Wire Gauge) – (Number of Holes) – (Sealant)

Example: *RPS-PL-12-3-T*

To order a Replacement Sealant only, order
RS – (Gland) – (Wire Gauge) – (Number of Holes) – (Sealant)

Example: *RS-PL-12-3-T*

Catalog Numbering System

PL Gland
- PL

Modifiers are added in parentheses to indicate optional mounting methods. See specifications chart for the proper modifiers.

Wire Gauge
- 20
- 18
- 16
- 14
- 12
- 10
- 8

Cap Style
- A – has mounting thread only
- B – has cap end threaded

Number of Wires Sealed
- 1
- 2
- 3
- 4
- 6
- 8
- 10
- 12
- 18

Sealant
- T – Teflon
- G – Grafoil

Other sealant materials also available.

PL Gland – Wire Gauge – Cap Style – Number of Wires Sealed – Sealant – Wire Length Cap Side – Wire Length Body Side

Example: *PL-12-A3-T, 24/36*
(With Non-Standard Wire Length)

Example: *PL-12-A3-T*
(With Standard Wire Length)

Example: *PL-18(J)-A2-T, 24/36*
(With Thermocouple Material Conductors)

Example: *PL-12-A3-T-XX*
(Without Conductors)

(Power Lead) Sealing

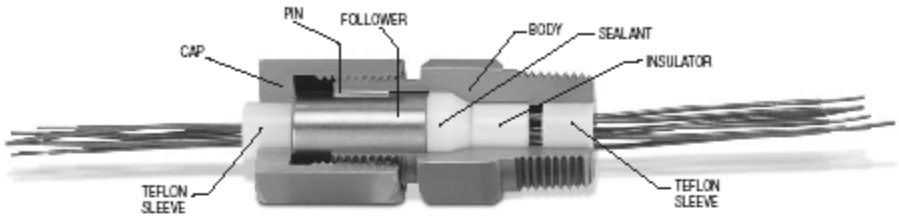

PL Selection Guide

Wire Gauge	Standard Number of Wires Offered								
	1	2	3	4	6	9	10	12	18
20		X	X	X	X	X			X
18	X	X	X	X	X	X	X	X	
16		X	X	X	X	X	X	X	
14	X	X	X	X	X	X	X	X	
12		X	X	X	X				
10		X	X	X					
8		X	X						

The number of wires offered is dependent on the mounting port size. See the Specifications charts on the subsequent pages for details.

Torque (ft-lbs)

	Number of Holes	Grafoil	Teflon
PL-20	2,3,4	90-100	60-70
PL-20	6,8	150-165	90-100
PL-20	18	250-265	125-140
PL-18	1	20-30	12-15
PL-18	2,3,4	90-100	60-70
PL-18	6,8	150-165	90-100
PL-18	10,12	250-265	125-140
PL-16	2,3,4	90-100	60-70
PL-16	6,8	150-165	90-100
PL-16	10,12	250-265	125-140
PL-14	1	25-30	12-15
PL-14	2	90-100	60-70
PL-14	3,4,6,8	150-165	90-100
PL-14	10,12	250-265	125-140
PL-12	2,3,4,6	150-165	90-100
PL-10	2,3,4	150-165	80-90
PL-8	2	150-165	75-85
PL-8	3	250-265	125-140

All pressure and torque ratings were determined at 68° F (20° C) using solid Kapton-insulated copper conductors as the element.

For proper assembly of these sealing glands, see the Assembly Instructions provided on page 156.

APPENDIX F: PRESSURE TRANSDUCER CALIBRATION CURVES

Table 9: Calibration Curve for PX02C1-7.5KG5T

Nominal	As Read
psi	vdc
0	0.0012
3750	2.5076
7500	5.0073
3750	2.5103
0	0.001

Omega display setup	
Rd.5.0	
IN 1	0002
Rd 1	0000
IN 2	5010
Rd 2	7500

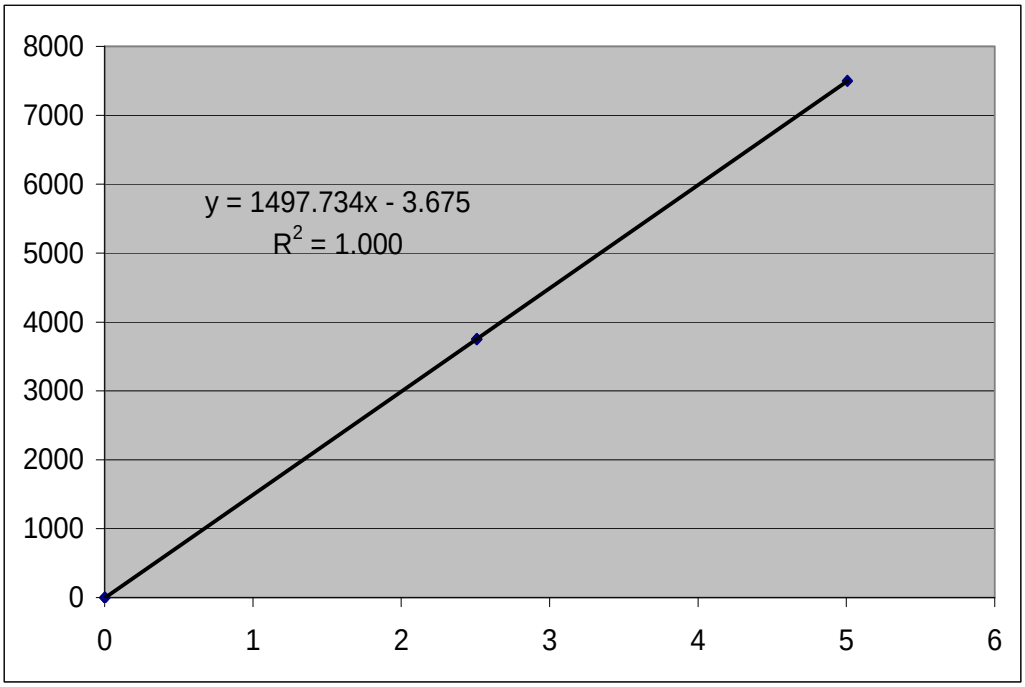

Table 10: Calibration Curve for PX309-7.5KG5V

Nominal	As Read	
psi	psi	vdc
0	0	0.001
1500	1497	0.998
3750	3748.5	2.499
5000	4997	3.331
7500	7506	5.004
7000	7005	4.67
5000	4997	3.331
3750	3748.5	2.499
1500	1497	0.998
0	0	0.001

Omega display setup	
Rd.5.0	
IN 1	0000
Rd 1	0002
IN 2	5001
Rd 2	7500

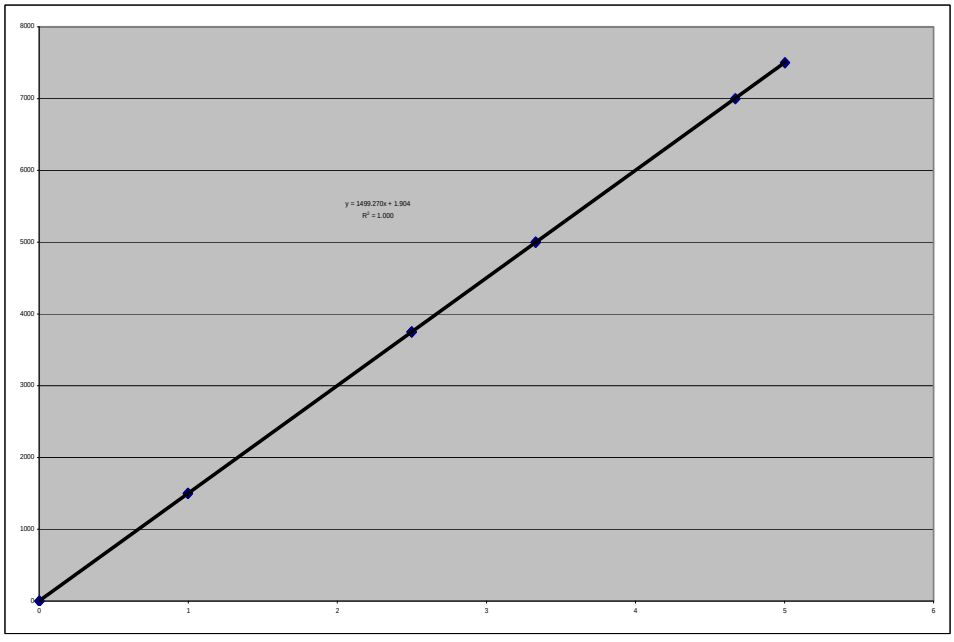

APPENDIX G: MATLAB CODE

```
% GageScope Data Smoother
% Rodolphe 'Gino' CARRO
% 04-09-2006

close all
clear all
Counter = 0;
Delta = 150;

bb = input('\nEnter the Batch Number: ');
Batch = num2str(bb);

if (bb < 10)
    Batch_Folder = strcat('MDA', '0', Batch);
else
    Batch = num2str(bb);
    Batch_Folder = strcat('MDA', Batch);
end

Current_Directory = pwd;
Batch_Directory = strcat (Current_Directory, '\', Batch_Folder);

if (isdir(Batch_Directory) == 1)
    cd (Batch_Directory);
else fprintf('%s is not an existing folder \n', Batch_Folder);
end

Sample_Folder = strcat(Batch_Folder, '-01');
ss = 2;

while (isdir(Sample_Folder) == 1)
    Sample = num2str(ss);
    if (ss < 10)
        Sample_Folder = strcat(Batch_Folder, '-0', Sample);
    else
        Sample_Folder = strcat(Batch_Folder, '-', Sample);
    end

    ss = ss + 1;
end

Number_of_Samples = ss -2;
fprintf('\nThere are %d Samples available for Batch Number 0%d \n',
Number_of_Samples, bb);
ss = 1;

while (ss <= Number_of_Samples)
    Sample = num2str(ss);
    if (ss < 10)
        Sample_Folder = strcat(Batch_Folder, '-0', Sample);
    else
        Sample_Folder = strcat(Batch_Folder, '-', Sample);
```

```
    end
    if (isdir(Sample_Folder) == 1)
        cd (Sample_Folder),
        Pressure_File = strcat(Sample_Folder, '-01.asc');
        Light_File = strcat(Sample_Folder, '-02.asc');
        fid = fopen (Pressure_File);
        if fid ==-1
            fprintf ('\nThere is no data recorded for Sample %s \n',
Sample_Folder);
            Counter = Counter + 1;
        else
            Pressure_Data_Original = dlmread (Pressure_File, '\t');
            Light_Data_Original = dlmread (Light_File, '\t');
            Pressure_Data_Original_Size = size (Pressure_Data_Original,1);
            for (Row = 1 : 2 : Pressure_Data_Original_Size / 2)
                Pressure_Data_Original(Row,:) = [];
                Light_Data_Original(Row,:) = [];
            end
            Pressure_Data_Original_Size = size (Pressure_Data_Original,1);
            for (Row = 1 : 2 : Pressure_Data_Original_Size / 2)
                Pressure_Data_Original(Row,:) = [];
                Light_Data_Original(Row,:) = [];
            end
        %    Pressure_Data_Original_Size = size
(Pressure_Data_Original,1);
         %   for (Row = 1 : 2 : Pressure_Data_Original_Size / 2)
          %      Pressure_Data_Original(Row,:) = [];
           %     Light_Data_Original(Row,:) = [];
            %end

            P_Time = Pressure_Data_Original(:, 1);
            L_Time = Light_Data_Original(:, 1);
            Pressure_In = (Pressure_Data_Original(:, 2) * 1495.752 -
2.542779);
            Light_In = Light_Data_Original(:, 2);
            N = 37;

            %   function yout = smooth(yin,N)

            % SMOOTH.M: Smooths vector data
            % YOUT=SMOOTH(YIN,N) smooths the data in YIN using a running
            % mean over 2*N+1 successive point, N points on each side of
            % the current point. At the ends of the series skewed or one-
            % sided means are used.
            %           Olof Liungman, 1997
            %           Dept. of Oceanography, Earth Sciences Centre
            %           Göteborg University, Sweden

            %if nargin<2, error('Not enough input arguments!'), end

            [rows,cols] = size(Pressure_In);
            Pressure_In = (Pressure_In(:))';
            Light_In = (Light_In(:))';
```

```
l = length(Pressure_In);
Pressure_Out = zeros(1,l);
Light_Out = zeros(1,1);
P_Temp = zeros(2*N+1,l-2*N);
L_Temp = zeros(2*N+1,l-2*N);
P_Temp(N+1,:) = Pressure_In(N+1:l-N);
L_Temp(N+1,:) = Light_In(N+1:l-N);

for i = 1:N
  Pressure_Out(i) = mean(Pressure_In(1:i+N));
  Light_Out(i) = mean(Light_In(1:i+N));
  Pressure_Out(l-i+1) = mean(Pressure_In(l-i-N:l));
  Light_Out(l-i+1) = mean(Light_In(l-i-N:l));
  P_Temp(i,:) = Pressure_In(i:l-2*N+i-1);
  L_Temp(i,:) = Light_In(i:l-2*N+i-1);
  P_Temp(N+i+1,:) = Pressure_In(N+i+1:l-N+i);
  L_Temp(N+i+1,:) = Light_In(N+i+1:l-N+i);
end

Pressure_Out(N+1:l-N) = mean(P_Temp);
Light_Out(N+1:l-N) = mean(L_Temp);

if size(Pressure_Out)~=[rows,cols],
    Pressure_Out = Pressure_Out';
    Light_Out = Light_Out';
end

Pressure_Light_Matrix = [P_Time, Pressure_Out, Light_Out];

%Saving the file
Smoothed_File = strcat('Smoothed-', Sample_Folder, '.asc');
dlmwrite (Smoothed_File, Pressure_Light_Matrix, '\t');
fclose(fid);


%finding the Minimum and Maximum Pressure
[M, N] = size (Pressure_Light_Matrix);
Max = Pressure_Light_Matrix(1, 2);
Min = Pressure_Light_Matrix(1, 2);
for Indice = 2 : 1 : M-1
    Previous = Pressure_Light_Matrix(Indice-1, 2);
    Current = Pressure_Light_Matrix(Indice, 2);
    Next = Pressure_Light_Matrix(Indice+1, 2);
    if Current > Previous
        CurrentMax = Current;
        if CurrentMax > Max
            Max = CurrentMax;
            MaxIndice = Indice;
        end
    end
    if Current < Next
        CurrentMin = Current;
```

```
                    if CurrentMin < Min
                        Min = CurrentMin;
                        MinIndice = Indice;
                    end
                end

            end

            if MaxIndice > M - Delta;
                MaxIndice = M - Delta;
            end

            if MinIndice < 111
                MinIndice = 111;
            end

            Max;
            MaxIndice;
            Min;
            MinIndice;

            i = 1;
            for Indice = MinIndice - 110 : 1 : MaxIndice + Delta
                ReducedP_Time(i, 1) = P_Time(Indice);
                ReducedPressure_Out(i, 1) = Pressure_Out(Indice);
                ReducedLight_Out(i, 1) = Light_Out(Indice);
                ReducedPressure_Light_Matrix = [ReducedP_Time,
ReducedPressure_Out, ReducedLight_Out];
                i = i + 1;
            end

            %Saving the reduced file (not quite working properly yet)
            Smoothed_R_File = strcat('Smoothed_R-', Sample_Folder,
'.asc');
            dlmwrite (Smoothed_R_File, ReducedPressure_Light_Matrix,
'\t');

        end
    end
    ss = ss + 1;
    cd ..;
end

cd ..;

Total = ss - Counter - 1;

fprintf('\n%d Samples have been analysed.\n\n', Total);
```

APPENDIX H: FINITE ELEMENT ANALYSIS

Here is a list of the assumptions used to conservatively simplify the Finite Element Model (FEM) representing the strand burner assembly:

- The complete strand burner assembly as represented on
- Figure 37 was modeled and meshed using Quad Shell 2D Mesh. A 3D meshing was deemed not necessary due to the simple (uniform and normal to nodes) load distribution.

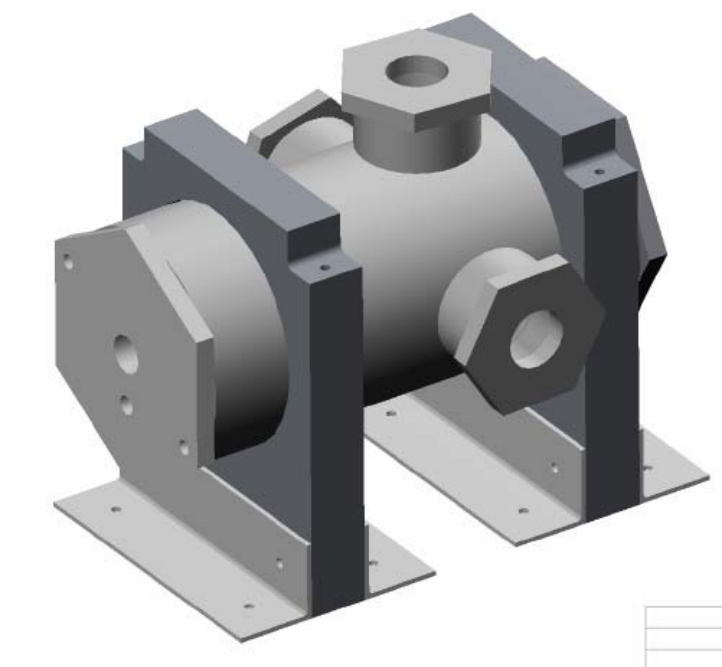

Figure 37: SB-II Configuration for FEM

- The thickness variation from the threads was not modeled throughout the assembly.
- The WINDOW FRAMES (SB-02-511) were not modeled separately but considered integral with the WINDOW FRAMES (SB-05-509).
- Isotropic AISI 4140 steel material properties was assigned to every metallic components, including the STRAND HOLDER (SB-02-501). Refer to
- Figure 38 for the detail of these properties.

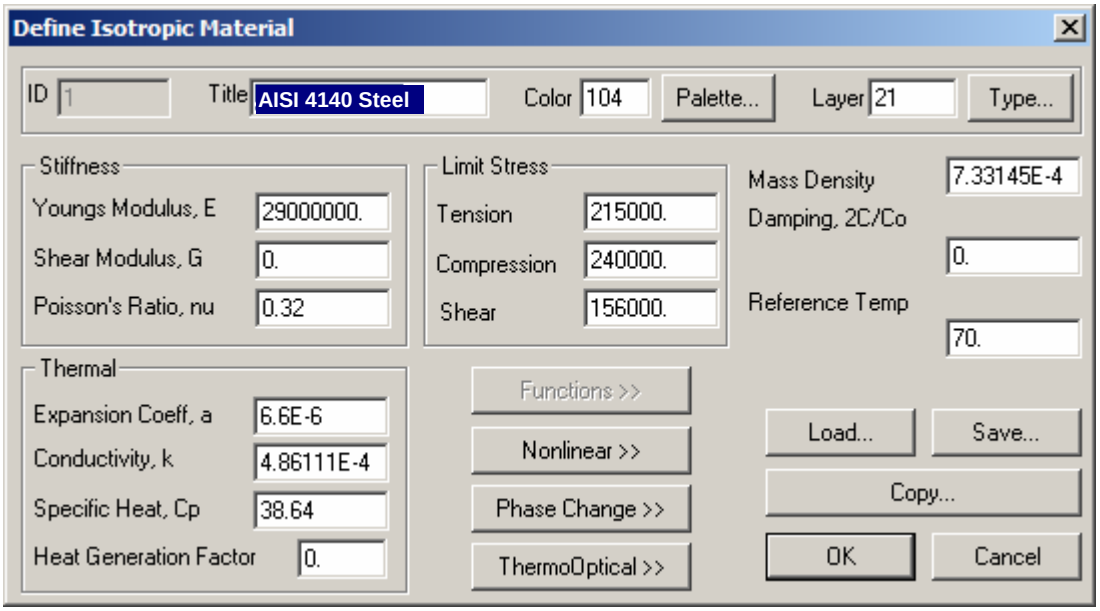

Figure 38: Isotropic AISI 4140 Steel Material Properties as Assigned to Metallic Components

- The isotropic material properties assigned to the four (4) WINDOWs (SB-02-301) were as defined in
- Figure 39.

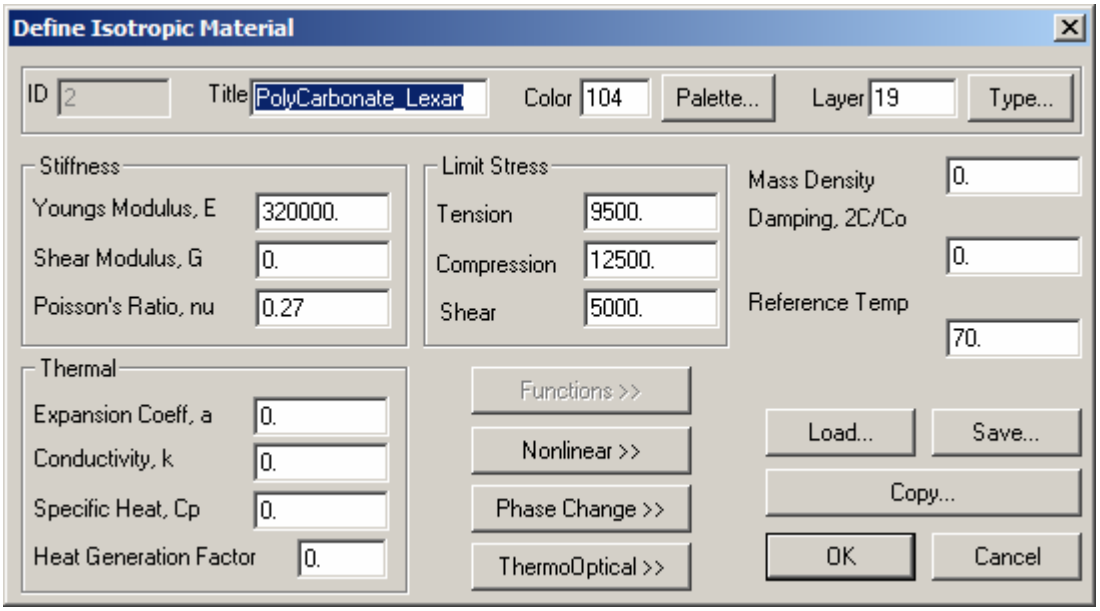

Figure 39: Isotropic Polycarbonate Material Properties as Assigned to the Windows

- A mid surface was generated for the MAIN BODY (SB-02-503) with three (3) co-planar 1.81 in apertures for the windows (Ref. Figure 40)

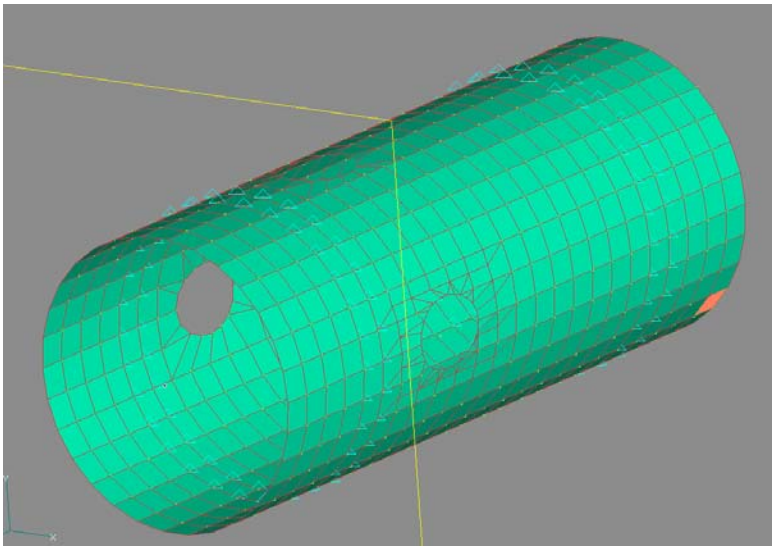

Figure 40: Main Body Mid-Surface with the Window Apertures

- The END-CAPs were modeled using the same principles as for the MAIN BODY as seen on Figure 41.

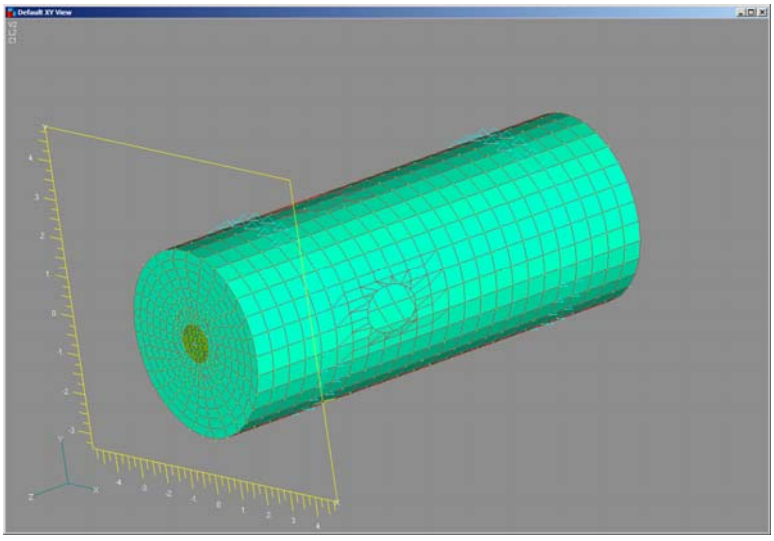

Figure 41: FEM Representation of the Forward End-Cap

- Then the four (4) WINDOWs were modeled using Quads and Tri Mesh (Ref.
- Figure 42) and assigned the properties of Lexan (
- Figure 39).

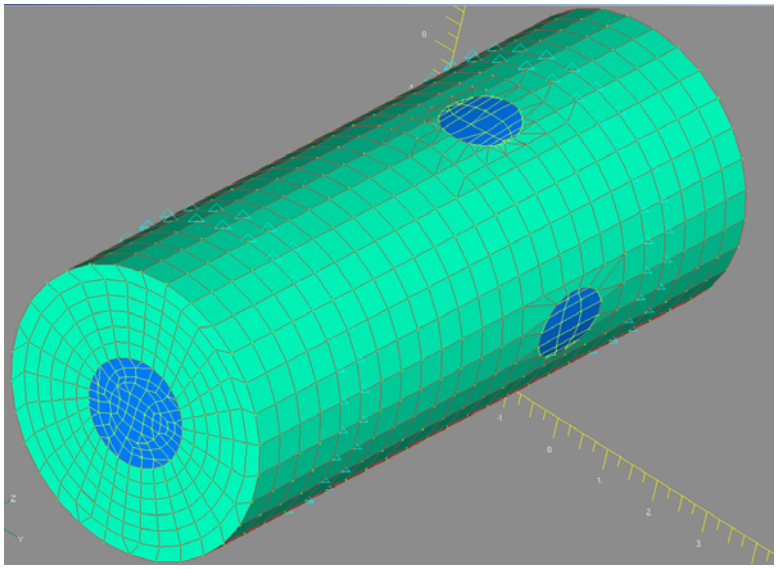

Figure 42: FEM Representation of the Lexan Windows

- The constrains were modeled as presented on Figure 43 to replicate the constrictive action provided by the strand burner braces (SB-02-513 and SB-02-515)

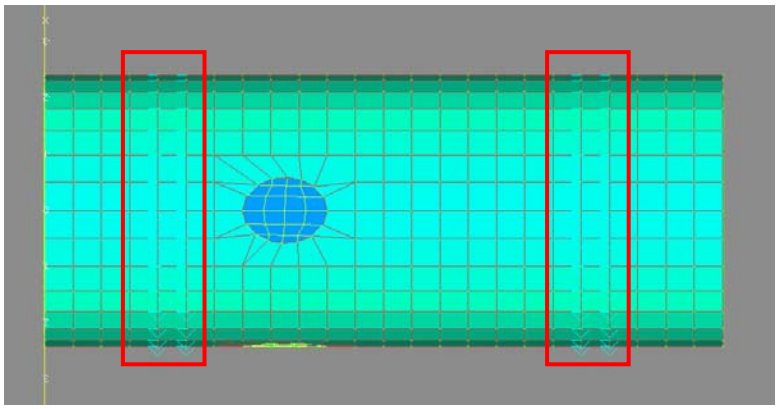

Figure 43: FEM Representation of the Constraints

- Every internal surface was subjected to a uniform and normal load distribution to reproduce a 340 atm (5000 psi) pressurization. Figure 44 shows a cross section of the FEM and the force vectors applied to the nodes.

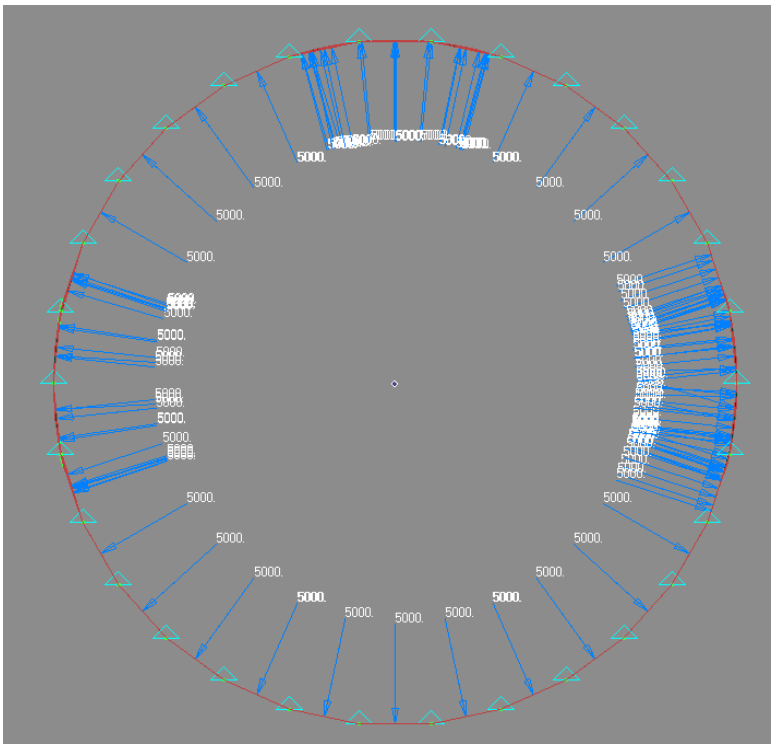

Figure 44: Cross Section View of the FEM and the Force Vectors

The model was then analyzed using the NE / Nastran for Windows 8.3 solver. The major and minor principal stresses are displayed on Figure 45 and Figure 46 respectively.

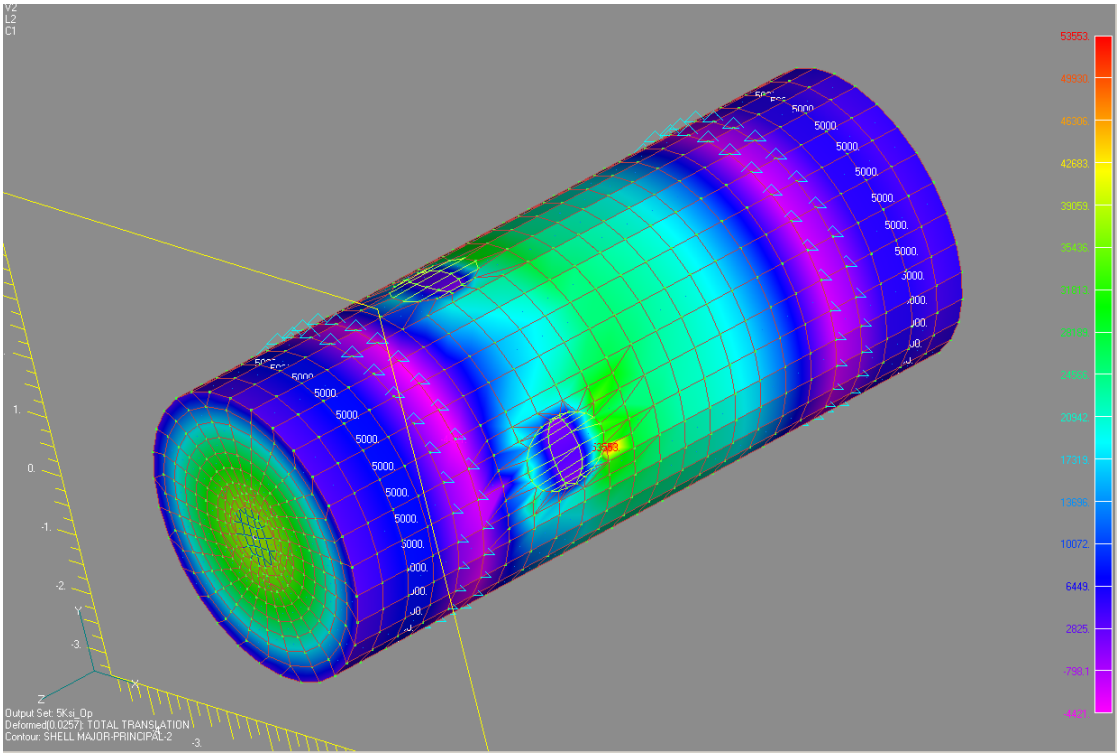

Figure 45: Major Principal Stresses

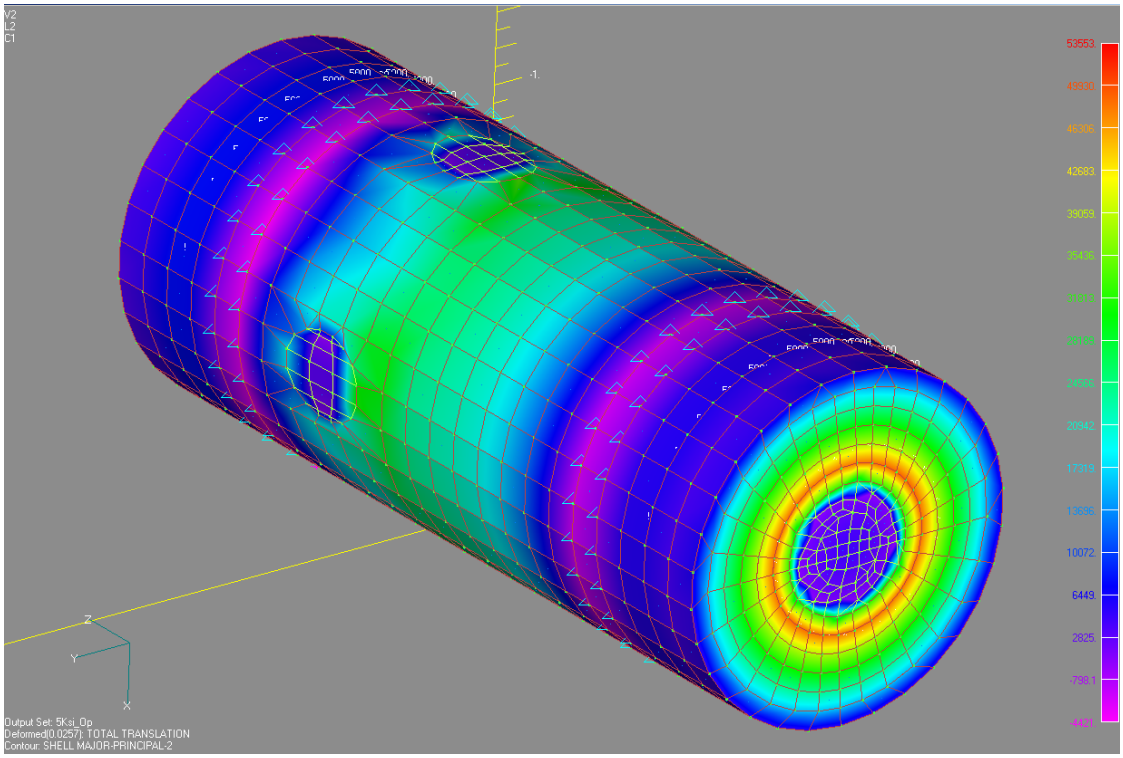

Figure 46: Minor Principal Stresses

Refer to Section 4.3 for a presentation of the findings from the FEA.

LIST OF REFERENCES

[1] Sutton, G. P. and Biblarz, O., *Rocket Propulsion Elements*, John Wiley, New York, 2001.

[2] Davenas, A., "Development of Modern Solid Propellant," *Journal of Propulsion and Power*, Vol. 19, No. 6, 2003, pp. 1108-1128.

[3] Brill, T. B. and Budenz, B. T., "Flash Pyrolysis of Ammonium Perchlorate-Hydroxyl-Terminated-Polybutadiene Mixtures Including Selected Additives," *Solid Propellant Chemistry, Combustion and Motor Interior Ballistics*, Vol. 185, Progress in Astronautics and Aeronautics, Yang, V., Brill, T., and Ren, W.-Z. (Ed.), AIAA, Reston, VA, 2000, pp. 3-32.

[4] Dokhan, A., Price, E. W., Seitzman, J. M., and Sigman, R. K., "The Effects of Bimodal Aluminum with Ultrafine Aluminum on the Burning Rates of Solid Propellants," *Proceedings of the Combustion Institute*, Vol. 29, 2002, pp. 2939-2945.

[5] Price, E. W. and Sigman, R. K., "Combustion of Aluminized Solid Propellants," *Solid Propellant Chemistry, Combustion, and Motor Interior Ballistics*, Vol. 185, *Progress in Astronautics and Aeronautics*, Yang, V., Brill, T., and Ren, W.-Z. (Ed.), AIAA, Reston, VA, 2000, pp. 663-687.

[6] Guirao, C. and Williams, F. A., "A Model for Ammonium Perchlorate Deflagration Between 20 and 100 atm," *AIAA Journal*, Vol. 9, No. 7, 1971, pp. 1345-1356.

[7] Sambamurthi, J. K., Price, E. W., and Sigman, R. K., "Aluminum Agglomeration in Solid-Propellant Combustion," *AIAA Journal*, Vol. 22, 1984, pp. 1132-1138.

[8] Groult, S. and Bizot, "Numerical Simulation of Heterogeneous AP/HTPB Propellant Combustion," AIAA Paper 2004-4039, 2004.

[9] Wang, X. and Jackson, T. L., "Modeling of Aluminized Composite Solid Propellants," AIAA Paper 2004-4041, 2004.

[10] Fitzgerald, R. P. and Brewster, M. Q., "Flame and Surface Structure of Laminate Propellants with Coarse and Fine Ammonium Perchlorate," *Combustion and Flame*, Vol. 136, 2004, pp. 313-326.

[11] Crawford B. L., Jr., Huggett C., Farrington D., and Wilfong R. E., "Direct Determination of Burning Rates of Propellant Powders," *Analytical Chemistry*, Vol. 19, No. 9, 1947.

[12] Glick R. L. and Haun D. V., "An Improved Closed Burner Method," AIAA Paper 90-1870, 1990.

[13] Stephens, M. A., Carro, R., Wolf, S., Sammet, T., Petersen, E. L., and Smith, C. "Performance of AP-Based Composite Propellant Containing Nanoscale Aluminum," AIAA Paper 2005-4470, July 2005.

[14] Lee, S. T., Hong, S. W., and Yoo, K. H., "Experimental Studies Relating to the Combustion Microstructure in Heterogeneous Propellants," AIAA Paper 1993-1753, June 1993.

[15] Miller, R. R., "Effect of Particle Size on Reduced Smoke Propellant Ballistics," AIAA Paper 1982-1096, June 1982.

[16] Small, J. L., Stephens, M. A., Deshpande, S., Petersen, E. L., and Seal, S., "Burn Rate Sensitization of Solid Propellants Using a Nano-Titania Additive," Paper 150, 20th International Colloquium on the Dynamics of Explosions and Reactive Systems, July 31-August 5, 2005, Montreal, Canada.

[17] Clarke E. Hermance, "Continuous Measurement of the Burning Rate of a Composite Solid Propellant," AIAA Paper 69-1967, 1969.

[18] Vladica S. Bozic, Djordje Dj. Blagojevic, and Bozidar A. Anicin, "Measurement System for Determining Solid Rocket Propellant Burning Rate Using Reflection Microwave Interferometry," AIAA Paper 1995-2709, 1995.

[19] D. Ribéreau, F. Dauch, G. Fouin, R. Lefrère, "Assessment of Solid Propellant Motor Internal Ballistic at Full-Scale with Ultrasound Measurement," AIAA Paper 2000-3844, 2000.

[20] R. A. Frederick, Jr., Marlow D. Moser "Research in Solid Propellant Ballistic at UAH," AIAA Paper 2005-3620, 2005.

[21] R. Carro, J. Arvanetes, A. Powell, M. Stephens, E. Petersen, and C. Smith, "High-Pressure Testing of Composite Solid Propellant Mixtures: Burner Facility Characterization," AIAA Paper 2005-3617, 41st AIAA/ASME/SAE/ASEE Joint Propulsion Conference & Exhibit, July 2005, Tucson, AZ.

[22] A. Russo, D. Reid, M. Stephens, A. LePage, T. Sammet, R. Carro, E. Petersen, S. Seal, "Anatase and Rutile Nano-crystalline Titania as Burn-rate Modifiers in Solid Rocket Propellants," July 2006.

[23] M. Stephens, T. Sammet, R. Carro, A. LePage, D. Reid, S. Seal and E. Petersen, "New Additives for Modifying the Burn Rate of Composite Solid Propellant," AIAA Paper

2006-4948, 42nd AIAA/ASME/SAE/ASEE Joint Propulsion Conference & Exhibit, July 2006, Sacramento, CA.

[24] D. L. Reid, A. E. Russo, R. V. Carro, M. A. Stephens, A. R. LePage, T. C. Spalding, E. L. Petersen, and S. Seal, "Nanoscale Additives Tailor Energetic Materials," *Nano Letters*, Vol. 7, No. 7, 2007, pp. 2157-2161.

[25] Stephens, M. A., Powell, A. S., Miranda, D. J., Shah, H. G., Nguyen, L. K., and Petersen, E. L., "A New Lab-Scale Mixing Facility for Composite Solid Propellants with Nanoadditives," Proceedings of the 41st JANNAF Combustion Meeting, CPIA, John Hopkins University, Baltimore, MD, December 2006.

[26] E. Petersen, J. Arvanetes, A. LePage, R. Carro, A. Powell, "Monitoring Strand Burner Combustion Products Using Emission Spectroscopy," AIAA Paper 2007-5767, 43rd AIAA/ASME/SAE/ASEE Joint Propulsion Conference & Exhibit, July 2007, Cincinnati, OH.

[27] A.I. Atwood, T.L. Boggs, P.O. Curran, T.P. Parr, D. M. Hanson-Parr, C. F. Price and J. Wiknich, "Burning Rate of Solid Propellant Ingredients, Part 2: Determination of Burning Rate Temperature Sensitivity," *Journal of Propulsion and Power*, Vol. 15, No. 6, November-December 1999.

[28] M.W. Beckstead, "A Model for Composite Modified Double Base Propellants," AIAA Paper 1982-355, 20th Aerospace Science Meeting, January 1982, Orlando, FL.

[29] J.P. Renie, J.R. Osborn, "Temperature and Pressure Sensitivity of Aluminized Propellants," 16th SAE/ASME Joint Propulsion Conference, July 1980, Hartford, CT.

[30] F. Cauty, "Investigation in Energetic Material Combustion: Solid Propellant Flame Structure and Temperature Profile" AIAA Paper 2007-5863, 43rd AIAA/ASME/SAE/ASEE Joint Propulsion Conference & Exhibit, July 2007, Cincinnati, OH.

[31] H. Gibby, "The Control of Ignition Transients Through Propellant Grain Inhibiting" AIAA Paper 2007-5863, 43rd AIAA/ASME/SAE/ASEE Joint Propulsion Conference & Exhibit, July 2007, Cincinnati, OH.

[32] W. Most, K. Parker, M Summerfield, "The ignition Transient in Solid Propellant Rocket Motors" AIAA Paper 1966-666, 2nd AIAA Propulsion Joint Specialist Conference, June 1966, Colorado Springs, CO.

[33] B. Favivni, M Di Giacinto, F. Serraglia, "Ignition Transient Pressure Oscillations in Solid Rocket Motors" AIAA Paper 2005-4165, 41st AIAA/ASME/SAE/ASEE Joint Propulsion Conference & Exhibit, July 2005, Tucson, AZ.

[34] A. Morita, T. Nagaoka, H. Isoda "Effect of Pressure Oscillation on the Burning Rate of Solid Propellant" AIAA Paper 1981-1521, 17th SAE/ASME Joint Propulsion Conference, Colorado Springs, CO, July 1981, AIAA.

[35] Y. Jinqi, L. Baoxuan, W Kexiu, C. Buxe, "Combustion Mechanism of a Negative Pressure Exponent Composite Solid Propellant" *Journal of Propulsion and Power*, Vol. 8, No. 1, 1992, pp. 37-44.

[36] F. Dauch, R. Frederick Jr., M. Moser, H. Coleman "Uncertainty Assessment of the Pulse-Echo Ultrasonic Burning Rate Measurement Technique" AIAA Paper 1999-2224, 35th AIAA/ASME/SAE/ASEE Joint Propulsion Conference & Exhibit, Los Angeles, CA, June 1999.

[37] K. Russell, H. Goldstein, "Investigation and Screening of M17 Propellant Production for Lots Subject to Poor Low Temperature Ballistic Performance" Final Technical Report No. DB-TR-7-61, Ammunition Group, Picatinny Arsenal, June 1961

ASME *Boiler and Pressure Vessel Code*, Section VIII, Division I, 1995.